PONTIFICIA UNIVERSIDAD CATOLICA DE CHILE
SCHOOL OF ENGINEERING

MODELING AND SIMULATION OF TIME-HARMONIC WAVE PROPAGATION IN CYLINDRICAL IMPEDANCE GUIDES: APPLICATION TO AN OIL WELL STIMULATION TECHNOLOGY

CARLOS ANDRÉS PÉREZ ARANCIBIA

Thesis submitted to the Office of Research and Graduate Studies
in partial fulfillment of the requirements for the degree of
Master in Engineering Sciences

Advisor:
MARIO DURÁN

Santiago de Chile, May 2010

PONTIFICIA UNIVERSIDAD CATOLICA DE CHILE
SCHOOL OF ENGINEERING

MODELING AND SIMULATION OF TIME-HARMONIC WAVE PROPAGATION IN CYLINDRICAL IMPEDANCE GUIDES: APPLICATION TO AN OIL WELL STIMULATION TECHNOLOGY

CARLOS ANDRÉS PÉREZ ARANCIBIA

Members of the Committee:
MARIO DURÁN
MARCELO GUARINI
RAFAEL BENGURIA
JEAN-CLAUDE NÉDÉLEC
JORGE VERA

Thesis submitted to the Office of Research and Graduate Studies
in partial fulfillment of the requirements for the degree of
Master in Engineering Sciences

Santiago de Chile, May 2010

To RUBY, *my parents,*
OSVALDO *and* HERMINDA,
and my brothers,
CÉSAR *and* NÉSTOR.

ACKNOWLEDGEMENTS

This thesis would not have been done without the help of many people, so it is a pleasure for me to thank those who made it possible.

First of all I would like to give thanks to the most important persons in my life; my parents, my brothers, my aunt Rita, and specially Ruby, for their infinite affection, support and patient.

I wish to thank my advisor, Mario Durán, whose encouragement from the initial to the final level enabled me to develop an understanding of the subject. It was an honor to work under his supervision during these last two years.

I am greatly indebted to my office mates: Ricardo Hein, Eduardo Godoy and Valeria Boccardo for sharing with me their good sense of humor, their ideas, their knowledge, their references and for their helpful comments on this manuscript.

I also would like to thank to Javier Jacobsen, Juan Cristóbal García-Huidobro, Juan Casanova, Gabriel Delgado, Pablo Troncoso, Enrique Mercadal and Álvaro Lorca, for sharing with me their time talking and speculating about philosophy, science, religion, music, movies, literature, politics and life in general. I realized that all these conversations indirectly or directly positively affected the development of this dissertation.

I wish to show my gratitude to the CONICYT scholarship for master's degree students for its financial aid during the last year; and to the Padre Alberto Hurtado scholarship for undergraduate students, without which I probably would have never attend at this university and perhaps, to no university at all.

Lastly, I offer my regards to all of those who supported me in any respect during the completion of the project.

CONTENTS

LIST OF FIGURES

RESUMEN

Esta tesis tiene como objetivo calcular el campo difractado y los estados resonantes que resultan de la radiación acústica de alta frecuencia emanada de un dispositivo que es sumergido en un pozo de petróleo para incrementar la permeabilidad de la formación rocosa que lo rodea. Simulaciones de alto desempeño son las que motivan este trabajo debido a su capacidad para determinar frecuencias óptimas de estimulación. Para lograr obtener dichas simulaciones, desarrollamos procedimientos matemáticos que permiten resolver problemas de propagación de ondas tiempo-harmónicas en una guía de ondas cilíndrica infinita localmente perturbada. La condición de borde de impedancia es ampliamente utilizada ya que resulta adecuada para captar los fenómenos de transmisión de energía producidos debido a las altas frecuencias a las cuales trabaja el dispositivo y la interacción entre el fluido y el medio poroso. El dominio no acotado es truncado introduciendo una condición de borde absorbente dada por el operador Dirichlet-a-Neumann, el cual es deducido por medio de una función de Green. La solución de los problemas resultantes es obtenida por medio del método de los elementos finitos. Problemas de referencia que comparan las soluciones exactas con las aproximadas, son resueltos para geometrías simples con el fin de probar la exactitud de los métodos numéricos aquí desarrollados.

Palabras Claves: Ecuación de Helmholtz, guía de onda cilíndrica, función de Green, problema de difracción de ondas directo, problema de resonancias, condición de borde de impedancia, operador Dirichlet-a-Neumann, método de los elementos finitos, perturbación compacta, estimulación acústica de pozos.

ABSTRACT

This thesis aims to compute the scattered field and the resonant states arising due to the high-frequency acoustic radiation produced by a device lowered into an oil well with the purpose of increasing the permeability of the porous rock surrounding it. Accurate simulations of these physical phenomena motivate this work due to their potential to improve the performance of this well stimulation method, by means of determining optimal emission frequencies. To obtain these simulations, we develop numerical procedures to solve time-harmonic wave propagation problems in a locally perturbed cylindrical waveguide. The impedance boundary condition is largely employed throughout this thesis because it is suitable to model the energy dissipation phenomenon resulting from the high-frequencies at which the device works, and the fluid/porous solid acoustic interaction (the interaction between the oil and the reservoir rock). The unbounded domain is truncated introducing an absorbing boundary condition obtained from the Dirichlet-to-Neumann map, which is deduced from a proper Green's function. The solution of the resultant problems is carried out via the finite element method. Benchmark problems are presented to show the efficacy and reliability of the numerical methods proposed.

Keywords: Helmholtz equation, cylindrical waveguide, Green's function, direct scattering problem, resonance problem, impedance boundary condition, Dirichlet-to-Neumann map, finite element method, compact perturbation, acoustic well stimulation method.

I. INTRODUCTION

1.1 Motivation

The decrease of oil recovery from a reservoir is one the most important problems in the oil-producing industry. As a result of this fact, the stimulation of oil wells is a key issue in the exploitation of this essential natural resource. There are two main causes for the reduction of oil well production. (1) Typically no more than 10% of the oil is recovered due to it flows from the formation to the well due to the natural pressure of the reservoir. The residual oil is difficult to recover because its low mobility and, to the fact that it is practically trapped in the reservoir unless the well is stimulated. Different methods have been developed to overcome this difficulty. The most commonly applied are steam, water and gas flooding; hydraulic and explosive fracturing; injection of surfactants; and layer burning (cf. Lake 1996). In the most successful case each stimulation method can enhance the oil recovery up to 50-70% of total oil in the reservoir (cf. Beresnev & Johnson 1994). (2) The second main cause is the local decrease of the reservoir's permeability around the producing wellbore due to the deposition of scales, precipitants and mud penetration during exploitation that form an impermeable barrier to fluid flow. Different method are used to combat local deposits, including solvent and acid injection, treatment by mechanical scrapers and high pressure fracturing. The most commonly employed are chemical solvents that dissolve the small debris particles that plug the rock's pores. Each of these methods has important drawbacks and undesirable effects. For instance, some methods are expensive and highly polluting, while others require stopping the production producing damage to the oil well itself or having harmful ecological consequences such as contamination of underground water resources (cf. Beresnev & Johnson 1994).

An alternative approach to face option (2) that overcomes the drawbacks mentioned above, is the application of ultrasound. The idea of using mechanical vibrations to stimulate oil wells dates back to the early 50s, when increased oil recovery was observed as a consequence of cultural noise and earthquakes. A good review of the development of seismic stimulation in USA and Russia can be found in Beresnev & Johnson (1994), while

observations of the same phenomenon due to field tests made in China are reported by Guo et al. (2004).

According to Krylov et al. (1991), seismic waves become an ultrasound when they pass through a fractured porous media like the zone near the borehole. Therefore, knowledge of the ultrasound effect on the fluid flow in porous media is critical to the development of a technology based on the application of acoustic radiation.

The viability of ultrasound as a method to enhance oil recovery was first studied by Duhon & Campbell (1965). Their observations showed that ultrasonic energy did have a considerable effect on displacement efficiency. Since that work several studies have tried to elucidate the physical phenomenon underlying the positive effect of ultrasound in enhancing oil recovery (see Hamida & Babadagli (2007) for a review of them). As Hamida & Babadagli (2007) point out the following mechanisms are believed to be responsible for the observed improvement in percolation of oil within porous media:

(a) Increase in the relative permeability of the phases (Cherskiy et al. 1977).

(b) Non-linear acoustic effects such as in-pore turbulence, acoustic streaming, cavitation, and perturbation in local pressures. Such effects reduce the adherence of wetting films onto the rock matrix and may be relevant at high ultrasonic intensities.

(c) Reduction of surface tension, density and viscosity as a consequence of heating by ultrasonic radiation. Ultrasound may also be very useful in reducing viscosity of thixotropic fluids (Fairbanks & Chen 1971).

(d) Mechanical vibration of pore walls initiate peristaltic transport, by which fluid is *squeezed* into adjacent pores (Aarts & Ooms 1998, Aarts et al. 1999).

(e) Micro-emulsification of oil in the presence of natural or introduced surfactants (Abismail et al. 1999).

(f) Coalescence and dispersion of oil drops due to the Bjerkness forces (Mettin et al. 1997).

(g) Increase in rock permeability and porosity due to removal of fines and clays, paraffin wax and and asphalting (Venkitaraman et al. 1995, Roberts et al. 1996, 2000, Champion

et al. 2004, Wong et al. 2004, Poesio et al. 2004, Poesio & Ooms 2004, 2007, Poesio 2009).

(h) Oscillation and excitation of capillary trapped oil drops to pressure perturbation generated by cavitating bubbles and mechanical vibrations of rock and fluid (Graham & Higdon 2000*a*,*b*, 2002*a*,*b*).

The proven good properties of ultrasound have led to the development of the so-called *acoustic well stimulation* (AWS) *method*, which nowadays has a broad acceptance in oil-producing industry. This method consists in the application of an ultrasonic field radiated by a transducer (or a configuration of several of them) that is lowered into the well to the zone that is in direct contact with the reservoir porous rock. Figure 1.1 (a) shows a diagram of the method, while Figure 1.1 (b) shows the acoustic device. This enhanced oil recovery method has shown to be effective in only about 40-50% of the cases studied. Due to these few successful cases studied, the AWS method still needs further research. Many patents, such as Pechkov et al. (1993), Ellingsen et al. (1994), Wegener, Maloney, Zornes, Reese & Fraim (2001), Wegener, Zornes, Maloney, Vienot & Fraim (2001), Meyer & Tarnawskyj (2002), Abramov, Abramov, Pechkov, Zolezzi-Garreton & Paredes-Rojas (2006), Abramov, Abramov, Zolezzi-Garreton, Paredes-Rojas & Pechkov (2006), Barrientos et al. (2006); and studies, such as Venkitaraman et al. (1995), Westermark et al. (2001), Westermark & Brett (2002), Mullakaev, Abramov & Pechkov (2009), Mullakaev, Abramov, Abramov, Gradov & Pechkov (2009), have been carried out so as to improve its performance.

The referred works study the influence of ultrasound on oil percolation assuming that the acoustic energy is efficiently transmitted from the device's surface to the reservoir rock. However, this assumption is not quite true, because in real conditions that energy transmission may be seriously affected by geometrical and physical effects have not yet been studied. For instance, most of the energy could be radiated to infinity along the direction of the well (up and down from the device) as leaky modes (i.e. modes that radiate energy along the direction of a waveguide) and consequently it would not be able to penetrate the reservoir rock; or it could remain trapped near the device as trapped modes

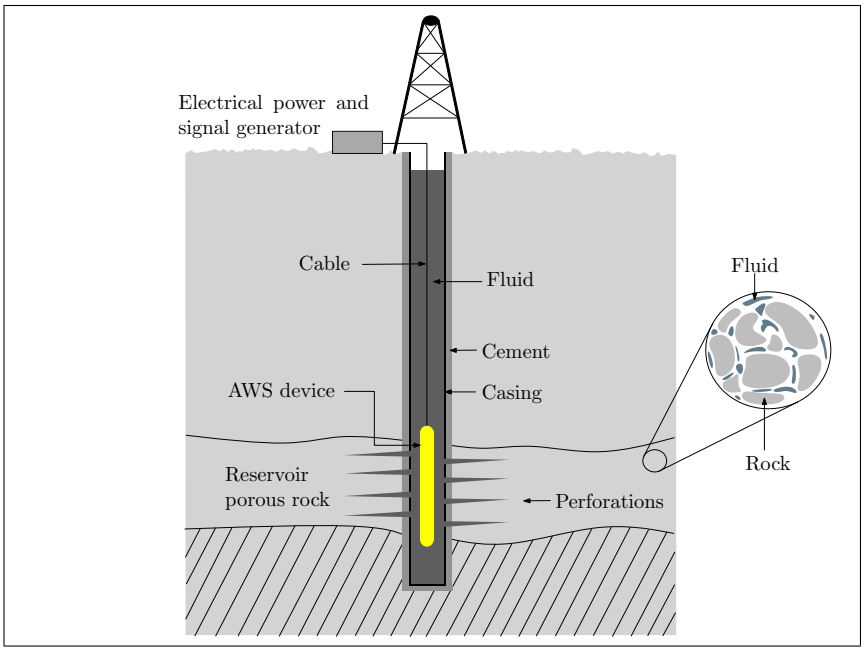

(a) Diagram of a completed well and the acoustic well stimulation method.

(b) Photograph of the acoustic device employed for the acoustic stimulation of oil wells, taken from Mullakaev, Abramov & Pechkov (2009).

FIGURE 1.1. Diagram of the acoustic well stimulation method and a photograph of the acoustic device.

(i.e. modes that do not radiate energy to infinity along the waveguide direction). On the other hand, the operation of the AWS method may trigger the occurrence of resonance phenomena, which might result in damage to the well and the device. In this context, a simple mathematical model is crucial to improve the design of the acoustic device due to numerical simulations of the AWS method may predict how the acoustic energy is distributed inside

the well, allowing us to find optimal emission frequencies in the sense that the energy is effectively radiated towards the damaged zone. Moreover, it can be used to determine the resonance frequencies in order to avoid them or excite them if this makes it possible to take advantage of their consequences.

1.2 Geophysical background information

Many works dealing with phenomenological models for the acoustic wave propagation in boreholes can be found in the geophysical literature. Most of them attempt to simulate the borehole acoustic logging system, which is the central component of the non-invasive in-situ assessment of rock formation properties. This system consists of a tool cylindrical in shape, composed by acoustic sources of excitation and a sensor, that is lowered into the hole to record the geologic formations penetrated by the borehole, resorting to the use of data inversion techniques (cf. Paillet & Cheng 1991, Tang & Cheng 2004).

These references use the scalar wave equation and the Biot model for the wave propagation in porous media (cf. Biot 1956*a*,*b*) - or the linear elastodynamic equations in the simplified case - to compute the different kind of waves allowed to propagate along the fluid inside the borehole, and in the rock and soil surrounding it. A few of them, the most relevant ones, are Cheng & Toksoz (1981), Tubman et al. (1984), Stephen et al. (1985), Schmitt & Bouchon (1985), Schmitt et al. (1988), Liu et al. (1996), Tadeu et al. (2000), Liu & Sinha (2003) and Michler et al. (2009). A survey of the numerical procedures employed in these articles is presented by Cheng & Blanch (2008). Most of these works regard simple geometries, consider an acoustic tool considerably different to the one employed by the AWS method and attempt to solve full-wave problems.

Unfortunately, this model is not quite suitable for our goals due to two main reasons:

(a) Contrary to the full wave model used to perform simulations of the acoustic logging, the AWS method may be assumed to be time-harmonic. The forced oscillations produced by the AWS device are at a specific frequency (cf. Mullakaev, Abramov & Pechkov

2009). It drives the system conformed by the device and the well to achieve a stationary regime. Consequently, wave propagation becomes time-harmonic as time goes by, allowing us to assume that the temporal part of the wave fields is given by $\mathrm{e}^{-\mathrm{i}\omega t}$, where ω is the angular frequency. This assumption leads to a great simplification of the methods employed to carry out the computations because the temporal variable can be extracted from the partial differential equations involved.

(b) There is a substantial difference between the boreholes considered in the acoustic logging simulations, and the completed wells in which the AWS method usually operates. A borehole consists of a hole drilled in the ground inside which the fluid is in interaction with the porous rock and the soil that surround the well. Contrariwise, in a completed well - like the one shown in Figure 1.1 (a) - the fluid and the porous rock are in contact only through the perforations' surface, which are small holes made in the reservoir rock. All the rest of the well's surface is covered by a steel pipe, the so-called casing (cf. Hyne 2001). Furthermore, the perforations lead us to consider a complicated computational domain difficult to handle by the methods usually employed in the acoustic logging simulations, like finite-difference schemes.

1.3 Aims and claims

In this thesis we propose a phenomenological model for the wave propagation problems arising when an oil well is stimulated by AWS method. The well is assumed to be filled with oil and we regard it as an infinite waveguide with a local perturbation placed where the perforations and the acoustic device are located (see Figure 1.1 (a)). A lossy boundary condition is set on the well's walls. It allows us to confine the computational domain to inside the well avoiding to solve a fluid/porous-solid interaction problem. The resulting model is based on the Helmholtz equation, which rules the scalar time-harmonic acoustic waves in fluids; and the impedance boundary condition, which models pretty well the energy dissipation throughout the boundaries of the domain. From a mathematical point of view two problem are set; a direct *scattering problem* seeking to determine the

total acoustic pressure field produced by the radiating device; and a *resonance problem*, seeking to determine the resonance frequencies (trapped modes and complex resonances).

We claim that the solution of the scattering problem provides a way of determining the frequencies at which it is possible to obtain optimal results of the AWS method, in the sense that most of the energy radiated by the obstacle is effectively transmitted through the perforations to the sealed pores of the reservoir rock. On the other hand, we claim that from the solution of the resonance problem it is possible to determine resonance frequencies at which it is possible to observe energy accumulation inside the perforations. Such resonance frequencies are highly relevant due to two reasons: they can lead to damage to the well and the device itself, as usually happens in waveguides when resonance frequencies are excited (cf. Parker & Stoneman 1989) ; or they may provide a way to optimize the energy, due to the fact that the energy remains trapped near the fluid/porous-solid interface where the sealed pores of the reservoir rock are in direct contact with the fluid medium.

1.4 Mathematical background information

Scalar time-harmonic wave propagation problems in unbounded spatial domains, like the ones we attempt to solve here, pose a unique challenge to numerical computation since the unbounded region is inappropriate for direct discretization. During the last decades several numerical techniques have been developed to solve these problems. They may be classified into four main categories: boundary integral/boundary element methods (cf. Colton & Kress 1983, Bonnet 1995, Nédélec 2001), infinite elements (cf. Astley 2000, Gardes 2000, Astley 2008), absorbing layers (cf. Bérenger 1994, Bermúdez et al. 2008, Givoli 2008), and *absorbing boundary conditions* (cf. Engquist & Majda 1977, Givoli et al. 1998, Givoli 1999, 2004, 2008). Surveys of these methods are found in Harari (2006), Thomson (2006), Ihlenburg (1998) and Marburg & Nolte (2008).

For the particular unbounded domain studied in this dissertation, a waveguide, relevant works on this matter are: Linton & Evans (1992) for integral equation methods; Wu & Fang (1995) and Singer & Turkel (2004) for absorbing layers; Goldstein (1982), Harari et al.

(1998) and Bendali & Guillaume (1999) for absorbing boundary conditions; and Pagneux et al. (1996), Amir et al. (1997), Hazard & Lunéville (2008) for multimodal techniques.

Extensive literature relating to resonance problems in non-perturbed waveguides (in two and three dimensions) with obstacles placed inside, has been published during the last decades.The literature distinguishes two sorts of eigenfunctions; trapped modes and leaky modes. Trapped modes correspond to real resonances of the Helmholtz operator in an unbounded domain, that is confined to the vicinity of the obstacle and do not radiate energy, i.e. they are undamped and no energy is radiated to infinity. Therefore, they are of great physical importance because at the trapped-mode frequencies the response to forced excitation can be quite high. Mathematically, trapped modes are also of considerable interest because they imply non-uniqueness in the associated scattering problem. Contrary to trapped modes, leaky modes radiate energy to infinity. They may be damped due to radiation losses when they are associated to complex resonances of the Helmholtz operator; or may be undamped, when they are associated to real resonances.

Results on sufficient conditions for the existence and non-existence of leaky and trapped modes are studied by many authors such as: Ursell (1991), Evans et al. (1993, 1994), McIver & Linton (1995), McIver et al. (2002), Aslanyan et al. (2000), Linton & McIver (1998*a*), Linton et al. (2002), Davies & Parnovski (1998) and Duan & McIver (2004). Semi-analytic techniques based on matched eigenfunction expansions, integral equations and approximated transcendental equations are developed by Linton & Evans (1992), Linton & McIver (1998*b*), Evans & Linton (1994), McIver et al. (2001) and Duan & McIver (2004) to solve some of these problems. A good review of those works is presented by Linton & McIver (2007).

From a purely numerical point of view, recent works have dealt with the problem of the effective computation of resonances and resonance states of problems like those. Hein et al. (2004), Duan et al. (2007) and Hein & Koch (2008) have successfully employed

the perfectly matched layer technique introduced by Bérenger (1994), for two and three-dimensional waveguides with different kind of obstacles inside, while a new full numerical method that is simple to implement is presented by Levitin & Marletta (2008).

All references mentioned in this section consider lossless boundary conditions, i.e. Neumann, Dirichlet or Robin with a real parameter. Nevertheless, some references dealing with impedance waveguide problems are Rawlins (1978, 1995), Rawlins & Mahmood-Ul-Hassan (2003) and Rawlins (2007), which arise in the context of guides lined with absorbent materials.

1.5 Methodology

The model for the AWS method proposed here leads to scalar time-harmonic wave propagation problems in an unbounded spatial domain. To deal with the unbounded domain we perform an absorbing boundary condition that relies on the computation of the so-called Dirichlet-to-Neumann (DtN) map. This kind of artificial boundary condition presents advantages over other techniques because it is perfectly transparent to incident waves and it does not show a strong dependence on arbitrary parameters like these needed to implement the perfectly matched layer technique.

In waveguides with a lossless boundary condition, the construction of this operator can be performed in two ways: from the separation of variables technique and from the Green's function for the suitable boundary value problem. However, when the impedance boundary condition is imposed (i.e. the Robin boundary condition with a proper complex parameter) it is not possible to use the separation of variable techniques because the functions that appear are not orthogonal in any known sense. This situation prompts us to study the Green's function for the Helmholtz operator in an infinite circular cylindrical waveguide with the impedance boundary condition, which is also useful to implement the boundary integral/boundary element method. This Green's function has not been studied yet, thus a detailed deduction and analysis is performed using the Fourier transform, complex analysis

techniques, the limiting absorption principle and several results relating to the zeros of the so-called Dini function.

The introduction of this absorbing boundary condition allow us to redefine the problems in a bounded region making them suitable for a numerical discretization. Consequently, the variational formulation is applied to discretize the problems using the *finite element method*. This procedure transforms the scattering problem in a linear algebraic system of equations, while the resonance problem results in a non-linear resonance problem that is solved finding the local maxima of a real valued function. Benchmark problems are designed to test the proposed numerical procedures.

Finally, simulations of AWS method in a realistic geometry are worked out solving the scattering problem for different frequencies and determining for each frequency the energy proportion transmitted from the radiating surface to the reservoir rock. On the other hand, the resonance problem is solved to determine the real resonance frequencies. For each resonance frequency the proportion of energy trapped in the perforation is determined.

It is important to observe that problems like the ones addressed here are frequently found in various fields of application such as acoustics, aerodynamics, electromagnetism, plasma physics and so on. Therefore the mathematical methods developed herein may be applied to other fields without important modifications.

1.6 Outline

The structure of this dissertation is as follows. The next chapter concentrates on the construction of the mathematical model and the set-up of the problems solved in this thesis. Chapter III shows the deduction and analysis of the Green's function. The DtN map based on the Green's function and the variational formulation are presented in Chapter IV. Subsequently, Chapter V focuses on all the numerical procedures needed to perform the computations as well as the benchmark problems that validate them. Next, in Chapter VI, the numerical results for a realistic geometry are shown. Finally, Chapter VII presents the conclusions of this work.

II. PHENOMENOLOGICAL MODEL

2.1 The geometry of an oil well

An oil well is created through two successive processes called drilling and completion (cf. Hyne 2001). The first process begins by drilling a hole in the ground, which may be straight down or in some angle. Once the hole is drilled, a logging tool is lowered into the well to determine the composition of each rock layer. If oil is detected, the well's walls are covered by a long length metal pipe called casing, that is set to the well's walls by a layer of cement. After that completion process begins by shooting with explosives the portion of the casing that passes the zone where oil was detected. The explosives form small holes called perforations, that allow oil flow from the reservoir into the well (see Figure 1.1). Henceforth, we call *perforating zone* the region where the perforations are located, while the rest of the well is referred as the *casing zone*.

The casing zone has a regular shape. Actually, it is a circular cylinder with almost constant surface acoustic properties because it is composed by an homogeneous material that is usually steel. On the contrary, the perforating zone has an irregular shape and surface acoustic properties that depend on the position over the boundary due to the fact that its surface is composed in part by the perforated casing, and in part by reservoir porous rock that surounds the perforations. These features lead us to regard the well as an infinite locally-perturbed vertically oriented waveguide. More precisely, it is assumed that the well is a circular cylinder in $\mathbb{R}^3$, with a local perturbation. We mean by local perturbation that the domain admits a decomposition by three sets in which two of them, the unperturbed parts, are perfect semi-infinite right circular cylinders, while the other one, the perturbed part, is a compact set with Lipshitz boundary located among the unperturbed domains. Throughout this dissertation we assume that the perturbed part of the domain corresponds to the perforating zone and the unperturbed domains corresponds to the casing zone.

Up to this point the open set

$$\Omega_w := \Omega_e^- \cup \Gamma_H^- \cup \Omega_i \cup \Gamma_H^+ \cup \Omega_e^+ \subset \mathbb{R}^3 \tag{2.1}$$

represents the well as was described above. The symbol Ω_i denotes the perturbed domain while Ω_e^- and Ω_e^+ denote the unperturbed domains. The unperturbed domain are precisely defined by

$$\Omega_e^- := \left\{(x_1, x_2, x_3) \in \mathbb{R}^3 : x_1^2 + x_2^2 < R^2,\ x_3 \in (-\infty, H)\right\} \tag{2.2a}$$

$$\Omega_e^+ := \left\{(x_1, x_2, x_3) \in \mathbb{R}^3 : x_1^2 + x_2^2 < R^2,\ x_3 \in (-H, +\infty)\right\} \tag{2.2b}$$

where $R > 0$ is the radius of the casing and $H > 0$ is large enough such that $\Omega_i \subset \{(x_1, x_2, x_3) \in \mathbb{R}^3 : |x_3| < H\}$. The artificial boundaries involved are denoted by Γ_H^- and Γ_H^+ and are defined by

$$\Gamma_H^- := \left\{(x_1, x_2, x_3) \in \mathbb{R}^3 : x_1^2 + x_2^2 < R^2, x_3 = -H\right\}. \tag{2.3a}$$

$$\Gamma_H^+ := \left\{(x_1, x_2, x_3) \in \mathbb{R}^3 : x_1^2 + x_2^2 < R^2, x_3 = H\right\}. \tag{2.3b}$$

It stems from (2.3) that the boundaries of Ω_i, Ω_e^- and Ω_e^+ can be expressed as

$$\partial\Omega_i := \Gamma_H^- \cup \Gamma_i \cup \Gamma_H^+, \tag{2.4a}$$

$$\partial\Omega_e^- := \Gamma_H^- \cup \Gamma_e^-, \tag{2.4b}$$

$$\partial\Omega_e^+ := \Gamma_H^+ \cup \Gamma_e^+, \tag{2.4c}$$

where

$$\Gamma_e^- := \left\{(x_1, x_2, x_3) \in \mathbb{R}^3 : x_1^2 + x_2^2 = R^2,\ x_3 \in (-\infty, -H]\right\}, \tag{2.5a}$$

$$\Gamma_e^+ := \left\{(x_1, x_2, x_3) \in \mathbb{R}^3 : x_1^2 + x_2^2 = R^2,\ x_3 \in [H, \infty)\right\}. \tag{2.5b}$$

Finally, the acoustic device is assumed to occupy the compact domain $\Omega_d \subset \Omega_i$, where Γ_d denotes its radiating surface. Let us observe that the definitions made above allow us to express the unbounded computational domain (i.e. the domain where we want to solve the problems) as

$$\Omega := \Omega_w \setminus \overline{\Omega_d}. \tag{2.6}$$

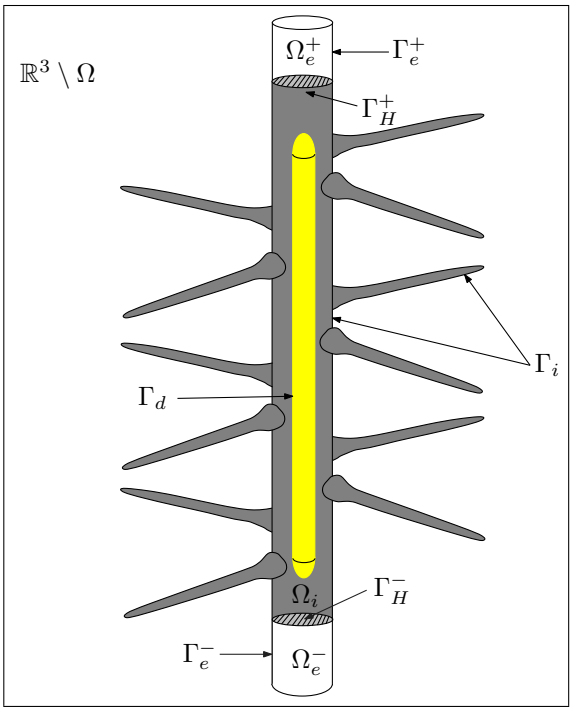

FIGURE 2.1. Diagram of the modeled geometry.

Figure 2.1 depicts a detailed diagram of the domains that we use throughout this thesis.

2.2 Linear acoustics

Here, the oil is assumed to be a compressible ideal fluid with hydrostatic equilibrium density and pressure ρ_0 and p_0 respectively. Around these fixed quantities we consider a small amplitude time-spatial dependent perturbation, $\rho(\boldsymbol{x}, t)$ and $P(\boldsymbol{x}, t)$. It allows us to obtain the linearized continuity equations and Euler equations around the hydrostatic equilibrium states in absence of external volumetric forces. These equations, together with the isentropic relation between the pressure and the density (i.e. the linear material law),

read as follows:

$$\frac{\partial \rho}{\partial t} + \rho_0 \,\text{div}\ \boldsymbol{V} = 0, \tag{2.7a}$$

$$\frac{\partial \boldsymbol{V}}{\partial t} + \frac{1}{\rho_0}\nabla P = 0, \tag{2.7b}$$

$$P = \left(\frac{\partial P}{\partial \rho_0}\right)_s \rho, \tag{2.7c}$$

where $\boldsymbol{V}(\boldsymbol{x}, t)$ is the velocity vector field and $(\partial P/\partial \rho_0)_s = c^2$, with $c > 0$ being the speed of sound in the fluid. Let us observe that (2.7) can be reduced to the following scalar equation for the pressure field:

$$\Delta P = c^2 \frac{\partial^2 P}{\partial t^2}, \tag{2.8}$$

which is the classical linear hyperbolic wave equation or d'Alembert equation. More details about the deduction of the wave equation can be found in Morse & Ingard (1986), Kinsler et al. (1999) and Filippi et al. (1999).

In this work we assume that there is only one source of sound, the acoustic device. As was already discussed in the introduction, it is a time-harmonic excitation that interacts with the fluid throughout its surface. We mean by time-harmonic excitation, that the acoustic source produces a pure mono-frequency motion at a specific frequency, $f = 2\pi\omega$, with ω being the angular frequency. Thus, when the system reaches the stationary regime it is expected that the temporal dependence of the pressure field becomes $\mathrm{e}^{-\mathrm{i}\,\omega t}$. Of course, in this case the physically correct pressure field is

$$P(\boldsymbol{x}, t) = \mathfrak{Re}\left\{p(\boldsymbol{x})\,\mathrm{e}^{-\mathrm{i}\,\omega t}\right\}, \tag{2.9}$$

because imaginary pressure values have no sense.

Replacing (2.9) in (2.8) we obtain that the spatial component of the pressure field satisfies the Helmholtz equation

$$\Delta p + k^2 p = 0 \tag{2.10}$$

where $k := \omega/c$ is the wave number.

Some modifications of (2.10) take place when dissipation is considered. It leads to a complex wave number that is a function of the angular frequency, i.e.

$$k = \frac{\omega}{c} + \mathrm{i}\,\beta,\ \beta \geqslant 0. \tag{2.11}$$

According to Kinsler et al. (1999) the dissipation or damping constant, β, in (2.11), models different physical phenomena. For instance, if the viscosity of the fluid is considered, the damping constant is given by

$$\beta = \frac{\omega}{c}\frac{1}{\sqrt{2}}\left(\frac{\sqrt{1+\tau_s^2\omega^2}-1}{1+\tau_s^2\omega^2}\right)^{1/2},\ \tau_s = \frac{1}{\rho_0 c^2}\left(\frac{4}{3}\eta + \eta_B\right), \tag{2.12}$$

where η and η_b are the coefficients of shear and bulk viscosity respectively; if thermal conduction is taken into account the damping constant is

$$\beta = \frac{\omega^2}{2\rho_0 c^3}\frac{(\gamma-1)\kappa}{c_{\mathcal{P}}}, \tag{2.13}$$

where κ is the thermal conductivity, $c_{\mathcal{P}}$ is the specific heat at constant pressure and γ is the adiabatic constant; and if the coupled effect between the viscosity and the thermal conduction is modeled the damping constant is

$$\beta = \frac{\omega^2}{2\rho_0 c^3}\left(\frac{4}{3}\eta + \frac{(\gamma-1)\kappa}{c_{\mathcal{P}}}\right), \tag{2.14}$$

where the bulk viscosity effect is avoided.

Let us observe that the speed of sound might depend on the position if the fluid is not homogeneous, thus in general the wave number is a function of the spatial variables. From a computational point of view this situation leads to a tough problem unless we assume that the spatial dependence of the wave number is compactly supported in the interior domain. Consequently, we assume that the wave number is given by the following complex valued function:

$$k : \mathbb{R}_+ \times \Omega \to \mathbb{C}, (\omega, \boldsymbol{x}) \mapsto k(\omega, \boldsymbol{x}) := k_i(\omega, \boldsymbol{x}) + k_e(\omega) \tag{2.15}$$

where supp $\{k_i(\omega, \cdot)\} \subset \Omega_i \setminus \overline{\Omega_d}$.

Remark II.1. *At this point it is important to remark that henceforth we assume that the oil well is infinite in length and is filled with oil. From a physical point of view, these assumptions mean that we are avoiding the possibility that incoming waves get in to the perforating zone of the well from its upper and lower ends. Under realistic conditions a fraction of the energy radiated by the device is reflected on the upper (oil-air interface) and the lower (the bottom of the well) ends of the well, and then it travels as acoustic waves toward the device. Despite that, we neglect these waves because the well's ends are far away from the obstacle and thus the dissipation severely attenuates them before reaching the perforating zone.*

2.3 Boundary conditions

As was pointed out in the introduction, a key point of this dissertation is to characterize energy loss through the well's walls. This is a very important phenomenon in this model due two main reasons: the high frequency range at which the AWS method works; and the well-known sound absorption properties of porous materials. Here we claim that a feasible way to model the energy loss is given by the use of the impedance boundary condition. Two reasons support this statement. On one hand we have that this boundary condition has been successfully applied to quantify the surface energy loss in ducts (cf. Munjal 1987), like the pipe placed in the casing zone of well; and on the other hand, we find that it has been extensively used to characterize the sound transmission between fluid and several kinds of porous materials (cf. Delany & Bazley 1970, Miki 1990, Allard & Champoux 1992) like the reservoir porous rock.

More specifically, we assume that the well's walls are locally reacting surfaces. These are surfaces for which the acoustic field at a given point depends only on the properties of the surface at that point and not on the configuration of the incident wave. This property can be mathematically represented by the normal acoustic impedance, which is the ratio of the pressure field to the normal velocity of the particles on the surface, i.e.

$$Z_n := \frac{P}{\boldsymbol{V}\cdot\boldsymbol{n}} \text{ on } \partial\Omega_w, \tag{2.16}$$

with $\boldsymbol{n}$ being the normal unit vector pointing outward of Ω_w. In the stationary regime it can be expressed as

$$Z_n = \mathrm{i}\ \omega\rho_0 \left(\frac{1}{p}\frac{\partial p}{\partial n}\right)^{-1} = \rho c\,\zeta \text{ on } \partial\Omega_w, \tag{2.17}$$

where $\zeta = \chi + \mathrm{i}\,\xi$ is the dimensionless specific impedance of the surface. Therein χ and ξ are respectively the resistive and the reactive component of the dimensionless specific impedance. The usefulness of the impedance model is that under the assumption that the well's walls are locally reacting surfaces, we can impose the following boundary condition

$$\frac{\partial p}{\partial n} - \alpha\, p = 0 \ \text{ on } \ \partial\Omega_w = \Gamma_e^- \cup \Gamma_i \cup \Gamma_e^+, \quad \text{with} \quad \alpha := \mathrm{i}\,k/\zeta, \tag{2.18}$$

known as the impedance or Robin boundary condition.

The resistive part of the dimensionless specific impedance plays a very important role because it is associated to energy loss through the boundary. In fact, the time-averaged energy flux density through a boundary during a period $T = 2\pi/\omega$ is given by (cf. Filippi et al. 1999)

$$I = -\frac{1}{\omega\rho_0 T}\int_0^T \mathfrak{Re}\left\{p\,\mathrm{e}^{-\mathrm{i}\,\omega t}\right\}\mathfrak{Re}\left\{\mathrm{i}\,\nabla p\cdot\boldsymbol{n}\,\mathrm{e}^{-\mathrm{i}\,\omega t}\right\}\,\mathrm{d}t. \tag{2.19}$$

Therefore, replacing (2.18) in (2.19), it is possible to infer that

$$I_{loss} = \frac{|p|^2}{2\rho_0 c|\zeta|^2}\chi, \tag{2.20}$$

and consequently the resistive part of the specific surface impedance is such that $\chi \geqslant 0$. Let us observe that under the assumptions $\beta = \mathfrak{Im}\,k \geqslant 0$ and $\chi = \mathfrak{Re}\,\zeta \geqslant 0$, we get that α fulfills the condition $\mathfrak{Im}\,\alpha \geqslant 0$.

The geometry of the well gives us crucial information about the spatial dependence of the impedance parameter. In the casing zone of the well the normal impedance does not change with the position due to the homogeneity of the metal pipe. On the contrary, in the perforating zone the impedance parameter is a point dependent function due to the variability of the geometry and the acoustic properties of materials involved (cement, casing and porous rock). It stems from here that the impedance parameter is assumed a compactly

supported function of the spatial variables, i.e.,

$$\alpha : \mathbb{R}_+ \times \partial\Omega_w \to \mathbb{C}, (\omega, \boldsymbol{x}) \mapsto \alpha(\omega, \boldsymbol{x}) = \alpha_i(\omega, \boldsymbol{x}) + \alpha_e(\omega) \tag{2.21}$$

where supp $\{\alpha_i(\omega, \cdot)\} \subset \Gamma_i$.

Finally, we assume that AWS device has an acoustically hard surface mathematically described by the Neumann boundary condition (cf. Filippi et al. 1999). The effect of the radiating surface is modeled by a non-homogeneus term appearing in the boundary condition, which we assume known and given by the function $g \in H^{-1/2}(\Gamma_d)$. Consequently the pressure field fulfills the condition

$$\frac{\partial p}{\partial n} = g \ \text{ on } \ \Gamma_d. \tag{2.22}$$

The choice of a surface source of excitation instead, for instance, a volumetric one, is motivated by the article of Mullakaev, Abramov & Pechkov (2009), where the AWS device is designed as a *surface-based source supply*. Nevertheless, other kinds of sources can be easily added to the model if their effect on the equations is confined to a compact subset of Ω_i.

For the kind of source chosen we can easily obtain the effective time-averaged acoustic energy supplied by the device. Then, by using (2.19) we infer that the effective time-averaged energy flux density (or power density) supplied by the AWS device is

$$I_{rad} = \frac{1}{2\omega\rho_0}\mathfrak{Im}\{p\bar{g}\}. \tag{2.23}$$

2.4 Set-up of the problems

In this section we set the problems that we attempt to solve in the following chapters. As was already indicated in the introduction, they correspond to a direct wave scattering problem and a resonance problem.

The scattering problem consists of the computation of the total pressure field produced by the AWS device submerged in the well. Making use of the equations deduced in previous sections, we realize that it is given by the solution of the following problem:

Find $p : \Omega \to \mathbb{C}$, $p \in H^1_{loc}(\Omega)$, such that:

$$\begin{cases} \Delta p + k^2 p &= 0 \quad \text{in} \quad \Omega, \\ \dfrac{\partial p}{\partial n} - \alpha\, p &= 0 \quad \text{on} \quad \Gamma_e^- \cup \Gamma_i \cup \Gamma_e^+, \\ \dfrac{\partial p}{\partial n} &= g \quad \text{on} \quad \Gamma_d, \\ + \text{ radiation condition at } |\boldsymbol{x}| \to \infty, \text{ if } \mathfrak{Im}\,\alpha_e = \mathfrak{Im}\,k_e = 0, \end{cases} \tag{2.24}$$

where p is the pressure field, $g \in H^{-1/2}(\Gamma_d)$ is the surface acoustic source and

$$H^1_{loc}(\Omega) = \left\{ u \in L^2_{loc}(\Omega) : |\nabla u| \in L^2_{loc}(\Omega) \right\}$$

is the space consisting of functions that are locally square integrable as well as their gradients, i.e. they are absolutely integrable on every compact subset of Ω.

Let us observe that in absence of dissipation, i.e. when the wave number and the impedance parameter are real numbers, a radiation condition is needed to allow only outgoing wave solutions of the problem. Such radiation condition differs greatly from the classical Sommerfeld condition and will be stated afterwards in this dissertation.

To introduce the artificial boundary conditions on the transparent boundaries, Γ_H^- and Γ_H^+, we equivalently reformulate the scattering problem (2.24) as the following three coupled problems (cf. Johnson & Nédélec 1980):

Find $p_i : \Omega_i \setminus \overline{\Omega_d} \to \mathbb{C}$, $p_i \in H^1(\Omega_i \setminus \overline{\Omega_d})$, $p_e^- : \Omega_e^- \to \mathbb{C}$, $p_e^- \in H^1_{loc}(\Omega_e^-)$ and $p_e^+ : \Omega_e^+ \to \mathbb{C}$, $p_e^+ \in H^1_{loc}(\Omega_e^+)$ such that:

$$\begin{cases} \Delta p_i + k^2 p_i = 0 & \text{in} \quad \Omega_i \setminus \overline{\Omega_d}, \\ \dfrac{\partial p_i}{\partial n} - \alpha\, p_i = 0 & \text{on} \quad \Gamma_i, \\ \dfrac{\partial p_i}{\partial n} = g & \text{on} \quad \Gamma_d, \\ \dfrac{\partial p_i}{\partial n} = \dfrac{\partial p_e^+}{\partial n} & \text{on} \quad \Gamma_H^+, \\ \dfrac{\partial p_i}{\partial n} = \dfrac{\partial p_e^-}{\partial n} & \text{on} \quad \Gamma_H^-, \end{cases} \tag{2.25}$$

$$\begin{cases} \Delta p_e^- + k^2 p_e^- = 0 & \text{in} \quad \Omega_e^-, \\ \dfrac{\partial p_e^-}{\partial n} - \alpha\, p_e^- = 0 & \text{on} \quad \Gamma_e^-, \\ p_e^- = p_i & \text{on} \quad \Gamma_H^-, \\ + \text{ radiation condition at } |\boldsymbol{x}| \to \infty, \text{ if } \mathfrak{Im}\,\alpha_e = \mathfrak{Im}\, k_e = 0 \end{cases} \tag{2.26}$$

and

$$\begin{cases} \Delta p_e^+ + k^2 p_e^+ = 0 & \text{in} \quad \Omega_e^+, \\ \dfrac{\partial p_e^+}{\partial n} - \alpha\, p_e^+ = 0 & \text{on} \quad \Gamma_e^+, \\ p_e^+ = p_i & \text{on} \quad \Gamma_H^+, \\ + \text{ radiation condition at } |\boldsymbol{x}| \to \infty, \text{ if } \mathfrak{Im}\,\alpha_e = \mathfrak{Im}\, k_e = 0, \end{cases} \tag{2.27}$$

where the solution of (2.24) can be recovered by setting

$$p_i = p|_{\Omega_i}\,, \quad p_e^- = p|_{\Omega_e^-} \quad \text{and} \quad p_e^+ = p|_{\Omega_e^+}\,.$$

Up to this point we refer to (2.25) as the *interior problem*, to (2.26) as the *lower exterior problem* and to (2.27) as the *upper exterior problem*.

On the other hand, the resonance problem consists in finding an angular frequency that has associated a wave number $k \neq 0$ and a non-identically zero acoustic field $p : \Omega \to \mathbb{C}$,

$p \in H^1_{loc}(\Omega)$, that satisfies the homogenous problem:

$$\begin{cases} \Delta p + k^2 p &= 0 \quad \text{in} \quad \Omega, \\ \dfrac{\partial p}{\partial n} - \alpha\, p &= 0 \quad \text{on} \quad \Gamma_e^- \cup \Gamma_i \cup \Gamma_e^+, \\ \dfrac{\partial p}{\partial n} &= 0 \quad \text{on} \quad \Gamma_d, \\ + \text{ radiation condition at } |\boldsymbol{x}| \to \infty, \text{ if } \mathfrak{Im}\,\alpha_e = \mathfrak{Im}\,k_e = 0\ . \end{cases} \tag{2.28}$$

As well as the scattering problem, the resonance problem can be equivalently reformulated so as to introduce the artificial boundary conditions on Γ_H^- and Γ_H^+. Thus (2.28) may be set as:

Find an angular frequency that leads to a wave number $k \neq 0$ and to non-identically zero functions $p_i : \Omega_i \setminus \overline{\Omega_d} \to \mathbb{C}$, $p_i \in H^1(\Omega_i \setminus \overline{\Omega_d})$, $p_e^- : \Omega_e^- \to \mathbb{C}$, $p_e^- \in H^1_{loc}(\Omega_e^-)$ and $p_e^+ : \Omega_e^+ \to \mathbb{C}$, $p_e^+ \in H^1_{loc}(\Omega_e^+)$ such that:

$$\begin{cases} \Delta p_i + k^2 p_i &= 0 \quad \text{in} \quad \Omega_i \setminus \overline{\Omega_d}, \\ \dfrac{\partial p_i}{\partial n} - \alpha\, p_i &= 0 \quad \text{on} \quad \Gamma_i, \\ \dfrac{\partial p_i}{\partial n} &= 0 \quad \text{on} \quad \Gamma_d, \\ \dfrac{\partial p_i}{\partial n} &= \dfrac{\partial p_e^-}{\partial n} \quad \text{on} \quad \Gamma_H^-, \\ \dfrac{\partial p_i}{\partial n} &= \dfrac{\partial p_e^+}{\partial n} \quad \text{on} \quad \Gamma_H^+, \end{cases} \tag{2.29}$$

$$\begin{cases} \Delta p_e^- + k^2 p_e^- &= 0 \quad \text{in} \quad \Omega_e^-, \\ \dfrac{\partial p_e^-}{\partial n} - \alpha\, p_e^- &= 0 \quad \text{on} \quad \Gamma_e^-, \\ p_e^- &= p_i \quad \text{on} \quad \Gamma_H^-, \\ + \text{ radiation condition at } |\boldsymbol{x}| \to \infty, \text{ if } \mathfrak{Im}\,\alpha_e = \mathfrak{Im}\,k_e = 0. \end{cases} \tag{2.30}$$

and

$$\begin{cases} \Delta p_e^+ + k^2 p_e^+ &= 0 \quad \text{in} \quad \Omega_e^+, \\ \dfrac{\partial p_e^+}{\partial n} - \alpha\, p_e^+ &= 0 \quad \text{on} \quad \Gamma_e^+, \\ \qquad p_e^+ &= p_i \quad \text{on} \quad \Gamma_H^+, \\ + \text{ radiation condition at } |\boldsymbol{x}| \to \infty, \text{ if } \mathfrak{Im}\,\alpha_e = \mathfrak{Im}\,k_e = 0. \end{cases} \tag{2.31}$$

It is important to note that due to the regular shape of the exterior domains and due to the fact that both the impedance parameter and the wave number are assumed to be constant complex numbers in the exterior domains, the exterior problems (2.26-2.27) and (2.30-2.31) can be solved analytically if we assume that the solutions of the interior problems, (2.25) and (2.29), are known data.

Remark II.2. *Let us observe that at each resonance frequency, given by (2.28), the scattering problem (2.24) has not a unique solution. It is in virtue of the fact that we can freely add to the solution of (2.24), a eigenfunction multiplied by an arbitrary constant, obtaining as a result another distinct solution of (2.24).*

III. THE GREEN'S FUNCTION OF THE INFINITE IMPEDANCE CIRCULAR CYLINDRICAL WAVEGUIDE

A powerful mathematical tool to solve impedance boundary value problems for the Helmholtz operator, is the Green's function. It is often employed in wave scattering, resonance and inverse problems defined on bounded and unbounded domains, where it is used as a benchmark solution to test numerical schemes or it is applied in conjunction with numerical methods such as the boundary element method and the mixed boundary element and finite element method. For a broader framework about the Green's functions and their use for solving time-harmonic problems, see Nédélec (2001), Colton & Kress (1983) and Bonnet (1995).

In this chapter we are interested in finding the Green's function for the Helmholtz operator in a infinite circular cylindrical waveguide with impedance boundary condition. In the particular problem that we want to solve in this dissertation, this Green's function is employed to represent the solution of the exterior problems (2.26-2.27) and (2.30-2.31). These representations allow us, in Chapter IV, to obtain the so-called Dirichlet-to-Neumann map that makes possible to solve the problems (2.24) and (2.28) by means of the finite element method.

For a infinite cylindrical waveguide with a Dirichlet or Neumann boundary condition, the Green's function can be obtained by a series provided by the method of separation of variables (see for instance Stuwe & Werner (1996) and Duffy (2001) for examples of a Neumann and a Dirichlet boundary condition, respectively) usually referred to as the eigenfunction expansion. This representation is highly appreciated because it is easy to implement on a computer as it does not require that the Fourier transform be numerically inverted, as other Green's functions do in problems arising, for example, on impedance half-planes and half-spaces (Durán et al. 2006, 2007). Moreover, such representation is suitable to achieve directly the asymptotic behavior at infinity and the radiation condition that the Green's function satisfies, which differs from the classical Sommerfeld radiation condition.

The separation of variables method works well when the Laplace operator - acting on a subspace of $L^2(\Omega')$, where $\Omega' = \{\boldsymbol{x} \in \mathbb{R}^2 : |\boldsymbol{x}| < R\}$ is the waveguide's cross section - is compact and self-adjoint, and consequently its eigenfunctions form a complete orthonormal basis of $L^2(\Omega')$, which is the case when the boundary condition is Dirichlet or Neumann. However, when the impedance boundary condition is imposed, the Laplacian is no longer self-adjoint for all the possible values of the impedance parameter (it is self-adjoint only for negative real values of the impedance parameter). In spite of that, a real impedance parameter leads to eigenfunctions that are still orthogonal and the theory of Dini series (cf. Watson 1966, Chapter 18) may be used to apply the separation of variables method to our problem. If instead, the impedance parameter is a proper complex number, i.e. it has a non-zero imaginary part, the eigenfunctions are no longer orthogonal and then it is necessary to develop another way to construct the Green's function that does not depend on the orthogonality and completeness of the eigenfunctions.

In this chapter we perform a detailed deduction of the eigenfunction expansion of the Green's function for the Helmholtz operator in an infinite impedance circular cylindrical waveguide. This deduction is carried out via a Fourier transform and the theory of Green's functions for non-self-adjoint singular Sturm-Liouville problems. The eigenfunction expansion makes it necessary to study the eigenvalues of the Laplacian generated by the roots of the Dini function $zJ_n'(zR) - \alpha J_n(zR)$, where α is the impedance parameter and $J_n(z)$ is the Bessel function of the first kind with integer order $n \geqslant 0$. Properties of these roots for $\alpha \in \mathbb{R}$, available in Spigler (1975), Ahmed & Calogero (1978) and Landau (1999), are used here. Furthermore, new results for the properties of these roots are performed for complex values of α by means of a Mittag-Leffler expansion. One particularly important result has to do with the existence of non-simple eigenvalues for specific values of α. The limiting absorption principle is employed to analyze the complete undamped case (i.e. real wave number and real impedance parameter) where the existence of propagative modes (which include surface propagative modes) allows obtaining the far-field and the radiation condition that the Green's function satisfies.

The outline of this chapter is as follows. The next section describes both the problem's set up and the Fourier transform used to compute the Green's function. Next, Section 3.2 summarizes the properties of the Bessel functions used throughout this chapter. Subsequently, in Section 3.3, the spectral Green's function - the solution of the problem in the Fourier domain - is found. In Section 3.4, the singularities of spectral Green's function are studied in detail so as to obtain, in Section 3.5, its series expansion by means of contour integration. Thereafter, Section 3.6 addresses the inversion of the Fourier transform, using again contour integration and the limiting absorption principle.

3.1 The Green's function of the infinite right circular cylinder

The sought Green's function is given by the solution of the following problem in the sense of distributions: Find $G(\boldsymbol{x},\cdot) \in \mathcal{D}'(\Omega_\infty)$ such that:

$$\begin{cases} \Delta_{\boldsymbol{y}} G(\boldsymbol{x},\boldsymbol{y}) + k^2 G(\boldsymbol{x},\boldsymbol{y}) &= -\delta_{\boldsymbol{x}}(\boldsymbol{y}), \quad \boldsymbol{y} \in \Omega_\infty, \\ \dfrac{\partial G(\boldsymbol{x},\boldsymbol{y})}{\partial n_{\boldsymbol{y}}} - \alpha\, G(\boldsymbol{x},\boldsymbol{y}) &= 0, \qquad \boldsymbol{y} \in \Gamma_\infty, \end{cases} \tag{3.1}$$

where

$$\Omega_\infty = \left\{ \boldsymbol{x} = (x_1, x_2, x_3) \in \mathbb{R}^3 : x_1^2 + x_2^2 < R^2, x_3 \in \mathbb{R} \right\} = \Omega' \times \mathbb{R}, \tag{3.2a}$$

$$\Gamma_\infty = \left\{ \boldsymbol{x} = (x_1, x_2, x_3) \in \mathbb{R}^2 : x_1^2 + x_2^2 = R^2, x_3 \in \mathbb{R} \right\} = \partial\Omega' \times \mathbb{R}, \tag{3.2b}$$

and $\delta_{\boldsymbol{x}} \in \mathcal{D}'(\Omega_\infty)$ is Dirac's delta distribution supported at a fixed point $\boldsymbol{x} \in \Omega_\infty$ where $\mathcal{D}'(\Omega_\infty)$ denotes the dual space of $\mathcal{D}(\Omega_\infty)$, i.e. the dual of the space of functions infinitely differentiable and compactly supported in Ω_∞.

Due to the physical considerations pointed out in Chapter II, the wave number and the impedance parameter are respectively $k \in \mathbb{C},\ \mathfrak{Im}\, k \geqslant 0$[1] and $\alpha \in \mathbb{C},\ \mathfrak{Im}\, \alpha \geqslant 0$, because the time dependence of the wave is assumed given by $\mathrm{e}^{-\mathrm{i}\,\omega t}$, where ω is the angular

[1]The condition $\mathfrak{Im}\, k \geqslant 0$ and $\mathfrak{Im}\, k^2 \geqslant 0$ are the same, since $\mathfrak{Re}\, k \geqslant 0$ always holds.

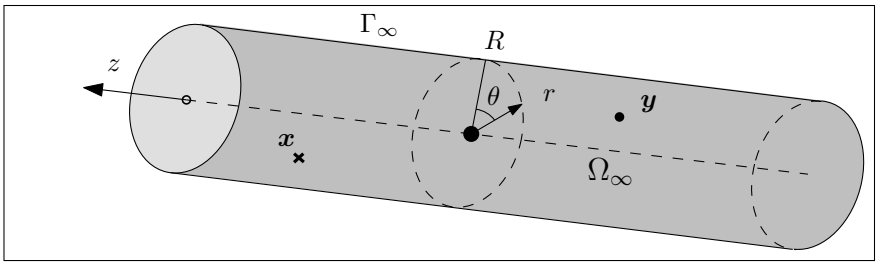

FIGURE 3.1. Domain of the Green's function problem.

frequency. Let us remark that throughout this chapter we assume that k and α do not depend on the spatial variables.

Once again we have to point out that in absence of dissipation, i.e. when α and k are real numbers, it is necessary to add a radiation condition to (3.1) in order to obtain a unique outgoing wave solution. Such radiation condition differs greatly from the classical Sommerfeld radiation condition and is stated later on, so that, for the time being we assume that k or α are not real numbers.

To achieve a solution of (3.1) we use integral transformation methods like the ones described in Duffy (2001). Hence, first we express (3.1) in cylindrical coordinates (see Figure 3.1) to obtain

$$\begin{cases} \dfrac{1}{r}\dfrac{\partial}{\partial r}\left(r\dfrac{\partial G}{\partial r}\right)+\dfrac{1}{r^2}\dfrac{\partial^2 G}{\partial \theta^2}+\dfrac{\partial^2 G}{\partial z^2}+k^2 G=-\dfrac{\delta_\rho(r)\,\delta_\zeta(z)\,\delta_\vartheta(\theta)}{r}, & \boldsymbol{y}\in\Omega_\infty, \\ \dfrac{\partial G}{\partial r}-\alpha\, G = 0, & \boldsymbol{y}\in\Gamma_\infty, \end{cases} \tag{3.3}$$

where $\rho\in(0,R)$, $\boldsymbol{y}=(r\cos\theta, r\sin\theta, z)$ is the *observation point* and $\boldsymbol{x}=(\rho\cos\vartheta,\rho\sin\vartheta,\zeta)$ is the *source point*.

In order to solve (3.3) we resort to the use of the Fourier transform, which is defined as follows: Let $u\in\mathcal{D}((-\pi,\pi)\times\mathbb{R})$, then its Fourier transform $\widehat{u}:\mathbb{N}_0\times\mathbb{R}\to\mathbb{C}$ is defined by

$$\widehat{u}(n,\xi)=\int_{[-\pi,\pi]\times\mathbb{R}} u(\theta,z)\cos(n\theta)\,\mathrm{e}^{-\mathrm{i}\,z\xi}\,\mathrm{d}\xi\,\mathrm{d}\theta$$

and its inverse is defined as

$$u(\theta, z) = \frac{1}{4\pi^2} \int_{\mathbb{N}_0 \times \mathbb{R}} \widehat{u}(n, \xi) \cos(n\theta)\, \mathrm{e}^{\mathrm{i}\, z\xi}\, \epsilon_n \mathrm{d}\xi\, \mathrm{d}n$$

where $\mathbb{N}_0 = \mathbb{N} \cup \{0\}$ and

$$\epsilon_n = \begin{cases} 1 & \text{for} \quad n = 0 \\ 2 & \text{for} \quad n \geqslant 1. \end{cases}$$

Assuming that for every fixed $\boldsymbol{x} \in \Omega_\infty$ and $r \in [0, R]$, $G \in \mathcal{D}'((-\pi, \pi) \times \mathbb{R})$, we can formally apply the Fourier transform to (3.3) to obtain the following integral representation (which, for the time being, is interpreted in the sense of distributions)

$$G(\boldsymbol{x}, \boldsymbol{y}) = \frac{1}{4\pi^2} \int_{\mathbb{N}_0 \times \mathbb{R}} g_n(r, \rho; k^2 - \xi^2) \cos(n(\theta - \vartheta))\, \mathrm{e}^{\mathrm{i}\, \xi(z-\zeta)} \epsilon_n\, \mathrm{d}\xi\, \mathrm{d}n \tag{3.4}$$

where the kernel g_n is referred to as the *spectral Green's function* and corresponds to the Green's function of the Bessel differential equation with an impedance boundary condition, i.e.

$$\begin{cases} -\dfrac{\mathrm{d}}{\mathrm{d}r}\left(r \dfrac{\mathrm{d}g_n}{\mathrm{d}r}\right) + \dfrac{n^2}{r} g_n - \lambda r\, g_n &= \delta_\rho, \quad 0 < r < R \\ \dfrac{\mathrm{d}g_n}{\mathrm{d}r} - \alpha g_n &= 0 \qquad r = R \\ \lim\limits_{r \to 0^+} |g_n(r, \rho; \lambda)| &< \infty, \end{cases} \tag{3.5}$$

where $\lambda = k^2 - \xi^2$, $\rho \in (0, R)$ and $n \in \mathbb{N}_0$.

3.2 Properties of the Bessel functions

This section summarizes some properties of the Bessel functions of first kind $J_n(z)$ and second kind $Y_n(z)$ with order $n \in \mathbb{N}_0$, that will be largely employed throughout this chapter.

- The Bessel functions $J_n(z)$ and $Y_n(z)$ are analytic in the whole complex plane except $Y_n(z)$ which has a branch cut along the negative real axis (cf. Abramovitz & Stegun 1972, p. 358).

- Their asymptotic form for small arguments, i.e. their behavior as $|z| \to 0$ (cf. Abramovitz & Stegun 1972, p. 360, eq. 9.1.7, 9.1.8 and 9.1.9) is given by:

$$J_n(z) \sim \frac{1}{n!}\left(\frac{z}{2}\right)^n \tag{3.6}$$

$$Y_n(z) \sim \begin{cases} \frac{2}{\pi}\,\mathrm{Ln}\left(\frac{z}{2}\right) & \text{if} \quad n = 0, \\ -\frac{(n-1)!}{\pi}\left(\frac{2}{z}\right)^n & \text{if} \quad n > 0. \end{cases} \tag{3.7}$$

- Their asymptotic form for large argument, i.e. their behavior as $|z| \to \infty$ (cf. Abramovitz & Stegun 1972, p. 364, eq. 9.2.1 and 9.2.2)) is given by:

$$J_n(z) \sim \sqrt{\frac{2}{\pi z}}\cos\left(z - \frac{n\pi}{2} - \frac{\pi}{4}\right), \tag{3.8}$$

$$Y_n(z) \sim \sqrt{\frac{2}{\pi z}}\sin\left(z - \frac{n\pi}{2} - \frac{\pi}{4}\right), \ |\arg z| < \pi. \tag{3.9}$$

- Some recurrence relations (cf. Abramovitz & Stegun 1972, p. 361, eq. 9.1.27) are

$$J_n'(z) = -J_{n+1}(z) + \frac{n}{z}J_n(z), \tag{3.10}$$

$$Y_n'(z) = -Y_{n+1}(z) + \frac{n}{z}Y_n(z), \tag{3.11}$$

  where $J_n'(z)$ and $Y_n'(z)$ denote the derivatives of the Bessel functions $J_n(z)$ and $Y_n(z)$, respectively.

- The wronskian (cf. Abramovitz & Stegun 1972, p. 360, eq. 9.1.16) is

$$W\left[J_n, Y_n\right](z) = J_n(z)Y_n'(z) - J_n'(z)Y_n(z) = \frac{2}{\pi z}. \tag{3.12}$$

- Some analytic continuation formulas (cf. Abramovitz & Stegun 1972, p. 361, eq. 9.1.35 and 9.1.36) are

$$J_n(-z) = (-1)^n J_n(z), \tag{3.13}$$

$$Y_n(-z) = (-1)^n \left\{Y_n(z) + 2\,\mathrm{i}\,J_n(z)\right\}. \tag{3.14}$$

3.3 The spectral Green's function

To solve (3.5) we resort to the theory of Green's functions of one variable. Let us note that for the particular case $\alpha \in \mathbb{R}$, (3.5) defines the Green's function of a singular self-adjoint Sturm-Liouville problem. It has a well-known solution for the cases $\alpha = 0$ and $\alpha = \infty$, provided by the Fourier-Bessel expansion. Some references that deal with this topic are Duffy (2001), Folland (1994) and Stakgold (2000). Herein we generalize those results for an almost arbitrary impedance parameter $\alpha \in \mathbb{C}$ (see Section 2.3).

To construct g_n, we divide the interval $(0, R)$ into two disjoint subintervals $(0, \rho)$ and (ρ, R). Since the Dirac's delta distribution is supported only at $r = \rho$, a candidate to be a solution of (3.5) must satisfy the homogeneous equation (3.5) in $(0, \rho)$ and in (ρ, R). Moreover, it has to fulfill the respective boundary condition imposed on $r = 0$ and on $r = R$. Therefore, if $r \in (0, \rho)$ the solution of (3.5) is

$$\varphi_1(r; \lambda) = J_n\big(\sqrt{\lambda} r\big) \tag{3.15}$$

whereas if $r \in (\rho, R)$ the solution is given by

$$\begin{aligned} \varphi_2(r; \lambda) \;\; = \;\; & \Big[\sqrt{\lambda} J_n'(\sqrt{\lambda} R) - \alpha J_n(\sqrt{\lambda} R)\Big] Y_n(\sqrt{\lambda} r) \\ & - \Big[\sqrt{\lambda} Y_n'(\sqrt{\lambda} R) - \alpha Y_n(\sqrt{\lambda} R)\Big] J_n(\sqrt{\lambda} r). \end{aligned} \tag{3.16}$$

According to the procedure followed above, the solution of (3.5) ought to have the form

$$g_n(r, \rho; \lambda) = \begin{cases} c_1 \varphi_1(r, \lambda) & \text{if} \quad r \in (0, \rho)\,, \\ c_2 \varphi_2(r, \lambda) & \text{if} \quad r \in (\rho, R)\,, \end{cases} \tag{3.17}$$

where the coefficients c_1 and c_2 can be computed imposing the continuity requirements of g_n and the jump condition of the derivative at the source point (Duffy 2001, Chapter 2):

$$\begin{cases} \displaystyle\lim_{r \to \rho^+} \frac{\mathrm{d} g_n(r, \rho; \lambda)}{\mathrm{d} r} - \lim_{r \to \rho^-} \frac{\mathrm{d} g_n(r, \rho; \lambda)}{\mathrm{d} r} \;\; = \;\; -\frac{1}{\rho}, \\ \\ \displaystyle\lim_{r \to \rho^+} g_n(r, \rho; \lambda) - \lim_{r \to \rho^-} g_n(r, \rho; \lambda) \;\; = \;\; 0. \end{cases} \tag{3.18}$$

The continuity of g_n at $r = \rho$ compels g_n to have the form

$$g_n(r, \rho; \lambda) = C\varphi_1(r_<; \lambda)\varphi_2(r_>; \lambda), \tag{3.19}$$

where $r_< = \min\{r, \rho\}$, $r_> = \max\{r, \rho\}$ and the constant C can be computed imposing the condition (3.18). That condition leads to

$$g_n(r, \rho; \lambda) = -\frac{\varphi_1(r_<; \lambda)\varphi_2(r_>; \lambda)}{\rho W\left[\varphi_1, \varphi_2\right](\rho)}, \tag{3.20}$$

where W is the wronskian function defined by

$$\begin{aligned} W[\varphi_1, \varphi_2](r) &= \varphi_1(r; \lambda)\frac{\mathrm{d}\varphi_2(r; \lambda)}{\mathrm{d}r} - \varphi_2(r; \lambda)\frac{\mathrm{d}\varphi_2(r; \lambda)}{\mathrm{d}r} \\ &= \sqrt{\lambda}\left[\sqrt{\lambda}J_n'(\sqrt{\lambda}R) - \alpha J_n(\sqrt{\lambda}R)\right] W\left[J_n, Y_n\right](\sqrt{\lambda}r). \end{aligned} \tag{3.21}$$

Hence, employing (3.12) we obtain that the spectral Green's function is given by

$$\begin{aligned} g_n(r, \rho; \lambda) &= \frac{\pi}{2}\frac{\sqrt{\lambda}Y_n'(\sqrt{\lambda}R) - \alpha Y_n(\sqrt{\lambda}R)}{\sqrt{\lambda}J_n'(\sqrt{\lambda}R) - \alpha J_n(\sqrt{\lambda}R)}J_n(\sqrt{\lambda}r)J_n(\sqrt{\lambda}\rho) \\ &\quad -\frac{\pi}{2}\begin{cases} Y_n(\sqrt{\lambda}\rho)J_n(\sqrt{\lambda}r) & \text{if} \quad 0 < r \leqslant \rho < R, \\ Y_n(\sqrt{\lambda}r)J_n(\sqrt{\lambda}\rho) & \text{if} \quad 0 < \rho \leqslant r < R. \end{cases} \end{aligned} \tag{3.22}$$

Before continuing there is a need to clarify how the square root in the complex plane will be understood. We define it as the complex map

$$z \mapsto \sqrt{z}, \ -\pi < \arg z \leqslant \pi \tag{3.23}$$

with range $-\pi/2 < \arg\sqrt{z} \leqslant \pi/2$. Let us observe that under our definition of the square root (3.23), it does not contain the branch cut of $Y_n(z)$ and $Y_n'(z)$. Consequently $\varphi_2(r; \cdot)$ is analytic in $\{z \in \mathbb{C} : -\pi < \arg z \leqslant \pi\}$.

3.4 The singularities of the spectral Green's function

Now we study the singularities of g_n as a function of λ. There are two sets of candidate singularities of the spectral Green's function. The first one corresponds to the origin in the

λ-complex-plane due to the behavior of the Bessel functions of the second kind (3.7); and the second one corresponds to the solutions of $\sqrt{\lambda}J_n'(\sqrt{\lambda}R) - \alpha J_n(\sqrt{\lambda}R) = 0$. With respect to the origin we can obtain the following result:

Proposition III.1. *If $\alpha \neq n/R$ the point $\lambda = 0$ is a removable singularity of $g_n(r, \rho; \cdot)$ while if $\alpha = n/R$ the point $\lambda = 0$ is a simple pole and the residue is given by*

$$\operatorname*{Res}_{\lambda=0} g_n(r, \rho; \lambda) = -\frac{2(n+1)}{R^2}\left(\frac{r}{R}\right)^n\left(\frac{\rho}{R}\right)^n$$

for all $n \in \mathbb{N}_0$, $\rho \in (0, R)$, and $r \in [0, R]$.

PROOF. Assume $\alpha \neq n/R$. Hence, by replacing the derivatives of the Bessel functions by (3.10) and (3.11) and the Bessel functions by their asymptotic form for small arguments, (3.6) and (3.7), we can compute the limit directly to get

$$\begin{aligned}\lim_{\lambda\to 0} g_n(r, \rho; \lambda) &= \frac{1}{2n}\left(\frac{\rho}{R}\right)^n\left(\frac{r}{R}\right)^n\left(\frac{n+R\alpha}{n-R\alpha}\right) \\ &\quad + \frac{1}{2n}\begin{cases} \left(\frac{r}{\rho}\right)^n & \text{if} \quad 0 < r \leqslant \rho < R, \\ \left(\frac{\rho}{r}\right)^n & \text{if} \quad 0 < \rho \leqslant r < R, \end{cases}\end{aligned} \tag{3.24}$$

when $n > 0$ and

$$\lim_{\lambda\to 0} g_0(r, \rho; \lambda) = -\frac{1}{R\alpha} - \begin{cases} \ln\left(\frac{\rho}{R}\right) & \text{if} \quad 0 < r \leqslant \rho < R, \\ \ln\left(\frac{r}{R}\right) & \text{if} \quad 0 < \rho \leqslant r < R, \end{cases} \tag{3.25}$$

when $n = 0$. So, as $\rho > 0$, we conclude that the origin $\lambda = 0$ is a removable singularity of g_n for all $n \in \mathbb{N}_0$.

On the other hand, by employing (3.10) and (3.11) we obtain that

$$\begin{aligned}\sqrt{\lambda}Y_n'(\sqrt{\lambda}R) - \alpha Y_n(\sqrt{\lambda}R) &= \left(\frac{n}{R} - \alpha\right)Y_n(\sqrt{\lambda}R) - \sqrt{\lambda}Y_{n+1}(\sqrt{\lambda}R), \\ \sqrt{\lambda}J_n'(\sqrt{\lambda}R) - \alpha J_n(\sqrt{\lambda}R) &= \left(\frac{n}{R} - \alpha\right)J_n(\sqrt{\lambda}R) - \sqrt{\lambda}J_{n+1}(\sqrt{\lambda}R).\end{aligned}$$

Consequently, if $\alpha = n/R$ we have that

$$\begin{aligned} g_n(r,\rho;\lambda) &= \frac{\pi}{2}\frac{Y_{n+1}(\sqrt{\lambda}R)}{J_{n+1}(\sqrt{\lambda}R)}J_n(\sqrt{\lambda}r)J_n(\sqrt{\lambda}\rho) \\ &\quad -\frac{\pi}{2}\begin{cases} Y_n(\sqrt{\lambda}\rho)J_n(\sqrt{\lambda}r) & \text{if} \quad 0 < r \leqslant \rho < R, \\ Y_n(\sqrt{\lambda}r)J_n(\sqrt{\lambda}\rho) & \text{if} \quad 0 < \rho \leqslant r < R, \end{cases} \end{aligned} \tag{3.26}$$

and substituting the Bessel functions by their asymptotic forms, (3.6) and (3.7), in (3.26), we obtain that the residue of g_n at $\lambda = 0$ is

$$\lim_{\lambda\to 0}\lambda\, g_n(r,\rho;\lambda) = -\frac{2(n+1)}{R^2}\left(\frac{r}{R}\right)^n\left(\frac{\rho}{R}\right)^n$$

for all $n \in \mathbb{N}_0$. □

Continuing with the analysis of the singularities of g_n in the λ-complex-plane, we study the poles of the spectral Green's function given by the non-zero solutions of the equation $\sqrt{\lambda}J_n'(\sqrt{\lambda}R) - \alpha J_n(\sqrt{\lambda}R) = 0$, which with the aid of (3.10) can be expressed equivalently as

$$\begin{aligned} D_n(z,\alpha) &= zJ_n'(zR) - \alpha J_n(zR) \\ &= \left(\frac{n}{R} - \alpha\right)J_n(zR) - zJ_{n+1}(zR) \\ &= zJ_{n-1}(zR) - \left(\frac{n}{R} + \alpha\right)J_n(zR) \\ &= \left(\alpha - \frac{n}{R}\right)J_{n-1}(zR) + \left(\alpha + \frac{n}{R}\right)J_{n+1}(zR) = 0, \end{aligned} \tag{3.27}$$

where $\lambda = z^2$.

Let us observe that if z is a solution to (3.27) for some given $\alpha \in \mathbb{C}$, then $-z$ is a solution too by virtue of (3.13). Therefore, only the non-zero roots located in the complex half-plane $\mathfrak{Re}\, z \geqslant 0$ are analyzed. Furthermore, it is possible to note that as $D_n(\cdot,\alpha)$ is an analytic function, its zeros are isolated and form a countable set $\{z_{n,m} \in \mathbb{C},\ (n,m) \in \mathbb{N}_0 \times \mathbb{N}\}$. Moreover, for the particular cases $\alpha = \pm n/R$, it is possible to achieve explicitly the values of $z_{n,m}$ by replacing α in (3.27) obtaining that

$$z_{n,m} = j_{n\pm 1,m}/R,\ m \in \mathbb{N},$$

where $j_{n\pm1,m}$ is the m-th positive root of the Bessel function $J_{n\pm1}(z)$. It follows from here that in this particular case there are infinite simple real roots of (3.27).

TABLE 3.1. Summary of results concerning positive and imaginary roots of $zJ_n'(Rz) - \alpha J_n(Rz)$ for $\alpha \in \mathbb{R}$ and $n \in \mathbb{N}_0$.

$\alpha = n/R$	$z_{n,m} = j_{n+1,m}/R,\ m \in \mathbb{N}$
$\alpha = -n/R$	$z_{n,m} = j_{n-1,m}/R,\ m \in \mathbb{N}$
$\alpha > n/R$	$z_{n,1} = \mathrm{i}\, y_n\ (y_n > 0), 0 < z_{n,2} < z_{n,3} < \cdots$
$\alpha < n/R$	$0 < z_{n,1} < z_{n,2} < \cdots$

For an arbitrary $\alpha \in \mathbb{R}$, the equation (3.27) is well studied in the literature. The first important result about this equation was made by Dixon (1903) who proved that (3.27) has an infinite number of distinct non-zero simple real roots when $n > -1$. Resorting to Dixon's results, Spigler (1975) obtained an asymptotic and series expansion of the roots of (3.27). Therein he also proved the existence of two symmetric purely imaginary roots if and only if $\alpha > n/R > -1/R$. The generalization of these for arbitrary cylinder functions instead of $J_n(z)$, is available in Spigler (1978) . Properties of convexity and concavity of the zeros depending on $\alpha \in \mathbb{R}$ and $n > 0$ of these general functions, are presented in Elbert & Siafarikas (1992). Bounds for the small positive and imaginary zeros of (3.27) are developed in Ahmed & Calogero (1978), Ifantis & Siafarikas (1988) and Ifantis et al. (1988); and for the general cylinder functions in Ismail & Muldoon (1995). Recent results on the monoticity and multiplicity of the positive roots of (3.27) for $n, \alpha \in \mathbb{R}$ are presented in Landau (1999). Table 3.1 outlines the known results for $z_{n,m}$ for $\alpha \in \mathbb{R}$. It also establishes the notation assigned to the roots of $D_n(\cdot, \alpha)$ employed throughout the rest of this chapter.

The following proposition states some results on the roots of $D_n(\cdot, \alpha)$ for $\alpha \in \mathbb{C}$ that will be used at a later stage in this chapter.

Proposition III.2. *(a) The roots of $D_n(\cdot,\alpha)$ form a countable infinite set and their asymptotic behavior as $m \to \infty$ is given by*

$$z \sim j_{n+1,m} \sim \frac{\pi}{R}\left(\frac{4m+2n+1}{4}\right). \tag{3.28}$$

(b) Every non-zero root $z_{n,m}$ is simple if either; $\alpha \in \mathbb{R}$ or $\alpha \in \mathbb{C}$ with α fulfilling the condition $\alpha \neq \pm\sqrt{n^2/R^2 - z_{n,m}^2}$. Nevertheless, if $z_{n,m}$ is not simple, it has at most multiplicity two.

(c) If $\mathfrak{Im}\,\alpha \neq 0$, the function $D_n(\cdot,\alpha)$ has no imaginary and real roots.

(d) If $\mathfrak{Im}\,\alpha > 0$, the inequality $\mathfrak{Im}\, z_{n,m}^2 < 0$ holds for every $(n,m) \in \mathbb{N}_0 \times \mathbb{N}$.

PROOF. (a) From (3.8) and (3.27) we may infer straightforwardly that for a large $|z|$, it holds that

$$D_n(z,\alpha) \sim zJ_{n+1}(zR) \sim \sqrt{\frac{2z}{\pi}}\sin\left(z - \frac{n\pi}{2} - \frac{\pi}{4}\right),\ |z| \gg \left|\frac{n}{R} - \alpha\right|.$$

Hence, we obtain that the zeros of $D_n(\cdot,\alpha)$ have the asymptotic behavior given by (3.28). From here we may conclude directly that (3.27) has infinite number of zeros which have an imaginary part that converges to zero.

(b) In order to prove that the zeros are simple, we compute the value of $D_n'(\cdot,\alpha)$ at a non-zero root $z_{n,m}$. If the pole is simple, $D_n'(z,\alpha)\big|_{z=z_{n,m}} \neq 0$ where D_n' denotes the derivative of D_n with respect to its first variable. Employing the formula for the derivatives of the Bessel functions (3.10) and the equation (3.27) itself, we find that

$$D_n'(z,\alpha)\big|_{z=z_{n,m}} = -\frac{J_n(z_{n,m}R)}{z_{n,m}R}\left(R^2 z_{n,m}^2 - n^2 + R^2\alpha^2\right). \tag{3.29}$$

Therefore, if $\mathfrak{Im}\,\alpha \neq 0$, by the assumption $\alpha \neq \pm\sqrt{n^2/R^2 - z_{n,m}^2}$ we obtain that $D_n'(z,\alpha)\big|_{z=z_{n,m}} \neq 0$ by virtue of the fact that $z_{n,m}R \neq j_{n,m}$, where $j_{n,m}$ is the j-th positive zero of $J_n(z)$ (it follows directly replacing $z_{n,m}R$ by $j_{n,m}$ in (3.27) and by taking into account that $J_n'(z)$ and $J_n(z)$ have interlaced roots).

On the other hand, we can note from (Dixon 1903, eq. 2) or (Spigler 1975, eq. II.3), that

$$\int_0^R r J_n^2(zr)\,\mathrm{d}r = \frac{1}{2}R^2 J_n'^2(zR)\frac{\mathrm{d}}{\mathrm{d}R}\left[\frac{J_n(zR)}{zRJ_n'(zR)}\right]. \tag{3.30}$$

Thus, if $\alpha \in \mathbb{R}$, we employ (3.10) and (3.27) in the right side of (3.30) to obtain that

$$\int_0^R r J_n^2(z_{n,m}r)\,\mathrm{d}r \;=\; \frac{J_n^2(z_{n,m}R)}{2}\left(\frac{R^2 z_{n,m}^2 - n^2 + R^2\alpha^2}{z_{n,m}^2}\right). \tag{3.31}$$

Then, if $z_{n,m} \in \mathbb{R}$ we have

$$\int_0^R r J_n^2(z_{n,m}r)\,\mathrm{d}r > 0,$$

while if $z_{n,m} = \mathrm{i}\, y_1$ we have $J_n(\mathrm{i}\, y_1 r) = \mathrm{i}^{\,n} I_n(y_1 r)$, where $I_n(z)$ is the modified Bessel function of the first kind. Consequently

$$(-1)^n \int_0^R r I_n^2(y_1 r)\,\mathrm{d}r = \int_0^R r J_n^2(z_{n,m}r)\,\mathrm{d}r \neq 0,$$

$$D_n'(z,\alpha)\,\big|_{z=z_{n,m}} = -\frac{2z_{n,m}}{RJ_n(z_{n,m}R)}\int_0^R r J_n^2(z_{n,m}r)\,\mathrm{d}r \neq 0$$

and consequently, $z_{n,m}$ is simple.

Finally, following Landau (1999) we define the function

$$F_n(z) = \frac{zJ_n'(zR)}{J_n(zR)},$$

which allows us to express (3.27) as $F_n(z) = \alpha$. Differentiating F_n two times we get that it satisfies the differential equation

$$F_n''(z) = -2R - \frac{R + 2F_n(z)}{z}F_n'(z).$$

Therefore, if $z_{n,m}$ is a repeated root of $D_n(\cdot,\alpha)$, it satisfies

$$F_n'(z)\,\big|_{z=z_{n,m}} = 0,$$

and $F_n''(z)\,\big|_{z=z_{n,m}} = -2R \neq 0$. This proves that the multiplicity of any root is less or equal to 2.

(c) The Bessel functions can be represented by the following infinite product (cf. Abramovitz & Stegun 1972):

$$J_n(z) = \frac{(z/2)^n}{n!} \prod_{m=1}^{\infty} \left(1 - \frac{z^2}{j_{n,m}^2}\right),$$

where $j_{n,m} \in \mathbb{R}$ are the zeros of $J_n(z)$. It leads to

$$\frac{J_n'(zR)}{J_n(zR)} - \frac{\alpha}{z} = \frac{1}{z}\left(\frac{n}{R} - \alpha\right) + \sum_{m=1}^{\infty} \frac{2zR}{(zR)^2 - j_{n,m}^2} = 0,$$

which is equivalent to the equation (3.27), so that $z_{n,m}$ are the solutions of

$$\sum_{m=1}^{\infty} \frac{2(zR)^2}{(zR)^2 - j_{n,m}^2} = \alpha R - n, \tag{3.32}$$

for which the left side is the well-known Mittag-Leffler expansion of $zRJ_n'(zR)/J_n(zR)$, valid for every $z \neq j_{n,m}/R$ (cf. Ifantis et al. 1988, Ismail & Muldoon 1995, Ifantis & Siafarikas 1986). Now, suppose that there is a purely imaginary zero given by $z_{n,m} = \mathrm{i}\, y,\ y \in \mathbb{R}$. Replacing it in (3.32) we get

$$\sum_{m=1}^{\infty} \frac{2(yR)^2}{(yR)^2 + j_{n,m}^2} = \alpha R - n. \tag{3.33}$$

Then, since $\mathfrak{Im}\,\alpha \neq 0$ we have that this equation has no solution $y \in \mathbb{R}$ because the left side of (3.33) is real while the right side has a non zero imaginary part. It is a contradiction and then $D_n(\cdot, \alpha)$ has no imaginary zeros. The proof that real roots do not exist is completely analogous.

(d) Suppose $\mathfrak{Im}\,\alpha > 0$ and that there is a root z of $D_n(\cdot, \alpha)$ such that $z^2 = (x + \mathrm{i}\, y)/R^2$ with $y \geqslant 0$. Thus, replacing it in (3.32) we obtain

$$\sum_{m=1}^{\infty} \frac{2(x + \mathrm{i}\, y)(x - j_{n,m}^2 - \mathrm{i}\, y)}{(x - j_{n,m}^2)^2 + y^2} = \alpha R - n. \tag{3.34}$$

Performing the product in the nominator of each term of the series and taking the imaginary part of the equation, we obtain

$$\sum_{m=1}^{\infty} \frac{-2y j_{n,m}^2}{(x^2 - j_{n,m}^2)^2 + y^2} = R\,\mathfrak{Im}\,\alpha. \tag{3.35}$$

Therefore, since $j_{n,m}^2 > 0$ and $y \geqslant 0$, we obtain a contradiction and consequently $\mathfrak{Im}\, z^2 < 0$.

□

3.4.1 The non-simple roots of $zJ_n'(zR) - \alpha J_n(zR)$

The condition $\alpha \neq \pm\sqrt{n^2/R^2 - z_{n,m}^2}$ for $\alpha \in \mathbb{C}$, is necessary in order for $z_{n,m}$ to be a simple zero. Moreover, all the values of $\alpha \in \mathbb{C}$ for which it is possible to obtain a non-simple zero, form a countable infinite set. Such particular values of α, denoted by $\alpha_{n,l}$, where the subindex l arranges them in ascending order according to their absolute value, can be found searching the roots of the equation

$$D_n\left(\sqrt{\frac{n^2}{R^2} - \alpha^2}, \alpha\right) = 0 \tag{3.36}$$

in the α-complex-plane. Figure 3.2 shows the location of the values of α leading to a non-simple root of $D_n(\cdot, \alpha)$ for $R = 1$ and $n = 3$. The non-simple zero due to $\alpha = \pm 3$ corresponds to the root $z = 0$, therefore it does not contradict Proposition III.2 (b) in which the case $z \neq 0$ is analyzed

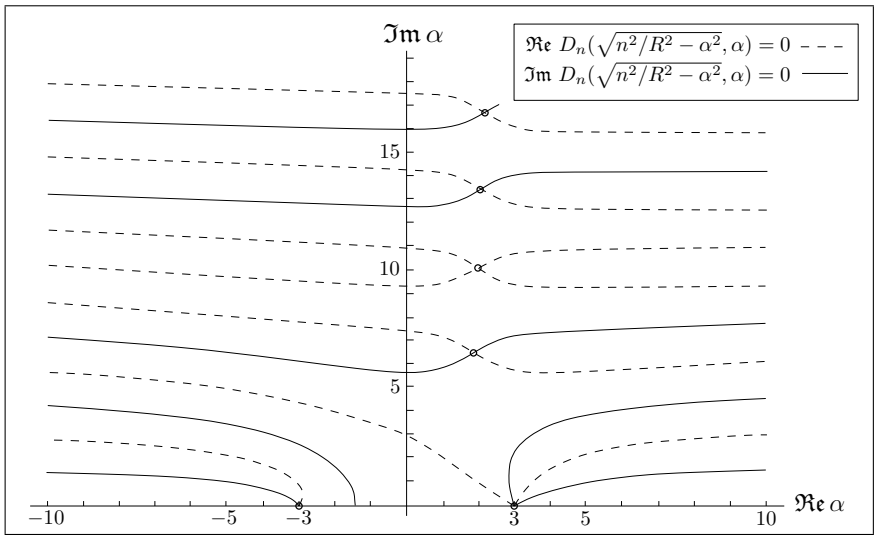

FIGURE 3.2. Location of the impedance parameters that lead to non-simple roots of the Dini function.

In Subsection 5.1.3 we develop a numerical algorithm to compute the values of these particular impedance parameters.

3.5 A series representation of the spectral Green's function

As it can be observed in (3.22), $g_n(r,\rho;\cdot)$ has a branch cut along the negative real line due to the complex square root. However, in the following proposition we show that $g_n(r,\rho;\cdot)$ is a meromorphic function in the whole λ-complex-plane, i.e. it is analytic everywhere except at its poles $\lambda_{n,m},\ (n,m)\in\mathbb{N}_0\times\mathbb{N}$ given by

$$\lambda_{n,m}=\begin{cases} z_{n,m}^2 & \text{if} \quad n\neq R\alpha,\ m\in\mathbb{N} \\ z_{n,m-1}^2 & \text{if} \quad n=R\alpha,\ m>1 \\ 0 & \text{if} \quad n=R\alpha,\ m=1, \end{cases} \tag{3.37}$$

where $z_{n,m},\ m\in\mathbb{N}$ are the non-zero roots of $D_n(\cdot,\alpha)$, which are sorted in increasing order according to their absolute value.

Proposition III.3. *The spectral Green's function (3.22) is meromorphic in the whole λ-complex-plane for every $\alpha\in\mathbb{C}$, $\rho\in(0,R)$, and $r\in[0,R]$.*

PROOF. Firstly, let us observe that $g_n(r,\rho;\cdot)$ is actually meromorphic in the whole complex plane except at the negative real axis. Consequently, to prove this proposition we only have to show that $g_n(r,\rho;\cdot)$ is also meromorphic in a region that contains the negative real axis. Without losing generality, let us assume that $\lambda\neq -y_n^2$ (where $\pm y_n\mathrm{i}$ are the imaginary roots of $D_n(\cdot,\alpha)$ arising when $\alpha>n/R$), and then the limits

$$\lim_{\varepsilon\to 0^+} g_n(r,\rho;|\lambda|e^{\mathrm{i}\,(\pi-\varepsilon)}) \text{ and } \lim_{\varepsilon\to 0^+} g_n(r,\rho;|\lambda|e^{-\mathrm{i}\,(\pi-\varepsilon)}) \tag{3.38}$$

exist by virtue of the fact that $g_n(r,\rho;\cdot)$ has no other poles on the negative real line (see Proposition III.2 (c)). Employing (3.20) we will compute the limits in (3.38) proving that they are equal. They will lead us to infer that the spectral Green's function is continuous in any region that contains the negative real line (except the poles). Immediately afterwards, a theorem of analytic continuation along curves will ensure that $g_n(r,\rho;\cdot)$ is meromorphic.

Let us claim that $\varphi_2(r;\cdot)$, defined in (3.16), is continuous in the whole complex plane as a function of λ, except at $\lambda = 0$ where it has a singularity due to the Bessel function of second kind. To show it we ought to compute

$$\varphi_2(r;\lambda)\Big|_{\lambda=|\lambda|\,\mathrm{e}^{\mathrm{i}\,\pi}}^{\lambda=|\lambda|\,\mathrm{e}^{-\mathrm{i}\,\pi}} = \lim_{\varepsilon\to 0^+}\varphi_2(r;|\lambda|e^{\mathrm{i}\,(\pi-\varepsilon)}) - \lim_{\varepsilon\to 0^+}\varphi_2(r;|\lambda|e^{-\mathrm{i}\,(\pi-\varepsilon)})$$

where

$$\begin{aligned}\varphi_2(r;\lambda)\Big|_{\lambda=|\lambda|\,\mathrm{e}^{\mathrm{i}\,\pi}}^{\lambda=|\lambda|\,\mathrm{e}^{-\mathrm{i}\,\pi}} &= \left(\beta J_n'(\beta R) - \alpha J_n(\beta R)\right) Y_n(\beta r)\Big|_{\beta=-\mathrm{i}\,|\lambda|^{1/2}}^{\beta=\mathrm{i}\,|\lambda|^{1/2}} \\ &- \left(\beta Y_n'(\beta R) - \alpha Y_n(\beta R)\right) J_n(\beta r)\Big|_{\beta=-\mathrm{i}\,|\lambda|^{1/2}}^{\beta=\mathrm{i}\,|\lambda|^{1/2}}.\end{aligned} \tag{3.39}$$

Then, replacing $Y_n'(z)$ and $J_n'(z)$ in (3.39) by the formulas for the derivatives, (3.10) and (3.11), and observing with the aid of the analytic continuation formulas, (3.13) and (3.14), that

$$\begin{aligned}\beta J_n(\beta r)Y_{n+1}(\beta R)\Big|_{\beta=-\mathrm{i}\,|\alpha|^{1/2}}^{\beta=\mathrm{i}\,|\alpha|^{1/2}} &= \beta J_n(\beta R)Y_{n+1}(\beta r)\Big|_{\beta=-\mathrm{i}\,|\alpha|^{1/2}}^{\beta=\mathrm{i}\,|\alpha|^{1/2}} \\ &= 2|\lambda|^{1/2}J_n(\mathrm{i}\,|\lambda|^{1/2}r)J_{n+1}(\mathrm{i}\,|\lambda|^{1/2}R)\end{aligned}$$

and

$$\begin{aligned}\beta J_{n+1}(\beta R)Y_n(\beta r)\Big|_{\beta=-\mathrm{i}\,|\lambda|^{1/2}}^{\beta=\mathrm{i}\,|\lambda|^{1/2}} &= \beta J_{n+1}(\beta r)Y_n(\beta R)\Big|_{\beta=-\mathrm{i}\,|\lambda|^{1/2}}^{\beta=\mathrm{i}\,|\lambda|^{1/2}} \\ &= 2|\lambda|^{1/2}J_{n+1}(\mathrm{i}\,|\lambda|^{1/2}R)J_n(\mathrm{i}\,|\lambda|^{1/2}r),\end{aligned}$$

we find that

$$\varphi_2(r;\lambda)\Big|_{\lambda=|\lambda|\,\mathrm{e}^{\mathrm{i}\,\pi}}^{\lambda=|\lambda|\,\mathrm{e}^{-\mathrm{i}\,\pi}} = 0,$$

and then $\varphi_2(r;\cdot)$ is continuous in the whole complex plane, except at $\lambda = 0$.

On the other hand, evaluating the remaining term of the Green's function in $\lambda = |\lambda|\,\mathrm{e}^{\mathrm{i}\,\pi}$ and $\lambda = |\lambda|\,\mathrm{e}^{-\mathrm{i}\,\pi}$, we obtain

$$\begin{aligned}\left.\frac{\varphi_1(r;\lambda)}{\rho W[\varphi_1(r;\lambda),\varphi_2(r;\lambda)](\rho)}\right|_{\lambda=|\lambda|\,\mathrm{e}^{\mathrm{i}\,\pi}} &= \left.\frac{J_n(\beta r)}{\beta J_n'(\beta R) - \alpha J_n(\beta R)}\right|_{\beta=\mathrm{i}\,|\lambda|^{1/2}} \\ &= \frac{J_n(\mathrm{i}\,|\lambda|^{1/2}r)}{\mathrm{i}\,|\lambda|J_n'\left(\mathrm{i}\,|\lambda|^{1/2}R\right) - \alpha J_n\left(\mathrm{i}\,|\lambda|^{1/2}R\right)}\end{aligned} \tag{3.40}$$

and

$$\begin{aligned}\left.\frac{\varphi_1(r;\lambda)}{\rho W[\varphi_1(r;\lambda),\varphi_2(r;\lambda)](\rho)}\right|_{\lambda=|\lambda|\,\mathrm{e}^{-\mathrm{i}\,\pi}} &= \left.\frac{J_n(\beta r)}{\beta J_n'(\beta R)-\alpha J_n(\beta R)}\right|_{\beta=-\mathrm{i}\,|\lambda|^{1/2}} \\ &= \frac{(-1)^n J_n(\mathrm{i}\,|\lambda|^{1/2} r)}{(-1)^n\left[\mathrm{i}\,|\lambda| J_n'\left(\mathrm{i}\,|\lambda|^{1/2}R\right)-\alpha J_n\left(\mathrm{i}\,|\lambda|^{1/2}R\right)\right]} \quad .\end{aligned} \tag{3.41}$$

Therefore, since (3.40) and (3.41) are equal and $\varphi_2(r;\cdot)$ is continuous, it follows that $g_n(r,\rho;\cdot)$ is continuous in any region that contains the negative real axis (except the poles).

Now, the fact that $g_n(r,\rho;\cdot)$ is meromorphic can be inferred directly from the following well-known theorem of analytic continuation along curves (cf. Silverman 1984, p. 206): If f is a function which is continuous on an open set U and analytic on U except possibly at the points of a simple analytic curve C in U, then f is actually analytic on all of U. □

Having stated the fact that $g_n(r,\rho;\cdot)$ is meromorphic, we proceed to present the main result of this section, which is a series expansion of g_n. To accomplish that, we need first the following Lemma.

Lemma III.1. *There are positive constants C_1 and C_2 depending on n such that*

$$|g_n(r,\rho;\lambda)| \leqslant \frac{C_1}{|\lambda|^{1/2}\sqrt{r\rho}}$$

provided that: (i) $|\lambda| \geqslant C_2$, and (ii) either $\mathfrak{Re}\,\sqrt{\lambda} = (4l+2n+3)\pi/4R$ for some integer l or $|\mathfrak{Im}\,\sqrt{\lambda}| \geqslant R^{-1}$.

PROOF. Let M_1 a positive constant such that the asymptotic forms of the Bessel functions for large arguments (3.8) and (3.9) are valid when $|\lambda| \geqslant M_1$. Thus, substituting the Bessel functions by their asymptotic forms in (3.15) and (3.16) we obtain, after some manipulation with the complex trigonometric functions, that the asymptotic form of φ_1 and

φ_2 is given by

$$\varphi_1(r;\lambda) \sim \left[\frac{2}{\pi\sqrt{\lambda}r}\right]^{1/2}\cos\left(\sqrt{\lambda}r-\frac{\pi(2n+1)}{4}\right),$$

$$\varphi_2(r;\lambda) \sim \frac{-2}{\pi\sqrt{Rr\lambda}}\left[\sqrt{\lambda}\cos\left(\sqrt{\lambda}(R-r)\right)+\left(\frac{n}{R}-\alpha\right)\sin\left(\sqrt{\lambda}(R-r)\right)\right],$$

for all $|\lambda| > M_1$.

Considering the properties of the complex trigonometric functions, $|\cos(x+\mathrm{i}\,y)| \leqslant 2\,\mathrm{e}^{|y|}$ and $|\sin(x+\mathrm{i}\,y)| \leqslant 2\,\mathrm{e}^{|y|}$ for every $x, y \in \mathbb{R}$, we get that for $|\lambda|$ large enough, the following inequalities hold

$$|\varphi_1(r_<;\lambda)| \leqslant \left[\frac{8}{\pi}\right]^{1/2}\frac{\mathrm{e}^{|\Im\mathrm{m}\sqrt{\lambda}|r_<}}{|\lambda|^{1/4}\sqrt{r_<}}, \tag{3.42}$$

$$|\varphi_2(r_>;\lambda)| \leqslant \frac{4}{\pi\sqrt{R}}\left[1+\frac{1}{M_1}\left|\frac{n}{R}-\alpha\right|\right]\frac{\mathrm{e}^{|\Im\mathrm{m}\sqrt{\lambda}|(R-r_>)}}{\sqrt{r_>}}, \tag{3.43}$$

for every $|\lambda| > M_1$. Multiplying (3.42) by (3.43), we obtain

$$|\varphi_1(r_<;\lambda)\varphi_2(r_>;\lambda)| \leqslant \frac{C}{|\lambda|^{1/4}\sqrt{r_<r_>}}\,\mathrm{e}^{\left|\Im\mathrm{m}\sqrt{\lambda}\right|(R-r_>+r_<)},$$

and since $r_> - r_< = \max(r,\rho) - \min(r,\rho) \geqslant 0$, we have $R - r_> + r_< \leqslant R$ and hence

$$|\varphi_1(r_<;\lambda)\varphi_2(r_>;\lambda)| \leqslant \frac{C}{|\lambda|^{1/4}\sqrt{r_<r_>}}\,\mathrm{e}^{\left|\Im\mathrm{m}\,\sqrt{\lambda}\right|R}. \tag{3.44}$$

On the other hand, the denominator of the spectral Green's function is $D_n(\sqrt{\lambda},\alpha)$ and its asymptotic behavior for large arguments is given by

$$D_n(\sqrt{\lambda},\alpha) \sim \left[\frac{2}{\pi\sqrt{\lambda}R}\right]^{1/2}\left\{\left(\frac{n}{R}-\alpha\right)\cos\left(\sqrt{\lambda}R-\frac{\pi(2n+1)}{4}\right) - \sqrt{\lambda}\sin\left(\sqrt{\lambda}R-\frac{\pi(2n+1)}{4}\right)\right\}.$$

So that for all $|\lambda| > M_1$ we have

$$\begin{aligned} |D_n(\sqrt{\lambda},\alpha)| \;\sim\; & \left|\frac{2\sqrt{\lambda}}{\pi R}\right|^{1/2} \left|\sin\left(\sqrt{\lambda}R - \frac{\pi(2n+1)}{4}\right)\right| \\ & \times \left|\frac{1}{\sqrt{\lambda}}\left(\frac{n}{R}-\alpha\right)\cot\left(\sqrt{\lambda}R - \frac{\pi(2n+1)}{4}\right) - 1\right|. \end{aligned} \tag{3.45}$$

Let us note that for any real x and y, we have

$$|\cos(x+\mathrm{i}\,y)|^2 \;=\; \cosh^2(y) - \sin^2(x) \tag{3.46}$$

$$|\sin(x+\mathrm{i}\,y)|^2 \;=\; \cosh^2(y) - \cos^2(x). \tag{3.47}$$

Thus, since $\cosh y \geqslant \mathrm{e}^{|y|}/2$, we have that placing $\cos x = 0$ in (3.47) the sine function can be bounded by $|\sin(x+\mathrm{i}\,y)| \geqslant \mathrm{e}^{|y|}/4$. If instead we have $|y| > 1$, the same bound holds due to the inequality

$$|\sin(x+\mathrm{i}\,y)|^2 = \cosh^2(y) - \cos^2(x) \geqslant \cosh^2(y) - 1 \geqslant \frac{\mathrm{e}^{2|y|}}{4} - 1 > \frac{\mathrm{e}^{2|y|}}{16}. \tag{3.48}$$

Consequently, from (3.46) and (3.48), we obtain that

$$|\cot(x+\mathrm{i}\,y)|^2 = \left|\frac{\cos(x+\mathrm{i}\,y)}{\sin(x+\mathrm{i}\,y)}\right|^2 \leqslant \frac{16\cosh^2(y)}{\mathrm{e}^{2|y|}} \leqslant 32\frac{\mathrm{e}^{2|y|}}{\mathrm{e}^{2|y|}}, \tag{3.49}$$

provided that either $\cos x = 0$ or $|y| > 1$.

Now, setting

$$\sqrt{\lambda}R - \frac{\pi(2n+1)}{4} = x + \mathrm{i}\,y, \tag{3.50}$$

we can make use of the inequality (3.49) and then choosing a constant $C_2 = \max\{M_1, M_2\}$, where

$$M_2 \geqslant 128\left|\frac{n}{R}-\alpha\right|^2,$$

we obtain that for every $|\lambda| \geqslant C_2$ the following inequality holds

$$\begin{aligned} \left|\frac{1}{\sqrt{\lambda}}\left(\frac{n}{R}-\alpha\right)\cot\left(\sqrt{\lambda}R - \frac{\pi(2n+1)}{4}\right) - 1\right| \quad & \geqslant \\ \left|1 - \frac{1}{|\lambda|^{1/2}}\left|\frac{n}{R}-\alpha\right|\left|\cot\left(\sqrt{\lambda}R - \frac{\pi(2n+1)}{4}\right)\right|\right| \quad & \geqslant \quad \frac{1}{2}. \end{aligned}$$

Then, employing it in (3.45), we obtain that

$$\left|D_n(\sqrt{\lambda},\alpha)\right| \geqslant |\lambda|^{1/4}\frac{\mathrm{e}^{\left|\Im\mathrm{m}\sqrt{\lambda}\right|R}}{8}\left|\frac{2}{\pi R}\right|^{1/2}, \tag{3.51}$$

and thus finally computing the quotient between (3.44) and (3.51), we get

$$|g_n(r,\rho;\lambda)| = \left|\frac{\varphi_1(r_<;\lambda)\varphi_2(r_>;\lambda)}{D_n(\sqrt{\lambda};\alpha)}\right| \leqslant \frac{C_1}{|\lambda|^{1/2}\sqrt{r_<r_>}},$$

where by definition $r_<r_> = \min\{r,\rho\}\max\{r,\rho\} = r\rho$. □

Theorem III.1. *Let $\lambda \neq \lambda_{n,m}$, then spectral Green's function (3.22) admits the following representation:*

$$g_n(r,\rho;\lambda) = \sum_{m=1}^{\infty}\operatorname*{Res}_{\nu=\lambda_{n,m}}\frac{g_n(r,\rho;\nu)}{\lambda-\nu},$$

with $n \in \mathbb{N}_0$, $r \in [0,R]$, and $\rho \in (0,R)$.

PROOF. Let γ_N be the contour depicted in the Figure 3.3, where N is a positive integer large enough such that

$$\begin{aligned}\frac{\pi}{4R}(4N+2n+3) &\geqslant C_2\\ \frac{\pi}{4R}(4N+2n+3) &\geqslant \frac{1}{R}\\ N &\geqslant 2|\lambda|,\end{aligned}$$

and C_2 is the second constant in Lemma III.1. Note that in the region bounded by γ_N the function g_n is meromorphic as a function of λ, i.e. holomorphic expect at the isolated points $\lambda = \lambda_{n,m}$ which are its poles, so that the residue theorem applies. Also, we have that by virtue of Lemma III.1, on γ_N the function g_n is bounded by $C_1\left(|\lambda|r\rho\right)^{-1/2}$ and thus there are no poles on it.

Hence, according to the residue theorem (cf. Silverman 1984)), the following equality holds for every $\lambda \neq \lambda_{n,m}$:

$$\frac{1}{2\pi\mathrm{i}}\int_{\gamma_N}\frac{g_n(r,\rho;\nu)}{\lambda-\nu}\,\mathrm{d}\nu = -g_n(r,\rho,\lambda) + \sum_{m=1}^{M(N)}\operatorname*{Res}_{\nu=\lambda_{n,m}}\frac{g_n(r,\rho;\nu)}{\lambda-\nu}, \tag{3.52}$$

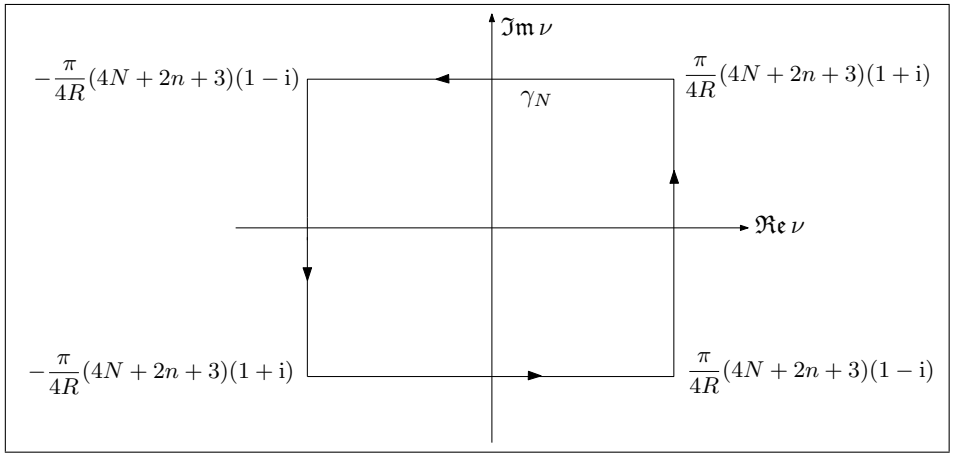

FIGURE 3.3. Integration contour used in the proof of the Theorem III.1.

where $M(N)$ is the number of poles $\nu = \lambda_{n,m}$ enclosed by γ_N, which is a monotone increasing function of N.

On the other hand, thanks to Lemma III.1 we have that the integral over γ_N can be bounded in the following way:

$$\left|\int_{\gamma_N} \frac{g_n(r,\rho;\nu)}{\lambda-\nu}\,\mathrm{d}\nu\right| \leqslant \int_{\gamma_N}\left|\frac{g_n(r,\rho;\nu)}{\lambda-\nu}\right|\,\mathrm{d}\nu \leqslant \frac{C_1}{\sqrt{r\rho}}\int_{\gamma_N}\frac{|\nu|^{-1/2}}{|\nu-\lambda|}\,\mathrm{d}\nu.$$

Then, as $N \geqslant 2|\lambda|$ we have that $|\lambda-\nu| \geqslant N$ and $|\nu| \leqslant \pi\sqrt{2}(4N+2n+3)/4R \leqslant \widetilde{C}N$ for every $\nu \in \gamma_N$. Consequently

$$\frac{C_1|\nu|^{1/2}}{|\lambda-\nu|} \leqslant \frac{\widetilde{C}}{N^{3/2}}, \quad \forall \nu \in \gamma_N \tag{3.53}$$

and noting that the length of the path γ_N is $l(\gamma_N) \leqslant 2\pi(4N+2n+3)/R$, we get

$$\left|\int_{\gamma_N} \frac{g_n(r,\rho;\nu)}{\lambda-\nu}\,\mathrm{d}\nu\right| \leqslant \frac{1}{\sqrt{r\rho}}\frac{\widehat{C}}{N^{1/2}}. \tag{3.54}$$

Next, taking the absolute value of (3.52), we obtain

$$\begin{aligned}\left|g(r,\rho;\lambda)-\sum_{m=1}^{M(N)}\operatorname*{Res}_{\nu=\lambda_{n,m}}\frac{g_n(r,\rho;\nu)}{\lambda-\nu}\right| &\leqslant \frac{1}{2\pi}\left|\int_{\gamma_N}\frac{g_n(r,\rho;\nu)}{\lambda-\nu}\,\mathrm{d}\nu\right| \\ &\leqslant \frac{1}{\sqrt{r\rho}}\frac{\widehat{C}}{N^{1/2}}\end{aligned} \tag{3.55}$$

and hence

$$\begin{aligned}g_n(r,\rho;\lambda) &= \lim_{N\to\infty}\sum_{m=1}^{M(N)}\operatorname*{Res}_{\nu=\lambda_{n,m}}\frac{g_n(r,\rho;\nu)}{\lambda-\nu} \\ &= \sum_{m=1}^{\infty}\operatorname*{Res}_{\nu=\lambda_{n,m}}\frac{g_n(r,\rho;\nu)}{\lambda-\nu}.\end{aligned} \tag{3.56}$$

Moreover, from (3.55) it is possible to conclude that

$$\lim_{N\to\infty}\sqrt{r\rho}\left|g_n(r,\rho;\lambda)-\sum_{m=1}^{M(N)}\operatorname*{Res}_{\nu=z_{n,m}^2}\frac{g_n(r,\rho;\nu)}{\lambda-\nu}\right|=0$$

uniformly for every $r\in[0,R]$ and $\rho\in(0,R)$. □

3.5.1 Computing the residues of the spectral Green's function

To find the residue of $g_n(r,\rho;\nu)/(\lambda-\nu)$ at $\nu=\lambda_{n,m}$, we will express the spectral Green's function as

$$g_n(r,\rho;\lambda)=\frac{N_n(\sqrt{\lambda},\alpha)}{D_n(\sqrt{\lambda},\alpha)}J_n(\sqrt{\lambda}r)J_n(\sqrt{\lambda}\rho)-\frac{\pi}{2}J_n(\sqrt{\lambda}r_<)Y_n(\sqrt{\lambda}r_>), \tag{3.57}$$

where D_n is defined in (3.27) and

$$N_n(z,\alpha)=\frac{\pi}{2}\left[zY_n'(zR)-\alpha Y_n(zR)\right]. \tag{3.58}$$

Let us observe that the last term in (3.57) contributes only to the residue at the pole $\nu=0$, arising when $\alpha=n/R$, was obtained in Proposition III.1 and is given by

$$\operatorname*{Res}_{\nu=0}\frac{g_n(r,\rho;\nu)}{\lambda-\nu}=-\frac{2(n+1)}{\lambda R^2}\left(\frac{r}{R}\right)^n\left(\frac{\rho}{R}\right)^n. \tag{3.59}$$

Therefore, this term in (3.57) does not exert any influence on the computation of the residues at the non-zero poles. Consequently, all other residues can be obtained with the following formula:

$$\operatorname*{Res}_{\nu=\lambda_{n,m}} \frac{g_n(r,\rho;\nu)}{\lambda-\nu} = \operatorname*{Res}_{\nu=z_{n,m}^2} \left[\frac{N_n(\sqrt{\nu},\alpha)}{D_n(\sqrt{\nu},\alpha)} \frac{J_n(\sqrt{\nu}r)J_n(\sqrt{\nu}\rho)}{\lambda-\nu} \right]. \tag{3.60}$$

At this stage we ought to distinguish two cases; $\nu=\lambda_{n,m}$ is a simple pole (i.e. $\lambda_{n,m}=z_{n,m}^2$ with $\alpha\in\mathbb{R}$ or $\mathfrak{Im}\,\alpha\neq 0$ with $\alpha\neq\pm\sqrt{n^2/R^2-z_{n,m}^2}$); or $\nu=\lambda_{n,m}$ is a double pole (i.e $\lambda_{n,m}=z_{n,m}^2$ with $\mathfrak{Im}\,\alpha\neq 0$ and $\alpha=\pm\sqrt{n^2/R^2-z_{n,m}^2}$).

When $\nu=\lambda_{n,m}$ is a simple pole, the following formula holds

$$\operatorname*{Res}_{\nu=\lambda_{n,m}} \left[\frac{N_n(\sqrt{\nu},\alpha)}{D_n(\sqrt{\nu},\alpha)} \frac{J_n(\sqrt{\nu}r)J_n(\sqrt{\nu}\rho)}{\lambda-\nu} \right] = \lim_{\nu\to z_{n,m}^2} \frac{2\sqrt{\nu}N_n(\sqrt{\nu},\alpha)}{D_n'(\sqrt{\nu},\alpha)} \frac{J_n(\sqrt{\nu}r)J_n(\sqrt{\nu}\rho)}{\lambda-\nu} \tag{3.61}$$

where D_n' denotes the derivative of D_n with respect to its first variable. Making use of the wronskian formula (3.12), we get that

$$\lim_{\nu\to z_{n,m}^2} N_n(\sqrt{\nu},\alpha) = \frac{1}{RJ_n(z_{n,m}R)}, \tag{3.62}$$

and from Proposition III.2 (b) it follows that

$$\lim_{\nu\to z_{n,m}^2} D_n'(\sqrt{\nu},\alpha) = -\frac{J_n(z_{n,m}R)}{z_{n,m}R}\left(R^2z_{n,m}^2-n^2+R^2\alpha^2\right). \tag{3.63}$$

Therefore

$$\operatorname*{Res}_{\nu=\lambda_{n,m}} \frac{g_n(r,\rho;\nu)}{\lambda-\nu} = \frac{2z_{n,m}^2 J_n(z_{n,m}r)J_n(z_{n,m}\rho)}{J_n^2(z_{n,m}R)(z_{n,m}^2-\lambda)\left(R^2z_{n,m}^2-n^2+R^2\alpha^2\right)} \tag{3.64}$$

when $\nu=\lambda_{n,m}\neq 0$ is a simple pole.

Now, let us assume that $\nu=\lambda_{n,m}$ is a double pole. Thus, the residue must be computed by the formula

$$\operatorname*{Res}_{\nu=\lambda_{n,m}} \frac{g_n(r,\rho;\nu)}{\nu-\lambda} = \lim_{\nu\to z_{n,m}^2} \frac{\mathrm{d}}{\mathrm{d}\nu}\left[\frac{(\nu-z_{n,m}^2)^2}{(\nu-\lambda)} \frac{N_n(\sqrt{\nu},\alpha)}{D_n(\sqrt{\nu},\alpha)} J_n(\sqrt{\nu}r)J_n(\sqrt{\nu}\rho) \right]. \tag{3.65}$$

After performing algebraic manipulation employing the properties of the Bessel functions and the equations that define non-simple roots, i.e. $D_n(z_{n,m},\alpha)=0$ and $\alpha^2=n^2/R^2-$

$z_{n,m}^2$, we obtain

$$\operatorname*{Res}_{\nu=\lambda_{n,m}} \frac{g_n(r,\rho;\nu)}{\lambda-\nu} = -\frac{4}{3}\frac{J_n(z_{n,m}r)J_n(z_{n,m}\rho)}{R^2J_n^2(z_{n,m}R)}\left[\frac{3z_{n,m}^2}{(z_{n,m}^2-\lambda)^2}+\frac{(2R\alpha-3n-2)}{z_{n,m}^2-\lambda}\right]$$
$$-\frac{J_{n+1}(z_{n,m}r)J_n(z_{n,m}\rho)}{R^2J_n^2(z_{n,m}R)}\frac{2z_{n,m}r}{z_{n,m}^2-\lambda}-\frac{J_n(z_{n,m}r)J_{n+1}(z_{n,m}\rho)}{R^2J_n^2(z_{n,m}R)}\frac{2z_{n,m}\rho}{z_{n,m}^2-\lambda}. \tag{3.66}$$

3.6 The spatial Green's function

In this section we recover the spatial Green's function from the integral representation and the spectral Green's function introduced in (3.4). Two different expressions of the spatial Green's function are obtained. The first one corresponds to a series expansion deduced as a result of Theorem III.1, and the second one shows explicitly the behavior of the Green's function at the source point.

3.6.1 Series representation

Thanks to Theorem III.1 we have that if $k^2-\xi^2 \neq \lambda_{n,m}$, then the spectral Green's function can be expressed as

$$g_n(r,\rho;k^2-\xi^2) = \sum_{m=1}^{\infty} \operatorname*{Res}_{\nu=\lambda_{n,m}} \frac{g_n(r,\rho;\nu)}{k^2-\xi^2-\nu}. \tag{3.67}$$

Paying attention to the condition $k^2-\xi^2 \neq \lambda_{n,m}$ and to Proposition III.2 (d), it may be noted that such condition holds if $\mathfrak{Im}\, k^2 > 0$ or $\mathfrak{Im}\, \alpha > 0$, by virtue of the fact that under either of those conditions, $\mathfrak{Im}(k^2-\xi^2)$ and $\mathfrak{Im}\, \lambda_{n,m}$ have opposite signs. This guarantees that every term in the series (3.67) belongs to $L^1(\mathbb{R})$ when it is viewed as a function of ξ, due to the functions $(k^2-\xi^2-z_{n,m}^2)^{-1}$ and $(k^2-\xi^2-z_{n,m}^2)^{-2}$, that appear in (3.64) and (3.66), have no singularities on the real line.

Therefore, assuming that $\mathfrak{Im}\, k^2 > 0$ or $\mathfrak{Im}\, \alpha > 0$, we utilize (3.4) and Theorem III.1 to obtain the following integral representation of the Green's function with the aid of the

Lebesgue convergence theorem

$$G(\boldsymbol{x},\boldsymbol{y}) = \frac{1}{4\pi^2}\sum_{n=0}^{\infty}\sum_{m=1}^{\infty}\epsilon_n\cos(n(\theta-\vartheta))\int_{\mathbb{R}}\operatorname*{Res}_{\nu=\lambda_{n,m}}\frac{g_n(r,\rho;\nu)}{k^2-\xi^2-\nu}\,\mathrm{e}^{\mathrm{i}\,\xi(z-\zeta)}\,\mathrm{d}\xi. \tag{3.68}$$

To compute the integral in (3.68) we need the following inverse Fourier transforms (Magnus & Oberhettinger 1954, p.116)

$$\int_{\mathbb{R}}\frac{\mathrm{e}^{\mathrm{i}\,z\xi}}{\xi^2+\lambda_{n,m}-k^2}\,\mathrm{d}\xi = \mathrm{i}\,\pi\frac{\mathrm{e}^{\mathrm{i}\,k_{n,m}|z|}}{k_{n,m}} \tag{3.69}$$

$$\int_{\mathbb{R}}\frac{\mathrm{e}^{\mathrm{i}\,z\xi}}{(\xi^2+\lambda_{n,m}-k^2)^2}\,\mathrm{d}\xi = \mathrm{i}\,\pi\frac{\mathrm{e}^{\mathrm{i}\,k_{n,m}|z|}}{2k_{n,m}^3}\left[\mathrm{i}\,k_{n,m}|z|-1\right], \tag{3.70}$$

where

$$k_{n,m} := \sqrt{k^2-\lambda_{n,m}} \tag{3.71}$$

are the so-called constant of propagation associated to the mode (n,m). Henceforth in this chapter, we assume k does not correspond to a cut-off frequency, i.e. $k_{n,m}\neq 0$.

The formulas (3.69) and (3.70) together with (3.64) and (3.66) lead to:

- If the pole of the spectral Green's function is $\lambda_{n,1}=0$, which occurs when $\alpha = n/R$, then we have that

$$\int_{\mathbb{R}}\operatorname*{Res}_{\nu=\lambda_{n,1}}\frac{g_n(r,\rho;\nu)}{k^2-\xi^2-\nu}\,\mathrm{e}^{\mathrm{i}\,\xi(z-\zeta)}\,\mathrm{d}\xi = \frac{2\pi\mathrm{i}\,(n+1)}{R^2}\left(\frac{r}{R}\right)^n\left(\frac{\rho}{R}\right)^n\frac{\mathrm{e}^{\mathrm{i}\,k|z-\zeta|}}{k}. \tag{3.72}$$

- If $\lambda_{n,m}=z_{n,m}^2$ is a simple pole of the spectral Green's function, i.e. $D_n(z_{n,m},\alpha)=0$ and $D_n'(z_{n,m},\alpha)\neq 0$, then we obtain that

$$\begin{aligned}&\int_{\mathbb{R}}\operatorname*{Res}_{\nu=\lambda_{n,m}}\frac{g_n(r,\rho;\nu)}{k^2-\xi^2-\nu}\,\mathrm{e}^{\mathrm{i}\,\xi(z-\zeta)}\,\mathrm{d}\xi \quad = \\ &\frac{2\pi\mathrm{i}\,z_{n,m}^2}{J_n^2(z_{n,m}R)\left(R^2z_{n,m}^2-n^2+R^2\alpha^2\right)}J_n(z_{n,m}r)J_n(z_{n,m}\rho)\frac{\mathrm{e}^{\mathrm{i}\,k_{n,m}|z-\zeta|}}{k_{n,m}}.\end{aligned} \tag{3.73}$$

- When $\lambda_{n,m} = z_{n,m}^2$ is a double pole of the spectral Green's function, i.e. $D_n(z_{n,m}, \alpha) = 0$ and $D_n'(z_{n,m}, \alpha) = 0$, we find that

$$\begin{aligned}
&\int_{\mathbb{R}} \operatorname*{Res}_{\nu=\lambda_{n,m}} \frac{g_n(r,\rho;\nu)}{k^2-\xi^2-\nu}\, \mathrm{e}^{\mathrm{i}\,\xi(z-\zeta)}\, \mathrm{d}\xi \quad = \\
&\frac{1}{2R^2 J_n^2(z_{n,m}R)} \left[z_{n,m}^2 J_n(z_{n,m}r) J_n(z_{n,m}\rho) \frac{[\mathrm{i}\,k_{n,m}|z-\zeta|-1]}{k_{n,m}^2} \right. \\
&+ z_{n,m} J_{n+1}(z_{n,m}r) J_n(z_{n,m}\rho) r + z_{n,m} J_n(z_{n,m}r) J_{n+1}(z_{n,m}\rho)\rho \\
&\left. + \frac{2}{3}(2R\alpha - 3n - 2) J_n(z_{n,m}r) J_n(z_{n,m}\rho) \right] \frac{\mathrm{e}^{\mathrm{i}\,k_{n,m}|z-\zeta|}}{\mathrm{i}\,k_{n,m}}.
\end{aligned} \tag{3.74}$$

Replacing (3.72), (3.73) and (3.74) in (3.68) when it corresponds, we get the series expansion of the Green's function. It is important to note that under the assumption $\mathfrak{Im}\, k^2 > 0$ or $\mathfrak{Im}\, \alpha > 0$, every term in the series representation of Green's function, decays exponentially in the direction of the axis of the waveguide (see Proposition III.2 (c)).

Results on the convergence of the series (3.68) for the particular case $\alpha = 0$ are found in Stuwe & Werner (1996). More specifically, in that work it is proved that for $(\boldsymbol{x}, \boldsymbol{y}) \in \overline{\Omega_\infty} \times \overline{\Omega_\infty} \setminus \{z = \zeta\}$ and $\mathfrak{Im}\, k^2 > 0$, the series converges uniformly. A generalization of this result for $\alpha \in \mathbb{C}$, $\mathfrak{Im}\, \alpha \geqslant 0$ seams to be possible to obtain from this work, but it is out of the scope of this work. Anyway, we assume that the uniform convergence of the series (3.68) for the domain stated above holds for an arbitrary impedance parameter α with $\mathfrak{Im}\, \alpha \geqslant 0$.

3.6.2 Local behavior at the source point

Let us replace the Bessel function of second kind $Y_n(z)$, by

$$Y_n(z) = \mathrm{i}\left[J_n(z) - H_n^{(1)}(z)\right]$$

in (3.22), where $H_n^{(1)}(z)$ is the Hankel function of the first kind (cf. Abramovitz & Stegun 1972). It leads to

$$\begin{aligned} g_n(r,\rho;\lambda) &= -\frac{\mathrm{i}\,\pi}{2}\frac{\sqrt{\lambda}H_n^{(1)'}(\sqrt{\lambda}R)-\alpha H_n^{(1)}(\sqrt{\lambda}R)}{\sqrt{\lambda}J_n'(\sqrt{\lambda}R)-\alpha J_n(\sqrt{\lambda}R)}J_n(\sqrt{\lambda}r)J_n(\sqrt{\lambda}\rho) \\ &\quad +\frac{\mathrm{i}\,\pi}{2}\begin{cases} J_n(\sqrt{\lambda}r)H_n^{(1)}(\sqrt{\lambda}\rho) & \text{if} \quad 0<r\leqslant\rho<R, \\ J_n(\sqrt{\lambda}\rho)H_n^{(1)}(\sqrt{\lambda}r) & \text{if} \quad 0<\rho\leqslant r<R, \end{cases} \end{aligned} \tag{3.75}$$

which may be written equivalently as

$$g_n(r,\rho;\lambda) = g_n^{\infty}(r,\rho;\lambda) + g_n^{c}(r,\rho;\lambda), \tag{3.76}$$

where

$$g_n^{\infty}(r,\rho;\lambda) = \frac{\mathrm{i}\,\pi}{2}\begin{cases} J_n(\sqrt{\lambda}r)H_n^{(1)}(\sqrt{\lambda}\rho) & \text{if} \quad 0<r\leqslant\rho<R, \\ J_n(\sqrt{\lambda}\rho)H_n^{(1)}(\sqrt{\lambda}r) & \text{if} \quad 0<\rho\leqslant r<R, \end{cases} \tag{3.77}$$

and

$$g_n^{c}(r,\rho;\lambda) = -\frac{\mathrm{i}\,\pi}{2}\frac{\sqrt{\lambda}H_n^{(1)'}(\lambda R)-\alpha H_n^{(1)}(\lambda R)}{\sqrt{\lambda}J_n'(\lambda R)-\alpha J_n(\lambda R)}J_n(\lambda r)J_n(\lambda\rho). \tag{3.78}$$

Now, setting (3.77) and (3.78) in the integral representation of the Green's function (3.4), we define

$$G^{\infty}(\boldsymbol{x},\boldsymbol{y}) := \frac{1}{4\pi^2}\int_{\mathbb{R}} \mathrm{e}^{\mathrm{i}\,\xi(z-\zeta)}\sum_{n=0}^{\infty} g_n^{\infty}(r,\rho;k^2-\xi^2)\cos(n(\theta-\vartheta))\epsilon_n\,\mathrm{d}\xi \tag{3.79}$$

and

$$G_c(\boldsymbol{x},\boldsymbol{y}) := \frac{1}{4\pi^2}\int_{\mathbb{N}_0\times\mathbb{R}} g_n^{c}(r,\rho;k^2-\xi^2)\cos(n(\theta-\vartheta))\,\mathrm{e}^{\mathrm{i}\,\xi(z-\zeta)}\epsilon_n\,\mathrm{d}\xi\,\mathrm{d}n, \tag{3.80}$$

from which the Green's function is expressed as $G = G^{\infty} + G_c$. Hence, as a result of Graf's addition theorem (Magnus & Oberhettinger 1954, p. 21, eq. 3(b)) we find that

$$\begin{aligned} &H_0^{(1)}\left(\sqrt{k^2-\xi^2}\sqrt{r^2+\rho^2-2r\rho\cos(\theta-\vartheta)}\right) \quad = \\ &\qquad \sum_{n=0}^{\infty}\epsilon_n H_n^{(1)}\left(\sqrt{k^2-\xi^2}\rho\right)J_n\left(\sqrt{k^2-\xi^2}r\right)\cos(n(\theta-\vartheta)) \ . \end{aligned} \tag{3.81}$$

Therefore, replacing (3.81) in (3.79) we obtain

$$G^{\infty}(\boldsymbol{x},\boldsymbol{y}) = \frac{\mathrm{i}}{8\pi}\int_{\mathbb{R}} H_0^{(1)}\left(\sqrt{k^2-\xi^2}\sqrt{r^2+\rho^2-2r\rho\cos(\theta-\vartheta)}\right)\,\mathrm{e}^{\mathrm{i}\,\xi(z-\zeta)}\,\mathrm{d}\xi, \tag{3.82}$$

and then, thanks to Weyrich's formula (Magnus & Oberhettinger 1954, p. 34),

$$\frac{\mathrm{i}}{2}\int_{\mathbb{R}} H_0^{(1)}\Big(\sqrt{k^2-\xi^2}\varrho\Big)\,\mathrm{e}^{\mathrm{i}\,\xi z}\,\mathrm{d}\xi = \frac{\mathrm{e}^{\mathrm{i}\,k\sqrt{\varrho^2+z^2}}}{\sqrt{\varrho^2+z^2}}, \tag{3.83}$$

which is valid for every $k\in\mathbb{C}$ such that $0\leqslant \arg\sqrt{k^2-\xi^2}<\pi,\ 0\leqslant\arg(k)<\pi$, that is our case, we get that the integral in (3.82) can be solved exactly to obtain

$$G^{\infty}(\boldsymbol{x},\boldsymbol{y}) = \frac{\mathrm{e}^{\mathrm{i}\,k\sqrt{(z-\zeta)^2+r^2+\rho^2-2r\rho\cos(\theta-\vartheta)}}}{4\pi\sqrt{(z-\zeta)^2+r^2+\rho^2-2r\rho\cos(\theta-\vartheta)}}, \tag{3.84}$$

where $G^{\infty}(\boldsymbol{x},\boldsymbol{y}) = \Phi(\boldsymbol{x}-\boldsymbol{y})$, with

$$\Phi(\boldsymbol{x}) = \frac{\mathrm{e}^{\mathrm{i}\,k|\boldsymbol{x}|}}{4\pi|\boldsymbol{x}|},$$

the fundamental solution of the Helmholtz equation in $\mathbb{R}^3$. It can be observed that G^{∞} contains the unique singularity of the Green's function located at $\boldsymbol{y}=\boldsymbol{x}$. Therefore, the remaining term G_c is *regular* in the sense that numerical techniques such as the Inverse Fast Fourier Transform may be applied with aim of approximating it (cf. Duffy 2004, Durán et al. 2006, 2007).

3.6.3 Undamped wave propagation and the far-field

Now we turn the attention to the complete undamped case, i.e. when the wave number and the impedance parameter are such that $\mathfrak{Im}\,k^2 = \mathfrak{Im}\,\alpha = 0$ and, consequently, all the poles of the spectral Green's function $\lambda_{n,m}$, are simple and lie on the real line.

When these conditions hold, the functions in the inverse Fourier transforms (3.69) and (3.70), no longer belong to $L^1(\mathbb{R})$ for all $m\in\mathbb{N}$ and $n\in\mathbb{N}_0$ because when $k^2>\lambda_{n,m}$ for some m and n, they have poles on the real line at $k_{n,m}=\sqrt{k^2-\lambda_{n,m}}$ and $-k_{n,m}$. Consequently, the integrals (3.69) and (3.70) lack meaning within the frame of Lebesgue integral and must be understood in a broader sense. To face that problem we appeal to the limiting

absorption principle (cf. Sveshnikov 1951, Nosich 1994), a mathematical procedure that allows us to obtain a suitable meaning in physical terms for (3.69) and (3.70), in a way that leads to a unique outgoing wave solution of (3.1).

To apply the limiting absorption principle we ought to add dissipation to the system perturbing either the wave number designated as $k_\varepsilon = k + \mathrm{i}\,\varepsilon,\ \varepsilon > 0$ or the impedance parameter as $\alpha_\varepsilon = \alpha + \mathrm{i}\,\varepsilon,\ \varepsilon > 0$. Subsequently, (3.1) can be solved resorting to the procedure described above to obtain an ε-dependent Green's function G_ε. Finally, taking the limit assuming the uniform convergence of the series

$$G = \lim_{\varepsilon \to 0} G_\varepsilon. \tag{3.85}$$

we get the unique outgoing wave solution of (3.1) that can be represented by the following series

$$G(\boldsymbol{x}, \boldsymbol{y}) = \frac{\mathrm{i}}{4\pi} \sum_{n=0}^{\infty} \sum_{m=1}^{\infty} \epsilon_n \cos(n(\theta - \vartheta)) \varphi_{n,m}(r) \varphi_{n,m}(\rho) \frac{\mathrm{e}^{\mathrm{i}\, k_{n,m}|z-\zeta|}}{k_{n,m}}, \tag{3.86}$$

where

$$\varphi_{n,m}(r) = \frac{\sqrt{2} z_{n,m} J_n\left(z_{n,m} r\right)}{J_n\left(z_{n,m} R\right) \sqrt{R^2 z_{n,m}^2 - n^2 + R^2 \alpha^2}},\ m \in \mathbb{N}, \tag{3.87}$$

if $\alpha \neq n/R,\ \lambda_{n,m} = z_{n,m}^2$ and

$$\varphi_{n,m}(r) = \begin{cases} \dfrac{\sqrt{2} J_n(j_{n+1,m-1} r/R)}{J_n\left(j_{n+1,m-1}\right) R} & \text{if} \quad m > 1, \\ \dfrac{\sqrt{2n+2}}{R} \left(\dfrac{r}{R}\right)^n & \text{if} \quad m = 1, \end{cases} \tag{3.88}$$

if $\alpha = n/R$ for some $n \in \mathbb{N}_0$. Let us observe that the set of functions $\{\sqrt{r}\varphi_{n,m}(r), m \in \mathbb{N}\}$ forms a complete orthonormal basis of $L^2((0, R))$. It can be deduced from the theory of Dini series (cf. Watson 1966) or equivalently, from the theory of singular self-adjoint Sturm-Liouville problems (cf. Stakgold 2000).

Unlike the damped case, in the undamped case the Green's function does not decay exponentially in the direction of the waveguide's axis. In fact, from the definition (3.71), we have that the term $\mathrm{i}\, k_{n,m}$ in (3.86) can be either purely real or purely imaginary. Thus,

when $k^2 > \lambda_{n,m}$, it holds that $k_{n,m} = \sqrt{k^2 - \lambda_{n,m}} > 0$, and then the mode in the series representation of the time-harmonic Green's function $\mathfrak{Re}(G(\boldsymbol{x}, \boldsymbol{y})\, \mathrm{e}^{-\mathrm{i}\,\omega t})$, that is

$$\mathfrak{Re}\left[\cos(n(\theta - \vartheta))\varphi_{n,m}(r)\varphi_{n,m}(\rho)\, \mathrm{e}^{\mathrm{i}\,[k_{n,m}|z-\zeta| - \omega t]}\right], \tag{3.89}$$

represents an unattenuated propagative mode that travels out from the point source located at $\boldsymbol{x} = (\rho\cos\vartheta, \rho\sin\vartheta, \zeta)$ in the direction of the waveguide's axis, with velocity $c_{n,m} = \omega/k_{n,m}$. On the other hand, when $k^2 < \lambda_{n,m}$ we have that $\mathrm{i}\, k_{n,m} < 0$, and then the mode (3.89) decays exponentially while it travels out from the source. The latter modes are the so-called evanescent modes and the former correspond to the propagative modes.

The following result states that in absence of dissipation the number of propagative modes is finite while the number of evanescent modes is infinite.

Proposition III.4. *The cardinality of the set*

$$\Lambda = \left\{(n,m) \in \mathbb{N}_0 \times \mathbb{N} : D(\sqrt{\lambda_{n,m}}, \alpha) = 0 \textit{ and } \lambda_{n,m} < k^2\right\} \tag{3.90}$$

is finite.

PROOF. First, let us observe that when $\alpha \in \mathbb{R}$ we have that $\lambda_{n,m} = z_{n,m}^2 \in \mathbb{R}$ and $z_{n,m}^2 \to \infty$ as $m \to \infty$ for every $n \in \mathbb{N}_0$. Then, there is $M \in \mathbb{N}$ such that $z_{n,m}^2 > k^2$ for every $m > M$ and every $n \in \mathbb{N}_0$. On the other hand, according to Ismail & Muldoon (1995) the following bound holds:

$$x_1^2 > \frac{(Rn - \alpha)(n+1)}{R(2R + nR - \alpha)}, \;\; \forall n > \alpha/R,$$

where x_1 is the first positive (real) root of $D_n(\cdot, \alpha)$. According to that, we can choose a $N > \max\{\alpha/R, 0\}$ such that

$$z_{n,1}^2 > \frac{(Rn - \alpha)(n+1)}{R(2R + nR - \alpha)} > k^2, \;\; \forall n > N,$$

and hence we obtain that $|\Lambda| < MN < \infty$. □

Now, since the evanescent modes decay exponentially, the far-field form of the Green's function is only composed by the propagative modes, i.e.

$$G^{ff}(\boldsymbol{x},\boldsymbol{y}) = \frac{\mathrm{i}}{4\pi}\sum_{(n,m)\in\Lambda}\epsilon_n\cos(n(\theta-\vartheta))\varphi_{n,m}(r)\varphi_{n,m}(\rho)\frac{\mathrm{e}^{\mathrm{i}\,k_{n,m}|z-\zeta|}}{k_{n,m}}. \tag{3.91}$$

This far-field form of G and the orthogonality of the functions

$$\left\{\sqrt{r}\varphi_{n,m}(r)\,\mathrm{e}^{\mathrm{i}\,n\theta},(n,m)\in\mathbb{N}_0\times\mathbb{N}\right\}$$

in the $L^2(\Omega')$ inner product (where Ω' is the waveguide's cross section), allow us to obtain directly the radiation condition which can be written as

$$\lim_{|L|\to\infty}\int_{\Gamma_L}\left\{\frac{\partial G}{\partial z}-\mathrm{i}\,k_{n,m}\mathrm{sign}(z-\zeta)\,G\right\}\mathrm{e}^{\mathrm{i}\,n\theta}\varphi_{n,m}(r)\,\mathrm{d}\sigma_{\boldsymbol{y}}=0,\quad\forall(n,m)\in\Lambda \tag{3.92}$$

where the convergence of the limit is uniformly for every $\boldsymbol{x}\in\Omega_\infty$, the surface Γ_L is defined by

$$\Gamma_L := \left\{\boldsymbol{x}=(x_1,x_2,x_3)\in\mathbb{R}^3 : x_1^2+x_2^2<R^2, x_3=L\right\} = \Omega'\times\{L\} \tag{3.93}$$

and the set of indices Λ is defined in (3.90).

An interesting phenomenon arising only when a non-dissipative impedance boundary condition is imposed on the waveguide's walls, is the propagation of a surface wave. This kind of wave decays exponentially to the interior of the waveguide, transporting energy only near the waveguide's surface. This wave is the result of the superposition of the surface wave modes that conform the series expansion of the Green's function. These modes appear for any real impedance parameter $\alpha>0$ due the negative poles of the spectral Green's function that arise when a purely imaginary root of $D_n(\cdot,\alpha)$ exists. It leads to the fact that the radial component of this modes (3.87) is

$$\varphi_{n,1}(r) = \frac{\sqrt{2}y_nI_n(y_nr)}{I_n(y_nR)\sqrt{R^2y_n^2+n^2-R^2\alpha^2}},$$

where $I_n(x)$ are the modified Bessel functions of the first kind (cf. Abramovitz & Stegun 1972) which are monotonically increasing functions. Figure 5.5 shows the surface wave

that composes the Green's function for the particular case $R = 1$, $k = 5$ and $\alpha = 2.5$, with source point $\boldsymbol{y} = (0, 0.5, 0)$.

3.7 Green's function of a semi-infinite circular cylinder

Once we have worked out the Green's function for the domain consisting of the whole cylinder, we can use it to easily obtain the Green's function suitable for the integral/series representation of the solution of the exterior problems (2.26-2.27) and (2.30-2.31). That is easy due to the *method of images*, which works pretty well when the boundary condition is either Dirichlet or Neumann. A deeper description of this method is found in Stakgold (1998), Duffy (2001) and Polyanin (2002).

The sought Green's functions for the integral/series representation of the solutions of exterior problems (2.26-2.27) and (2.30)- (2.31), are given by the solutions of the problems

$$\begin{cases} \Delta_{\boldsymbol{y}} G_e^{\pm}(\boldsymbol{x}, \boldsymbol{y}) + k^2 G_e^{\pm}(\boldsymbol{x}, \boldsymbol{y}) &= -\delta_{\boldsymbol{x}}(\boldsymbol{y}), \quad \boldsymbol{y} \in \Omega_e^{\pm} \\ \dfrac{\partial G_e^{\pm}(\boldsymbol{x}, \boldsymbol{y})}{\partial n_{\boldsymbol{y}}} - \alpha\, G_e^{\pm}(\boldsymbol{x}, \boldsymbol{y}) &= 0, \qquad \boldsymbol{y} \in \Gamma_e^{\pm} \\ G_e^{\pm}(\boldsymbol{x}, \boldsymbol{y}) &= 0, \qquad \boldsymbol{y} \in \Gamma_H^{\pm} \end{cases} \tag{3.94}$$

where the sets $\Omega_e^{\pm}$, $\Gamma_e^{\pm}$ and $\Gamma_H^{\pm}$ are defined in (2.2), (2.5) and (2.3) respectively. Again, as in the beginning of this chapter, we assume that $\mathfrak{Im}\, k^2 > 0$ as well as $\mathfrak{Im}\, \alpha > 0$, and subsequently, the undamped case is analysed by means of the limiting absorption principle.

Without loosing generality, we focus in finding G_e^{+}, since the computation of G_e^{-} is slightly different. According to the method of images, we have to consider two point sources, $\boldsymbol{x} \in \Omega_e^{+}$ and $\bar{\boldsymbol{x}} \in \Omega_\infty \setminus \overline{\Omega_e^{+}}$, where $\bar{\boldsymbol{x}} = (x_1, x_2, 2H - x_3)$ when $\boldsymbol{x} = (x_1, x_2, x_3)$. The system response to the coupling effect of these source terms is given by the superposition of the respective Green's functions, $G(\boldsymbol{x}, \boldsymbol{y})$ and $G(\bar{\boldsymbol{x}}, \boldsymbol{y})$. Both functions satisfy the first two equations in (3.94). Therefore, in order to impose the remaining Dirichlet

boundary condition on Γ_H^+, we define a new function

$$\widetilde{G}_e^+(\boldsymbol{x},\boldsymbol{y}) = G(\boldsymbol{x},\boldsymbol{y}) - G(\bar{\boldsymbol{x}},\boldsymbol{y}),$$

which satisfies

$$\widetilde{G}_e^+(\boldsymbol{x},\boldsymbol{y}) = 0,\ \boldsymbol{y}\in\Gamma_H^+.$$

Hence, restricting it to Ω_e^+, we get that the solution of (3.94) in the upper semi-infinite cylinder (i.e. in Ω_e^+) is:

$$G_e^+(\boldsymbol{x},\boldsymbol{y}) = \widetilde{G}_e^+\Big|_{\Omega_e^+}(\boldsymbol{x},\boldsymbol{y}).$$

If $\alpha \neq \pm\sqrt{n^2/R^2 - z_{n,m}^2}$, the solution of (3.94) can be expressed by the series

$$G_e^+(\boldsymbol{x},\boldsymbol{y}) = \frac{1}{2\pi}\sum_{n=0}^{\infty}\sum_{m=1}^{\infty}\epsilon_n\cos(n(\theta-\vartheta))\varphi_{n,m}(r)\varphi_{n,m}(\rho)\frac{\mathrm{e}^{\mathrm{i}\,k_{n,m}(z_>-H)}\sin(k_{n,m}(z_<-H))}{k_{n,m}} \tag{3.95}$$

which is valid for every $k^2 \neq \lambda_{n,m}$ (i.e. $k_{n,m}\neq 0$). Let us observe that here we use the same notation as in Section 3.3, that is, $z_< = \min\{z,\zeta\}$ and $z_> = \max\{z,\zeta\}$.

In the same manner as is achieved the radiation condition for G, we can obtain it for the Green's function of the semi-infinite circular cylinder. Thus, resorting to use of (3.95), we get that when $\mathfrak{Im}\,\alpha = \mathfrak{Im}\,k^2 = 0$, the far-field form of G_e^+ is given by

$$G_e^{+ff}(\boldsymbol{x},\boldsymbol{y}) = \frac{1}{2\pi}\sum_{(n,m)\in\Lambda}\epsilon_n\cos(n(\theta-\vartheta))\varphi_{n,m}(r)\varphi_{n,m}(\rho)\frac{\mathrm{e}^{\mathrm{i}\,k_{n,m}(z-H)}\sin(k_{n,m}(\zeta-H))}{k_{n,m}}. \tag{3.96}$$

It follows from here that the radiation condition can be expressed as

$$\lim_{L\to\infty}\int_{\Gamma_L}\left\{\frac{\partial G_e^+}{\partial z} - \mathrm{i}\,k_{n,m}\,G_e^+\right\}\mathrm{e}^{\mathrm{i}\,n\theta}\varphi_{n,m}(r)\,\mathrm{d}\sigma_{\boldsymbol{y}} = 0, \quad \forall (n,m)\in\Lambda \tag{3.97}$$

where the convergence of the limit is uniformly for every $\boldsymbol{x}\in\Omega_e^+$, the surface Γ_L is defined by (3.93) and the set of indices Λ is defined in (3.90).

On the other hand, taking into account the local behavior of G at its singularity located at $\boldsymbol{y} = \boldsymbol{x}$, we obtain an alternative representation of G_e^+ given by

$$G_e^+(\boldsymbol{x}, \boldsymbol{y}) = \Phi(\boldsymbol{x} - \boldsymbol{y}) - \Phi(\bar{\boldsymbol{x}} - \boldsymbol{y}) + G_c(\boldsymbol{x}.\boldsymbol{y}) - G_c(\bar{\boldsymbol{x}}, \boldsymbol{y}), \tag{3.98}$$

where Φ and G_c are defined in (3.84) and (3.80) respectively. Let us observe that the function

$$\Psi(\boldsymbol{x}, \boldsymbol{y}) = -\Phi(\bar{\boldsymbol{x}} - \boldsymbol{y}) + G_c(\boldsymbol{x}.\boldsymbol{y}) - G_c(\bar{\boldsymbol{x}}, \boldsymbol{y})$$

does not have any singularities for every $\boldsymbol{x}, \boldsymbol{y} \in \Omega_e^+$. Moreover, it can be proved that it is continuous in virtue of the fact that $G_c(\boldsymbol{x}, \boldsymbol{y})$ is continuous and for every $\boldsymbol{x}, \boldsymbol{y} \in \Omega_\infty$, and $\Phi(\bar{\boldsymbol{x}} - \boldsymbol{y})$ has its singularity outside Ω_e^+.

In a completely analogous manner it is possible to take $\boldsymbol{x} = (x_1, x_2, x_3) \in \Omega_e^-$ and $\bar{\boldsymbol{x}} = (x_1, x_2, -2H - x_3)$, to obtain that when $\alpha \neq \pm\sqrt{n^2/R^2 - z_{n,m}^2}$ and $k^2 \neq \lambda_{n,m}$, the Green's function of the lower semi-infinite cylinder is given by

$$G_e^-(\boldsymbol{x}, \boldsymbol{y}) = \frac{1}{2\pi} \sum_{n=0}^{\infty} \sum_{m=1}^{\infty} \epsilon_n \cos(n(\theta - \vartheta)) \varphi_{n,m}(r) \varphi_{n,m}(\rho) \frac{\mathrm{e}^{-\mathrm{i}\, k_{n,m}(z_< + H)} \sin(k_{n,m}(z_> + H))}{k_{n,m}}, \tag{3.99}$$

its far-field form is

$$G_e^{-ff}(\boldsymbol{x}, \boldsymbol{y}) = \frac{1}{2\pi} \sum_{(n,m) \in \Lambda} \epsilon_n cos(n(\theta - \vartheta)) \varphi_{n,m}(r) \varphi_{n,m}(\rho) \frac{\mathrm{e}^{-\mathrm{i}\, k_{n,m}(z + H)} \sin(k_{n,m}(\zeta + H))}{k_{n,m}},$$

and the radiation condition that it satisfies is

$$\lim_{L \to -\infty} \int_{\Gamma_L} \left\{ \frac{\partial G_e^-}{\partial z} + \mathrm{i}\, k_{n,m}\, G_e^- \right\} \mathrm{e}^{\mathrm{i}\, n\theta} \varphi_{n,m}(r)\, \mathrm{d}\sigma_{\boldsymbol{y}} = 0, \quad \forall (n, m) \in \Lambda. \tag{3.100}$$

As well as the Green's function of the upper semi-infinite cylinder, the representation (3.98) shows the local behavior of G_e^- near its singularity.

IV. DIRICHLET-TO-NEUMANN MAP ABSORBING BOUNDARY CONDITION

This chapter addresses the problem of finding a way to redefine the scattering problem (2.24) and the resonance problem (2.28) on a bounded domain. If we want to reduce them to a boundary value problems on a bounded domain, the first step is to introduce artificial boundaries that split the original domain into three disjoint sets; a bounded one, which contains the local perturbation; and two unbounded sets, which do not have any perturbation. Section 2.1 describes this procedure applied to our problem. There, the unbounded domain Ω is splitted by the artificial boundaries Γ_H^+ and Γ_H^- which divide it into three sets; the interior domain Ω_i, and the exterior domains Ω_e^+ and Ω_e^-. As a result of introducing these artificial boundaries we obtained the coupled problems, (2.25-2.26-2.27) and (2.29-2.30-2.31), which interact among themselves across the plane surfaces Γ_e^+ and Γ_e^-.

The main issue of the present chapter consist in resorting to the use of a suitable absorbing boundary condition imposed on Γ_H^+ and Γ_H^-, to uncouple (2.25-2.26-2.27) and (2.29-2.30-2.31), in order to achieve equivalent problems defined only on Ω_i. As was already pointed out in the introduction, good surveys of artificial boundary conditions can be found in Ihlenburg (1998), Thomson (2006) and Givoli (2008). In this dissertation we develop the DtN map, which is constructed from the Green's function obtained in the previous chapter. Some specific references about this kind of absorbing boundary condition applied to similar problems can be found in Goldstein (1982), Harari et al. (1998) and Givoli (1999).

4.1 Representation of exterior solution

In this section we seek for an explicit representation of the solution of the exterior problems. Without loss of generality, we focus on the problems (2.27) and (2.31) because the problems (2.26) and (2.30) may be treated in a similar way. To obtain these representations, we resort to the use of the Green's function shown in (3.95) and the Green's theorem in the following way: let us assume that $k \neq \sqrt{\lambda_{n,m}}$ and $p_e^+ : \Omega_e^+ \to \mathbb{C}$, $p_e^+ \in C^2(\Omega_e^+) \cap C^1(\overline{\Omega_e^+})$,

be a solution of either (2.26) or (2.30), and let $\varepsilon > 0$ small enough such that

$$B_\varepsilon(\boldsymbol{x}) = \left\{\boldsymbol{z} \in \mathbb{R}^3 : |\boldsymbol{x} - \boldsymbol{z}| < \varepsilon\right\} \subset \Omega_e^+, \tag{4.1}$$

where the point $\boldsymbol{x} \in \Omega_e^+$ is fixed. Now, let $L > H$ and define the set

$$\Omega_\varepsilon^L = \left(\Omega_e^+ \setminus B_\varepsilon\right) \cap \left(\mathbb{R}^2 \times (H, L)\right), \tag{4.2}$$

where L is large enough such that $B_\varepsilon \subset \Omega_\varepsilon^L$. Figure 4.1 depicts the domains defined above.

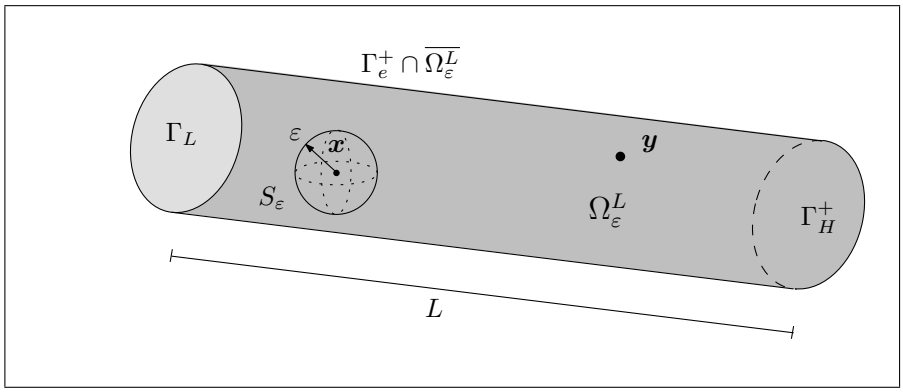

FIGURE 4.1. Domain used for the representation of the exterior solution.

The good properties of G_e^+ over Ω_ε^L allow us to use the Green's second identity that reads as follows:

$$\begin{aligned}\int_{\Omega_\varepsilon^L} \left[G_e^+(\boldsymbol{x},\boldsymbol{y})\Delta p_e^+(\boldsymbol{y}) - p_e^+(\boldsymbol{y})\Delta_{\boldsymbol{y}} G_e^+(\boldsymbol{x},\boldsymbol{y})\right] \mathrm{d}\boldsymbol{y} \\ = \int_{\partial\Omega_\varepsilon^L} \left[G_e^+(\boldsymbol{x},\boldsymbol{y})\frac{\partial p_e^+(\boldsymbol{y})}{\partial n} - p_e^+(\boldsymbol{y})\frac{\partial G_e^+(\boldsymbol{x},\boldsymbol{y})}{\partial n_{\boldsymbol{y}}}\right] \mathrm{d}\sigma_{\boldsymbol{y}},\end{aligned} \tag{4.3}$$

where the normal derivatives exist in the sense that the limits

$$\frac{\partial p_e^+(\boldsymbol{y})}{\partial n} = \lim_{\delta \to 0} n_{\boldsymbol{y}} \cdot \left\{\nabla p_e^+(\boldsymbol{y}) - \delta n_{\boldsymbol{y}}\right\}, \tag{4.4a}$$

$$\frac{\partial G_e^+(\boldsymbol{x},\boldsymbol{y})}{\partial n_{\boldsymbol{y}}} = \lim_{\delta \to 0} n_{\boldsymbol{y}} \cdot \left\{\nabla_{\boldsymbol{y}} G_e^+(\boldsymbol{x},\boldsymbol{y}) - \delta n_{\boldsymbol{y}}\right\}, \tag{4.4b}$$

exist uniformly for $\boldsymbol{y} \in \partial\Omega_\varepsilon^L$ and $\boldsymbol{x} \in \Omega_\varepsilon^L$. Herein ∇ and $\nabla_{\boldsymbol{y}}$ denote the gradient operator with respect to the variable $\boldsymbol{y}$, $n_{\boldsymbol{y}}$ denotes the outward pointing normal vector to Ω_ε^L, and $\partial\Omega_\varepsilon^L$ denotes the Ω_ε^L's boundary.

It can be observed that adding and subtracting $k^2 p_e^+(\boldsymbol{y}) G_e^+(\boldsymbol{x},\boldsymbol{y})$ to the function in the integral on the left-hand side of (4.3), it becomes

$$\int_{\Omega_\varepsilon^L} G_e^+(\boldsymbol{x},\boldsymbol{y}) \left[\Delta p_e^+(\boldsymbol{y}) - k^2 p_e^+(\boldsymbol{y})\right] \mathrm{d}\boldsymbol{y} - \int_{\Omega_\varepsilon^L} p_e^+(\boldsymbol{y}) \left[\Delta_{\boldsymbol{y}} G_e^+(\boldsymbol{x},\boldsymbol{y}) - k^2 G_e^+(\boldsymbol{x},\boldsymbol{y})\right] \mathrm{d}\boldsymbol{y} = 0, \tag{4.5}$$

in virtue of the fact that G_e^+ and p_e^+ satisfy the Helmholtz equation in Ω_ε^L, for every $L > H$ big enough and $\varepsilon > 0$ small enough.

On the other hand, the integral on the right hand side of (4.3), can be splitted into the following four integrals:

$$I_1 = \int_{\Gamma_e^+ \cap \overline{\Omega_\varepsilon^L}} \left[G_e^+(\boldsymbol{x},\boldsymbol{y}) \frac{\partial p_e^+(\boldsymbol{y})}{\partial n} - p_e^+(\boldsymbol{y}) \frac{\partial G_e^+(\boldsymbol{x},\boldsymbol{y})}{\partial n_{\boldsymbol{y}}} \right] \mathrm{d}\sigma_{\boldsymbol{y}} \tag{4.6a}$$

$$I_2 = \int_{\Gamma_H^+} \left[G_e^+(\boldsymbol{x},\boldsymbol{y}) \frac{\partial p_e^+(\boldsymbol{y})}{\partial n} - p_e^+(\boldsymbol{y}) \frac{\partial G_e^+(\boldsymbol{x},\boldsymbol{y})}{\partial n_{\boldsymbol{y}}} \right] \mathrm{d}\sigma_{\boldsymbol{y}} \tag{4.6b}$$

$$I_3 = \int_{S_\varepsilon} \left[G_e^+(\boldsymbol{x},\boldsymbol{y}) \frac{\partial p_e^+(\boldsymbol{y})}{\partial n} - p_e^+(\boldsymbol{y}) \frac{\partial G_e^+(\boldsymbol{x},\boldsymbol{y})}{\partial n_{\boldsymbol{y}}} \right] \mathrm{d}\sigma_{\boldsymbol{y}} \tag{4.6c}$$

$$I_4 = \int_{\Gamma_L} \left[G_e^+(\boldsymbol{x},\boldsymbol{y}) \frac{\partial p_e^+(\boldsymbol{y})}{\partial n} - p_e^+(\boldsymbol{y}) \frac{\partial G_e^+(\boldsymbol{x},\boldsymbol{y})}{\partial n_{\boldsymbol{y}}} \right] \mathrm{d}\sigma_{\boldsymbol{y}} \tag{4.6d}$$

where the sets Γ_e^+ and Γ_H^+ are defined in Section 2.1, Γ_L was introduced in (3.93) and S_ε corresponds to the boundary of B_ε (i.e. a sphere with radius ε and center at $\boldsymbol{x}$).

Adding and subtracting $\alpha p_e^+ G_e^+$ to the functions in the integral (4.6a) and noting that on Γ_e^+ the functions G_e^+ and p_e^+ satisfy the homogeneous impedance boundary condition, we get that (4.6a) becomes in $I_1 = 0$.

Likewise, since $p_e^+ = p_i$ on Γ_H^+ and G_e^+ satisfies the homogeneous Dirichlet boundary condition on Γ_H^+, the integral in (4.6b) becomes in

$$I_2 = -\int_{\Gamma_H^+} p_i(\boldsymbol{y}) \frac{\partial G_e^+(\boldsymbol{x},\boldsymbol{y})}{\partial n_{\boldsymbol{y}}} \mathrm{d}\sigma_{\boldsymbol{y}}. \tag{4.7}$$

Subsequently, by means of (3.98) we get that G_e^+ can be expressed as

$$G_e^+(\boldsymbol{x},\boldsymbol{y}) = \Phi(\boldsymbol{x}-\boldsymbol{y}) + \Psi(\boldsymbol{x},\boldsymbol{y}), \tag{4.8}$$

where Φ is the fundamental solution of the Helmholtz operator and $\Psi : \Omega_e^+ \times \Omega_e^+ \mapsto \mathbb{C}$ is a continuous function. Hence, from Nédélec (2001), Chapter 3, we know that

$$\lim_{\varepsilon\to 0}\int_{S_\varepsilon} \Phi(\boldsymbol{x}-\boldsymbol{y})\frac{\partial p_e^+(\boldsymbol{y})}{\partial n}\,\mathrm{d}\sigma_{\boldsymbol{y}} = 0 \tag{4.9a}$$

$$\lim_{\varepsilon\to 0}\int_{S_\varepsilon} p_e^+(\boldsymbol{y})\frac{\partial \Phi(\boldsymbol{x}-\boldsymbol{y})}{\partial n_{\boldsymbol{y}}}\,\mathrm{d}\sigma_{\boldsymbol{y}} = p_e^+(\boldsymbol{x}) \tag{4.9b}$$

and since Ψ is a continuos function, we have

$$\lim_{\varepsilon\to 0}\int_{S_\varepsilon} \Psi(\boldsymbol{x},\boldsymbol{y})\frac{\partial p_e^+(\boldsymbol{y})}{\partial n}\,\mathrm{d}\sigma_{\boldsymbol{y}} = 0 \tag{4.10a}$$

$$\lim_{\varepsilon\to 0}\int_{S_\varepsilon} p_e^+(\boldsymbol{y})\frac{\partial \Psi(\boldsymbol{x},\boldsymbol{y})}{\partial n_{\boldsymbol{y}}}\,\mathrm{d}\sigma_{\boldsymbol{y}} = 0. \tag{4.10b}$$

Using (4.9) and (4.10), we can compute the limit of (4.6c) as ε tends to zero, which is

$$\lim_{\varepsilon\to 0} I_3 = -p_e^+(\boldsymbol{x}). \tag{4.11}$$

From the previous chapter we know that when $\mathfrak{Im}\,\alpha > 0$ or $\mathfrak{Im}\,k > 0$, both the Green's function and its derivatives, decay exponentially in the direction of the waveguide. Therefore it is easy to see that

$$\lim_{L\to\infty} I_4 = 0. \tag{4.12}$$

However, when $\mathfrak{Im}\,\alpha = \mathfrak{Im}\,k = 0$, this statement is no longer true and we have to introduce a radiation condition to p_e^+. The suitable radiation condition for p_e^+ is

$$\lim_{L\to\infty}\int_{\Gamma_L}\left\{\frac{\partial p_e^+}{\partial z} - \mathrm{i}\,k_{n,m}p_e^+\right\}\mathrm{e}^{\mathrm{i}\,n\theta}\varphi_{n,m}(r)\,\mathrm{d}\sigma = 0, \quad \forall (n,m)\in\Lambda. \tag{4.13}$$

which is the shown in (3.97), the same that G_e^+ satisfies. Let us remark that the numbers $k_{n,m}$ with $(n,m) \in \mathbb{N}_0 \times \mathbb{N}$, are defined in (3.71) while the set of indices Λ is defined in (3.90). To take into consideration the radiation condition we express I_4 as the sum of two series; one containing the evanescent modes of the Green's function and the other

containing the propagative modes, i.e.,

$$\begin{aligned} I_4 \;=\; & -\frac{\mathrm{i}}{2\pi} \sum_{(n,m)\in(\mathbb{N}_0\times\mathbb{N})\setminus\Lambda} \epsilon_n \varphi_{n,m}(\rho) \frac{\sin(k_{n,m}(\zeta-H))\,\mathrm{e}^{\mathrm{i}\,k_{n,m}(L-H)}}{k_{n,m}} \\ & \qquad \times \int_{\Gamma_L} \left\{ \frac{\partial p_e^+}{\partial z} - \mathrm{i}\,k_{n,m} p_e^+ \right\} \cos(n(\theta-\vartheta)) \varphi_{n,m}(r)\,\mathrm{d}\sigma_{\boldsymbol{y}} \\ & -\frac{\mathrm{i}}{2\pi} \sum_{(n,m)\in\Lambda} \epsilon_n \varphi_{n,m}(\rho) \frac{\sin(k_{n,m}(\zeta-H))\,\mathrm{e}^{\mathrm{i}\,k_{n,m}(L-H)}}{k_{n,m}} \\ & \qquad \times \int_{\Gamma_L} \left\{ \frac{\partial p_e^+}{\partial z} - \mathrm{i}\,k_{n,m} p_e^+ \right\} \cos(n(\theta-\vartheta)) \varphi_{n,m}(r)\,\mathrm{d}\sigma_{\boldsymbol{y}}. \end{aligned} \tag{4.14}$$

Then, as $\mathrm{i}\,k_{n,m} < 0$ when $(n,m) \notin \Lambda$, we get that the first sum tends to zero as L goes to infinity. On the other hand, the second sum tends to zero too, due to the radiation condition (4.13).

Finally, from the results obtained above we find that (4.3) becomes in

$$p_e^+(\boldsymbol{x}) = -\int_{\Gamma_H^+} p_i(\boldsymbol{y}) \frac{\partial G_e^+(\boldsymbol{x},\boldsymbol{y})}{\partial n_{\boldsymbol{y}}}\,\mathrm{d}\sigma_{\boldsymbol{y}}, \quad \forall \boldsymbol{x} \in \Omega_e^+, \tag{4.15}$$

when L and ε tend to infinity and zero respectively. The relaxation of the condition $p_e^+ \in C^2(\Omega_e^+) \cap C^1(\overline{\Omega_e^+})$ to $p_e^+ \in H_{loc}(\Omega_e^+)$ stems straightforwardly from the density argument.

From (4.4) we have that the normal derivative in (4.15) can be computed in the following way:

$$\frac{\partial G_e^+}{\partial n_{\boldsymbol{y}}} = -\lim_{z\to H^+} \frac{\partial G_e^+}{\partial z}. \tag{4.16}$$

Therefore, under the assumption $\alpha \neq \pm\sqrt{n^2/R^2 - z_{n,m}^2}$ and the uniform convergence of the series that defines the Green's function, we get that

$$\frac{\partial G_e^+}{\partial n_{\boldsymbol{y}}} = -\frac{1}{2\pi} \sum_{n=0}^{\infty} \sum_{m=1}^{\infty} \epsilon_n \cos(n(\theta-\vartheta)) \varphi_{n,m}(r) \varphi_{n,m}(\rho)\,\mathrm{e}^{\mathrm{i}\,k_{n,m}(\zeta-H)}, \tag{4.17}$$

and so the integral representation of the exterior solution, (4.15), becomes in the series

$$p_e^+(\rho,\vartheta,\zeta) = \frac{1}{2\pi} \sum_{n=0}^{\infty}\sum_{m=1}^{\infty} \epsilon_n \varphi_{n,m}(\rho)\,\mathrm{e}^{\mathrm{i}\,k_{n,m}(\zeta-H)} \int_0^R \int_0^{2\pi} p_i(r,\theta,H) \cos(n(\theta-\vartheta)) \varphi_{n,m}(r) r\,\mathrm{d}\theta\,\mathrm{d}r, \tag{4.18}$$

which is valid for all $\rho \in [0, R),\ \vartheta \in [0, 2\pi)$, $\zeta > H$ and $k_{n,m} \neq 0$.

In a completely analogous way, applying the Green's theorem to p_e^- and G_e^- instead p_e^+ and G_e^+, and taking into account the radiation condition

$$\lim_{L\to-\infty} \int_{\Gamma_L} \left\{ \frac{\partial p_e^-}{\partial z} + \mathrm{i}\, k_{n,m} p_e^- \right\} \mathrm{e}^{\mathrm{i}\, n\theta} \varphi_{n,m}(r)\, \mathrm{d}\sigma = 0, \quad \forall (n,m) \in \Lambda. \tag{4.19}$$

we obtain the following representation for p_e^-

$$p_e^-(\boldsymbol{x}) = -\int_{\Gamma_H^-} p_i(\boldsymbol{y}) \frac{\partial G_e^-(\boldsymbol{x}, \boldsymbol{y})}{\partial n_{\boldsymbol{y}}}\, \mathrm{d}\sigma_{\boldsymbol{y}}, \quad \forall \boldsymbol{x} \in \Omega_e^-, \tag{4.20}$$

which becomes in

$$p_e^-(\rho,\vartheta,\zeta) = \frac{1}{2\pi} \sum_{n=0}^{\infty} \sum_{m=1}^{\infty} \epsilon_n \varphi_{n,m}(\rho)\, \mathrm{e}^{-\mathrm{i}\, k_{n,m}(\zeta+H)} \int_0^R \int_0^{2\pi} p_i(r,\theta,H) \cos(n(\theta-\vartheta)) \varphi_{n,m}(r) r\, \mathrm{d}\theta\, \mathrm{d}r, \tag{4.21}$$

if $\alpha \neq \pm\sqrt{n^2/R^2 - z_{n,m}^2}$. This representation is valid for all $\rho \in [0, R),\ \vartheta \in [0, 2\pi)$, $\zeta < -H$ and $k_{n,m} \neq 0$.

4.2 Dirichlet-to-Neumann map

Now we are in position to introduce the pseudodifferential operator that maps the trace of the solution of the interior problems (2.25) and (2.29) on Γ_H^+, into its normal derivative on Γ_H^+. More specifically, we seek for the map defined by

$$\begin{aligned} \mathcal{DN}^+ : H^{1/2}(\Gamma_H^+) &\to H^{-1/2}(\Gamma_H^+) \\ p_i|_{\Gamma_H^+} &\mapsto \frac{\partial p_i}{\partial n} \text{ on } \Gamma_H^+. \end{aligned}$$

This operator is the so-called DtN map, sometimes named Steklov-Poincaré and Carderòn operator. To obtain the explicit formula that defines it, we observe that from the problem decomposition made in Section 2.4, on Γ_H^+ the normal derivative of p_i and p_e^+ are equal. Thus, as the the representation of upper exterior solution (4.15) gives the exact solution of either (2.27) or (2.31), we can easily compute the normal derivative of p_e^+ on Γ_H^+ and replace it in (2.25) and (2.25) respectively, obtaining the following abstract form of the DtN

map

$$\frac{\partial p_i(\boldsymbol{x})}{\partial n_{\boldsymbol{x}}} = -\frac{\partial}{\partial n_{\boldsymbol{x}}} \left\{ \int_{\Gamma_H^+} p_i(\boldsymbol{y}) \frac{\partial G_e^+(\boldsymbol{x}, \boldsymbol{y})}{\partial n_{\boldsymbol{y}}} \, \mathrm{d}\sigma_{\boldsymbol{y}} \right\}, \quad \forall \boldsymbol{x} \in \Gamma_H^+. \tag{4.22}$$

Therefore, assuming that $\alpha \neq \pm\sqrt{n^2/R^2 - z_{n,m}^2}$ and performing the formula (4.22), i.e. taking derivative with respect to ζ on both sides of (4.18) and evaluating the resultant equation at $\zeta = H$, we obtain

$$\frac{\partial p_e^+}{\partial n} = \frac{\mathrm{i}}{2\pi} \sum_{n=0}^{\infty} \sum_{m=1}^{\infty} \epsilon_n k_{n,m} \varphi_{n,m}(\rho) \int_0^R \int_0^{2\pi} p_i(r, \theta, H) \cos(n(\theta - \vartheta)) \varphi_{n,m}(r) r \, \mathrm{d}\theta \, \mathrm{d}r \tag{4.23}$$

where the normal derivative must be interpreted as the normal derivative on Γ_H^+, with n outward pointing with respect to Ω_i. It stems from (4.23) that the DtN map for Γ_H^+ can be defined by

$$\begin{cases} \mathcal{DN}^+ : H^{1/2}(\Gamma_H^+) \mapsto H^{-1/2}(\Gamma_H^+) \\ \left[\mathcal{DN}^+ p_i\right](\rho, \vartheta) = \dfrac{\mathrm{i}}{2\pi} \displaystyle\sum_{m=1}^{+\infty} \sum_{n=0}^{+\infty} \epsilon_n k_{n,m} \varphi_{n,m}(\rho) \\ \qquad\qquad \times \displaystyle\int_0^R \int_0^{2\pi} p_i(r, \theta, H) \cos(n(\theta - \vartheta)) \varphi_{n,m}(r) r \, \mathrm{d}\theta \, \mathrm{d}r \end{cases} \tag{4.24}$$

when the condition $\alpha \neq \pm\sqrt{n^2/R^2 - z_{n,m}^2}$ holds.

Analogously, an abstract form of the DtN map for Γ_H^- can be obtained from the formula (4.20) and a explicit formula given by

$$\begin{cases} \mathcal{DN}^- : H^{1/2}(\Gamma_H^-) \mapsto H^{-1/2}(\Gamma_H^-) \\ \left[\mathcal{DN}^- p_i\right](\rho, \vartheta) = \dfrac{\mathrm{i}}{2\pi} \displaystyle\sum_{m=1}^{+\infty} \sum_{n=0}^{+\infty} \epsilon_n k_{n,m} \varphi_{n,m}(\rho) \\ \qquad\qquad \times \displaystyle\int_0^R \int_0^{2\pi} p_i(r, \theta, -H) \cos(n(\theta - \vartheta)) \varphi_{n,m}(r) r \, \mathrm{d}\theta \, \mathrm{d}r \end{cases} \tag{4.25}$$

can be found when the condition $\alpha \neq \pm\sqrt{n^2/R^2 - z_{n,m}^2}$ holds.

Finally, let us observe that the DtN maps are well defined for every physically correct wave number, thus we remove the condition $k \neq \sqrt{\lambda_{n,m}}$ defining by the function zero the value that the DtN maps take when $k = \sqrt{\lambda_{n,m}}$.

4.3 Variational formulation

From the definition of the DtN maps, (4.24) and (4.25), we get that all the information that the exterior problems set on the interior problem through the artificial boundaries, may by supplied by the DtN maps and thus we are able to uncouple them obtaining an uncoupled problem defined on a bounded computational domain. Consequently, using the DtN maps we can redefine the interior scattering problem (2.25) as follows

$$\begin{cases} \Delta p_i + k^2 p_i &= 0, & \text{in } \Omega_i \setminus \overline{\Omega_d}, \\ \dfrac{\partial p_i}{\partial n} - \alpha\, p_i &= 0, & \text{on } \Gamma_i, \\ \dfrac{\partial p_i}{\partial n} &= g, & \text{on } \Gamma_d, \\ \dfrac{\partial p_i}{\partial n} &= \mathcal{DN}^-\, p_i, & \text{on } \Gamma_H^-, \\ \dfrac{\partial p_i}{\partial n} &= \mathcal{DN}^+\, p_i, & \text{on } \Gamma_H^+. \end{cases} \tag{4.26}$$

As (4.26) is defined on a bounded domain, it is suitable to develop some numerical algorithms to solve it. Thus, with the finite element method in sight, we perform the variation formulation of this problem.

Multiplying the Helmholtz equation in (4.26) by the complex conjugate of a test function $q \in H^1(\Omega_i \setminus \overline{\Omega_d})$ we obtain

$$\int_{\Omega_i \setminus \overline{\Omega_d}} \left(\Delta p_i + k^2 p_i\right) \overline{q}\, \mathrm{d}\boldsymbol{x} = 0.$$

Using the first Green's identity we get that

$$\int_{\Omega_i \setminus \overline{\Omega_d}} (\Delta p_i + k^2 p_i)\overline{q}\, \mathrm{d}\boldsymbol{x} = \int_{\partial\Omega_i \cup \partial\Omega_d} \overline{q}\, \frac{\partial p_i}{\partial n}\, \mathrm{d}\sigma - \int_{\Omega_i \setminus \overline{\Omega_d}} \left(\nabla \overline{q} \cdot \nabla p_i - k^2 \overline{q}\, p_i\right) \mathrm{d}\boldsymbol{x}.$$

Then, noting that on each part of the boundary $\partial\Omega_i \cup \partial\Omega_d = \Gamma_H^- \cup \Gamma_H^+ \cup \Gamma_i \cup \Gamma_d$, there is a different boundary condition, we replace the normal derivative in the boundary integrals, by the correspondent term to achieve that

$$\int_{\partial\Omega_i \cup \partial\Omega_d} \overline{q}\, \frac{\partial p_i}{\partial n}\, \mathrm{d}\sigma = \int_{\Gamma_H^+} \overline{q}\, \mathcal{DN}^+ p_i\, \mathrm{d} + \int_{\Gamma_H^-} \overline{q}\, \mathcal{DN}^- p_i\, \mathrm{d}\sigma + \int_{\Gamma_d} \overline{q} g\, \mathrm{d}\sigma + \int_{\Gamma_i} \alpha\, \overline{q}\, p_i\, \mathrm{d}\sigma,$$

Therefore, the variational or weak formulation of (4.26) is

$$\begin{cases} \text{Find } p_i \in H^1(\Omega_i \setminus \overline{\Omega_d}) \text{ such that:} \\ a(p_i, q) \;\; = \;\; b(q), \quad \forall q \in H^1(\Omega_i \setminus \overline{\Omega_d}) \end{cases} \tag{4.27}$$

where

$$a(p_i, q) \;\; := \;\; \int_{\Omega_i \setminus \overline{\Omega_d}} \left(k^2 \overline{q}\, p_i - \nabla \overline{q} \cdot \nabla p_i\right)\, \mathrm{d}\boldsymbol{x} + \int_{\Gamma_i} \alpha\, \overline{q}\, p_i\, \mathrm{d}\sigma + \int_{\Gamma_H^+} \overline{q}\, \mathcal{DN}^+ p_i\, \mathrm{d}\sigma + \int_{\Gamma_H^-} \overline{q}\, \mathcal{DN}^- p_i\, \mathrm{d}\sigma \tag{4.28a}$$

$$b(q) \;\; := \;\; -\int_{\Gamma_d} \overline{q} g\, \mathrm{d}\sigma. \tag{4.28b}$$

In an analog way we can obtain the variational formulation of the resonance problem (2.28), which thanks to the DtN maps can be equivalently expressed as follows:

Find an angular frequency $\omega \in \mathbb{R}_+$ that leads to a wave number $k \neq 0$ and to a non identically zero function $p_i \in H^1(\Omega_i \setminus \overline{\Omega_d})$, such that:

$$\begin{cases} \Delta p_i + k^2 p_i \;\; = \;\; 0 \quad \text{in} \quad \Omega_i \setminus \overline{\Omega_d}, \\ \dfrac{\partial p_i}{\partial n} - \alpha p_i \;\; = \;\; 0 \quad \text{on} \quad \Gamma_d, \\ \dfrac{\partial p_i}{\partial n} \;\; = \;\; 0 \quad \text{on} \quad \Gamma_i, \\ \dfrac{\partial p_i}{\partial n} \;\; = \;\; \mathcal{DN}^+ p_i \quad \text{on} \quad \Gamma_h^+, \\ \dfrac{\partial p_i}{\partial n} \;\; = \;\; \mathcal{DN}^- p_i \quad \text{on} \quad \Gamma_h^-, \end{cases} \tag{4.29}$$

It comes from the variational formulation of the scattering problem (4.27), that the variational formulation of (4.29) can be written as:

$$\begin{cases} \text{Find } \omega \in \mathbb{R}_+ \text{ that leads to } k \neq 0 \text{ and } 0 \neq p_i \in H^1(\Omega_i \setminus \overline{\Omega_d}), \text{ such that:} \\ \\ a(p_i, q) \;\; = \;\; 0, \quad \forall q \in H^1(\Omega_i \setminus \overline{\Omega_d}) \end{cases} \tag{4.30}$$

where a is defined in (4.28a).

Axisymmetric problems. Let us observe that if the boundary datum g and the domains Ω_i and Ω_d present azimuthal symmetry in $\mathbb{R}^3$, i.e. they do not depend on the angular variable in cylindrical coordinates, it is expected to obtain a solution of (4.26) that does not depend on the angular variable too. Therefore, under these assumptions, the variational formulation of (4.26) can be rewritten as

$$\begin{cases} \text{Find } p_i \in H^1(\widetilde{\Omega}_i \setminus \widetilde{\Omega}_d) \text{ such that:} \\ \\ a(p_i, q) \;\; = \;\; b(q), \quad \forall q \in H^1(\widetilde{\Omega}_i \setminus \widetilde{\Omega}_d) \end{cases} \tag{4.31}$$

in which the bilinear form a and the linear functional b are:

$$\begin{aligned} a(p_i, q) \;\; &:= \;\; 2\pi \left\{ \int_{\widetilde{\Omega}_i \setminus \widetilde{\Omega}_d} \left(k^2 \overline{q}\, p_i - \nabla \overline{q} \cdot \nabla p_i \right) r \, \mathrm{d}\sigma + \int_{\widetilde{\Gamma}_i} \alpha\, \overline{q}\, p_i r \, \mathrm{d}\gamma \right. \qquad (4.32a) \\ &\qquad \left. + \int_{\widetilde{\Gamma}_H^+} \overline{q}\, \mathcal{DN}^+ p_i r \, \mathrm{d}\gamma + \int_{\widetilde{\Gamma}_H^-} \overline{q}\, \mathcal{DN}^- p_i r \, \mathrm{d}\gamma \right\} \\ b(q) \;\; &:= \;\; -2\pi \int_{\widetilde{\Gamma}_d} \overline{q} g r \, \mathrm{d}\gamma, \qquad (4.32b) \end{aligned}$$

where the modified domains (in two dimensions) involved are

$$\widetilde{\Omega}_i := \left\{(r,z) \in \mathbb{R}^2 : (r\cos(\theta), r\sin(\theta), z) \in \Omega_i, r > 0, \forall\theta \in [0, 2\pi)\right\}, \quad (4.33a)$$

$$\widetilde{\Omega}_d := \left\{(r,z) \in \mathbb{R}^2 : (r\cos(\theta), r\sin(\theta), z) \in \Omega_d, r > 0, \forall\theta \in [0, 2\pi)\right\}, \quad (4.33b)$$

$$\widetilde{\Gamma}_i := \left\{(r,z) \in \mathbb{R}^2 : (r\cos(\theta), r\sin(\theta), z) \in \Gamma_i, r > 0, \forall\theta \in [0, 2\pi)\right\}, \quad (4.33c)$$

$$\widetilde{\Gamma}_d := \left\{(r,z) \in \mathbb{R}^2 : (r\cos(\theta), r\sin(\theta), z) \in \Gamma_d, r > 0, \forall\theta \in [0, 2\pi)\right\}, \quad (4.33d)$$

$$\widetilde{\Gamma}_H^- := \left\{(r,z) \in \mathbb{R}^2 : (r\cos(\theta), r\sin(\theta), z) \in \Gamma_H^-, r > 0, \forall\theta \in [0, 2\pi)\right\}, \quad (4.33e)$$

$$\widetilde{\Gamma}_H^+ := \left\{(r,z) \in \mathbb{R}^2 : (r\cos(\theta), r\sin(\theta), z) \in \Gamma_H^+, r > 0, \forall\theta \in [0, 2\pi)\right\}, \quad (4.33f)$$

and the DtN maps involved become

$$\begin{cases} \mathcal{DN}^+ : H^{1/2}(\Gamma_H^+) \mapsto H^{-1/2}(\Gamma_H^+) \\ \left[\mathcal{DN}^+ p_i\right](\rho) = \dfrac{\mathrm{i}}{2\pi} \displaystyle\sum_{m=1}^{+\infty} k_{n,m}\varphi_{0,m}(\rho) \int_0^R p_i(r,0,H)\varphi_{0,m}(r) r \,\mathrm{d}r \end{cases} \quad (4.34)$$

and

$$\begin{cases} \mathcal{DN}^- : H^{1/2}(\Gamma_H^-) \mapsto H^{-1/2}(\Gamma_H^-) \\ \left[\mathcal{DN}^- p_i\right](\rho) = \dfrac{\mathrm{i}}{2\pi} \displaystyle\sum_{m=1}^{+\infty} k_{n,m}\varphi_{0,m}(\rho) \int_0^R p_i(r,0,-H)\varphi_{0,m}(r) r \,\mathrm{d}r \end{cases} \quad (4.35)$$

in virtue of the azimuthal symmetry of interior solution. It is important to observe that here $\mathrm{d}\sigma$ represents a element of area in the RZ-plane and $\mathrm{d}\gamma$ represents a line element in the same plane.

Under the assumption of axisymmetric domains, Ω_i and Ω_d, a similar procedure may be carried out for (4.29). However, under these conditions, we can only expect to find the resonance frequencies that lead to axisymmetric resonance states, i.e. functions p_i that do not depend on the angular variable.

V. NUMERICAL PROCEDURES

5.1 Computing the poles of the spectral Green's function

In this section we state some basic procedures to obtain numerical evaluations of the Green's function (3.68). To do that, we present two different methods to compute the zeros of $D_n(\cdot, \alpha)$ (which is defined in 3.27), based on standard algorithms for finding roots of real valued function when the impedance parameter is real, and based on the finite element method when the impedance parameter is a proper complex number. We are particularly interested in obtaining accurate approximations for the smallest $z_{n,m}$, since the bigger ones can be approximated by the asymptotic formula obtained in the Proposition III.2. Also, we develop a numerical procedure to compute the non-simple roots of $D_n(\cdot, \alpha)$, reported in the Subsection 3.4.1.

5.1.1 Real impedance case

As discussed above, in this case there is an infinite number of real positive roots of $D_n(\cdot, \alpha)$ and only one purely imaginary root in the positive imaginary axis. Consequently, the search of the imaginary root does not present difficulties because there are standard methods to solve that kind of problems. However, the search of the positive real roots produce more complications. To face them, let us note that the equation $D_n(z, \alpha) = 0$ can be expressed as

$$F_n(z) = \alpha, \tag{5.1}$$

so that to achieve a good approximation of $z_{n,m}$ we have to compute the intersection points of the horizontal line $w = \alpha$ and the real valued function $w = F_n(z)$. Thus, since $F_n'(z) < 0$ for all $0 < z \neq j_{n,m}/R$ and $n > -1$ (cf. Landau 1999) and F_n has poles in $j_{n,m}$, we have that there is at most one intersection point in every interval $[j_{n,m}/R, j_{m+1,n}/R]$. So that, to obtain the positive real roots of $D_n(\cdot, \alpha)$ we only have to search them in every interval $[j_{n,m}/R, j_{m+1,n}/R]$. Figure 5.1 shows the location of $z_{n,m}$ for $\alpha = 2.5,\ R = 1$ and $n = 1$.

From a numerical point of view, to obtain the value of $z_{n,m}$ we need first to have $j_{n,m}$, the positive zeros of the Bessel function $J_n(x)$. To compute them there are several efficient

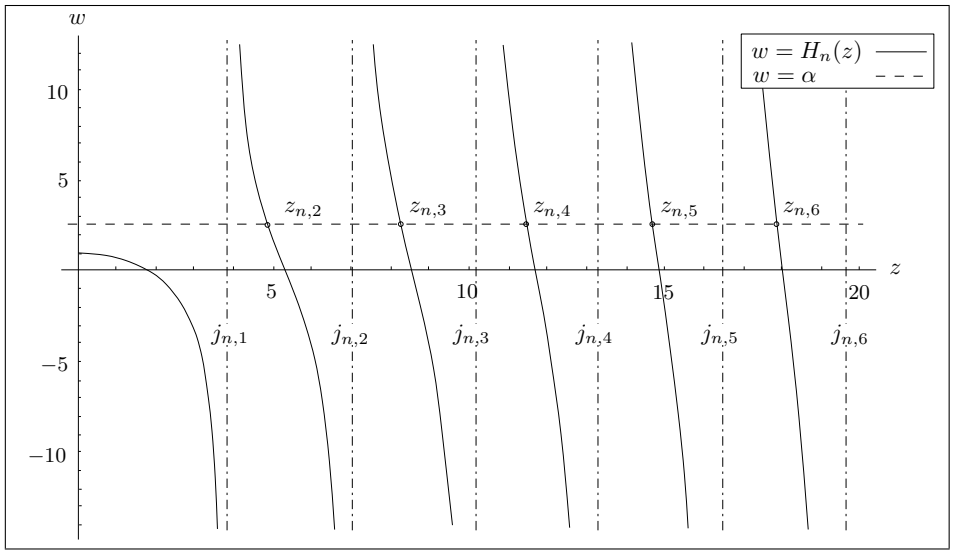

FIGURE 5.1. Roots of the Dini function for a real impedance parameter

numerical methods. Some of them are found in Segura & Gil (1999) and Vrahatis et al. (1995). Once the numbers $j_{n,m}$ are achieved, we may obtain $z_{n,m}$ using standard algorithms for finding zeros of functions that change their sign once in a given interval, such as are found in Brent (1973) (which is implemented in MATLAB).

5.1.2 Complex impedance case

When the impedance parameter is a proper complex number we can not use the method described above because nothing guarantees that the zeros are real. In fact, they have a non-zero imaginary part as can be seen from Figure 5.2, which shows the location of $z_{n,m}$ for $\alpha = 2.5 + \mathrm{i}\,,\ R = 1$ and $n = 1$. Consequently, we have to face the problem of finding $z_{n,m}$ on the whole complex plane.

To find these values we appeal to the Bessel differential equation. Let us note that the zeros of $D_n(\cdot, \alpha)$ can be characterized as the eigenvalues of the following differential

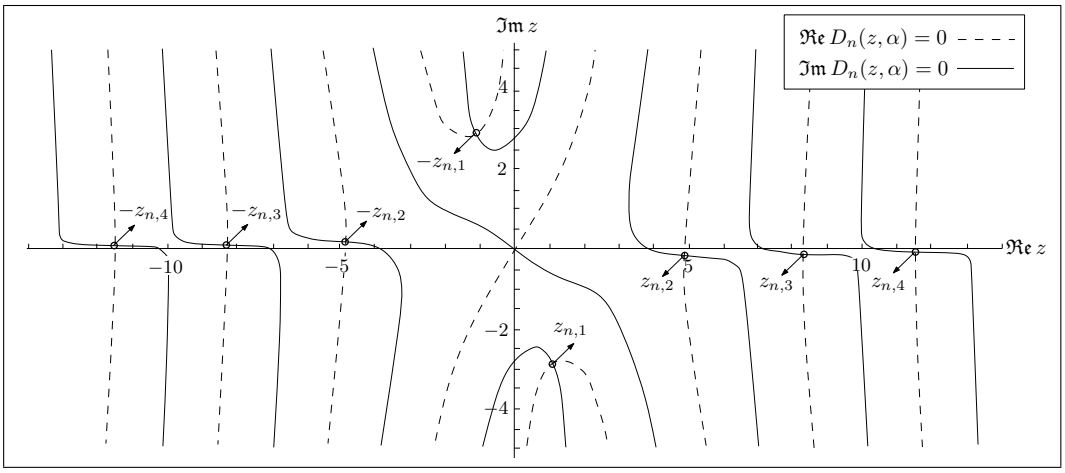

FIGURE 5.2. Roots of the Dini function for a complex impedance parameter.

problem for $\varphi \in C^1[0,R] \cap C^2(0,R)$

$$\begin{cases} -\left(r\varphi'\right)' + \dfrac{n^2}{r}\varphi &= r\lambda\varphi, \quad 0 < r < R \\ \varphi' - \alpha\varphi &= 0, \qquad r = R \\ \lim\limits_{r\to 0^+} \varphi(r) &< \infty. \end{cases} \tag{5.2}$$

where the eigenvalues and the eigenfunctions are $\lambda = z_{n,m}^2$ and $\varphi_{n,m}$, respectively, and where the functions $\varphi_{n,m}$ are defined in (3.87) and (3.88).

To achieve the numerical values of $z_{n,m}$, we transform the differential eigenvalue problem (5.2) into a generalized matrix eigenvalue problem by means of the finite element method or the finite difference method. To employ the finite element method, we discretize the interval $(0,R)$ at N regular subintervals $[r_n, r_{n+1}]$ of length $h = R/N$ where $r_n = nR/N$, $0 \leqslant n \leqslant N$, and we construct basis functions that are linear at every subinterval and satisfy $\psi_n(r_m) = \delta_{n,m}$. Thus, multiplying (5.2) by $r\psi \in H^1(0,R)$ and using integration by parts, the variational formulation is obtained. Next, making use of the Galerkin method with basis functions ψ_n, the discretized version of (5.2) is achieved and it

reads as follows:

$$\begin{cases} \text{Find } 0 \neq \lambda^{(h)} \in \mathbb{C} \text{ and } \mathbf{0} \neq \mathbf{x} \in \mathbb{C}^N \text{ such that:} \\ \\ \mathbf{A}_n\mathbf{x} \;\; = \;\; \lambda^{(h)}\mathbf{B}\mathbf{x}, \end{cases} \tag{5.3}$$

where the matrices $\mathbf{A}_n$, $\mathbf{B} \in \mathbb{C}^{N\times N}$ are defined by:

$$\begin{aligned} [\mathbf{A}_n]_{i,j} &= -\alpha R^2\psi_i(R)\psi_j(R) + \int_0^R r^2\psi_i\psi_j' \,\mathrm{d}r + n^2\int_0^R \psi_i\psi_j \,\mathrm{d}r, \quad i,j = 1,\ldots,N, \\ [\mathbf{B}]_{i,j} &= \int_0^R r^2\psi_i(r)\psi_j(r)\,\mathrm{d}r, \qquad\qquad\qquad\qquad\qquad\qquad\quad i,j = 1,\ldots,N. \end{aligned} \tag{5.4}$$

The generalized matrix eigenvalue problem (5.3) can be solved with ARPACK (or the MATLAB version of it implemented in the function `eigs.m`) to obtain the eigenvalues $\lambda^{(h)}$ with smallest absolute value. They correspond to the first N smallest approximate zeros of $D_n(\cdot,\alpha)$ and are denoted by $z_{n,m}^{(h)} = \sqrt{\lambda^{(h)}}$. Table 5.1 shows the results for the particular cases $n = 1,, 2, 3$ and 4, where the error is measured by $|D_n(z_{n,m}^{(h)},\alpha)|$.

Finally, plots of the Green's function for real and complex impedance case are shown in Figures 5.3 (for $\alpha = 2.5$) and 5.4 (for $\alpha = 2.5 + \mathrm{i}$) respectively, for $k = 5$, $R = 1$ and $\boldsymbol{y} = (0, 0.5, 0)$, where series representation of G is truncated at $m = n = 40$. The Figure 5.5 shows a plot of sum of the surface wave modes that compose the series representation of Green's function for the parameters $k = 5$, $\alpha = 2.5$, $R = 1$ and $\boldsymbol{y} = (0, 0.5, 0)$. In this case, there are only three surface wave modes arising due to the purely imaginary roots of $D_n(\cdot,\alpha)$, given by $z_{0,1} = 3.0679\mathrm{i}\,, z_{1,1} = 2.7700\mathrm{i}$ and $z_{2,1} = 1.7868\mathrm{i}\,$.

5.1.3 Computation of the non-simple poles of the spectral Green's function

This section deals with the problem of achieving numerical values of the impedance parameters that lead to non-simple roots of $D_n(\cdot,\alpha)$. According to the Subsection 3.4.1, to find them, we have to compute the solutions of the equation (3.36), i.e. to find complex numbers, $\alpha \in \mathbb{C}$, such that

$$f(\alpha) = 0, \tag{5.5}$$

TABLE 5.1. Numerical results of the finite element method applied to find the first five zeros of $D_n(\cdot,\alpha)$ for $R=1$, $n=0,1,2,3,4$ and $\alpha = 2.5+\mathrm{i}$. All the values were computed with $h=10^{-5}$.

n	m	$z_{n,m}^{(h)}$	$j_{n+1,m}/R$	$\lvert D_n(z_{n,m}^{(h)},\alpha)\rvert$
0	1	$0.9701-3.0594\mathrm{i}$	3.8317	$0.0834\cdot 10^{-5}$
	2	$3.1926-0.1935\mathrm{i}$	7.0156	$0.0055\cdot 10^{-5}$
	3	$6.6600-0.1322\mathrm{i}$	10.1735	$0.0025\cdot 10^{-5}$
	4	$9.9279-0.0950\mathrm{i}$	13.3237	$0.0057\cdot 10^{-5}$
	5	$13.1361-0.0736\mathrm{i}$	16.4706	$0.0042\cdot 10^{-5}$
1	1	$1.1116-2.8342\mathrm{i}$	5.1356	$0.5515\cdot 10^{-5}$
	2	$4.8468-0.1694\mathrm{i}$	8.4172	$0.0464\cdot 10^{-5}$
	3	$8.2396-0.1131\mathrm{i}$	11.6198	$0.0394\cdot 10^{-5}$
	4	$11.4909-0.0839\mathrm{i}$	14.7960	$0.0295\cdot 10^{-5}$
	5	$14.6947-0.0665\mathrm{i}$	17.9598	$0.0281\cdot 10^{-5}$
2	1	$1.5439-2.1842\mathrm{i}$	6.3802	$0.7108\cdot 10^{-5}$
	2	$6.2959-0.1511\mathrm{i}$	9.7610	$0.1933\cdot 10^{-5}$
	3	$9.7081-0.1009\mathrm{i}$	13.0152	$0.1558\cdot 10^{-5}$
	4	$12.9761-0.0762\mathrm{i}$	16.2235	$0.1356\cdot 10^{-5}$
	5	$16.1923-0.0613\mathrm{i}$	19.4094	$0.1206\cdot 10^{-5}$
3	1	$2.5572-1.4060\mathrm{i}$	7.5883	$0.5930\cdot 10^{-5}$
	2	$7.6507-0.1378\mathrm{i}$	11.0647	$0.4173\cdot 10^{-5}$
	3	$11.1088-0.0923\mathrm{i}$	14.3725	$0.3600\cdot 10^{-5}$
	4	$14.4068-0.0704\mathrm{i}$	17.6160	$0.3167\cdot 10^{-5}$
	5	$17.6441-0.0572\mathrm{i}$	20.8269	$0.2794\cdot 10^{-5}$
4	1	$3.8601-0.9877\mathrm{i}$	8.7715	$0.8437\cdot 10^{-5}$
	2	$8.9496-0.1277\mathrm{i}$	12.3386	$0.6867\cdot 10^{-5}$
	3	$12.4627-0.0858\mathrm{i}$	15.7002	$0.5919\cdot 10^{-5}$
	4	$15.7969-0.0660\mathrm{i}$	18.9801	$0.5265\cdot 10^{-5}$
	5	$19.0599-0.0540\mathrm{i}$	22.2178	$0.4756\cdot 10^{-5}$

where f is the complex map

$$\alpha \longmapsto \sqrt{n^2/R^2-\alpha^2}J_n'(\sqrt{n^2-\alpha^2R^2})-\alpha J_n(\sqrt{n^2-\alpha^2R^2}). \tag{5.6}$$

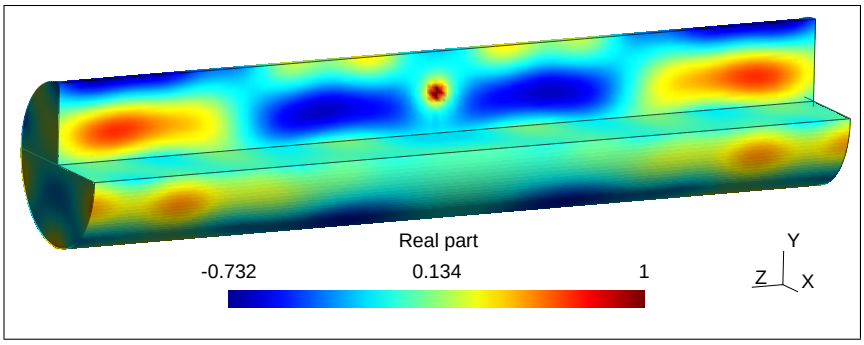

(a) $\mathfrak{Re}\, G$

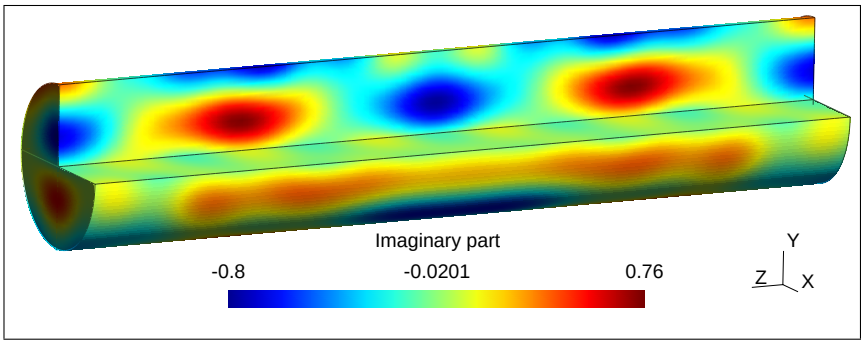

(b) $\mathfrak{Im}\, G$

FIGURE 5.3. Plot of the Green's function for a real impedance parameter.

Numerical procedures to obtain the values of $\alpha_{n,l}$ can be performed making use of the so-called *logarithmic residue based quadrature method*. Some references about this method are found in Delves & Lyness (1967), the paper that originated these kinds of methods, and in the book of Kravanja & Barel (2000), where big improvements of this algorithm are presented.

Herein we describe how to employ the Delves-Lyness algorithm to obtain such particular values of the impedance parameter. Therefore, first we have to identify the region in the complex plane where the function f is analytic. To do this, we observe that according to the physical meaning of the impedance boundary condition (see Chapter II), we only have to search for the values of α satisfying (3.36) in the upper complex plane, $\mathfrak{Im}\, \alpha \geqslant 0$. In order to identify it, we need to give an exact meaning to the square root in (5.6):

$$\alpha \longmapsto \sqrt{n^2 - \alpha^2 R}. \tag{5.7}$$

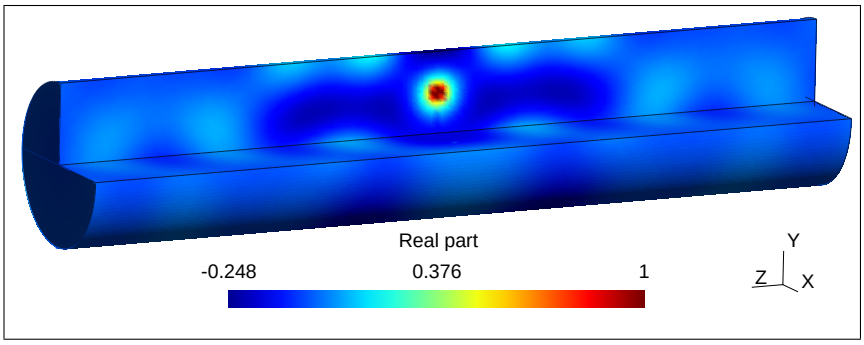

(a) $\mathfrak{Re}\, G$

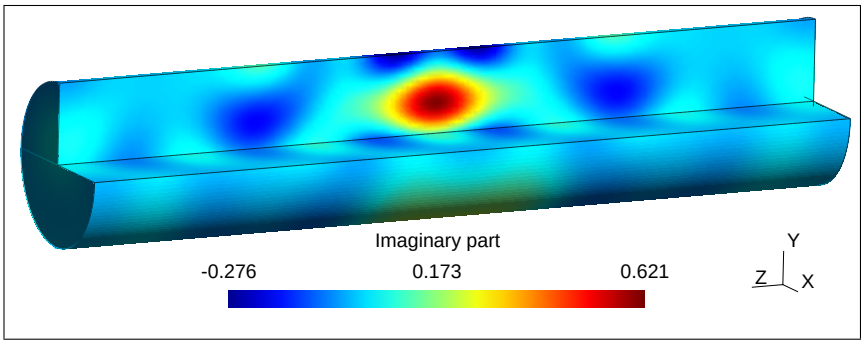

(b) $\mathfrak{Im}\, G$

FIGURE 5.4. Plot of the Green's function for a complex impedance parameter.

Then, we define $\sqrt{n^2 - \alpha^2 R}$ as the product between $\sqrt{n - \alpha R}$ and $\sqrt{n + \alpha R}$. The first root uses the analytic branch of the logarithm in the whole complex plane minus the non-negative imaginary axis; the second one uses an analytic branch of the logarithm in the whole complex plane minus the non-positive imaginary axis. Thus, the function in (5.7) is analytic in the simple connected region W, shown in Figure 5.6. Consequently, $f : W \to \mathbb{C}$ is analytic in the upper complex plane in virtue of the fact that W contains it and the Bessel functions $J_n(z)$ are analytic in the whole complex plane.

Now, let γ, a positively oriented Jordan curve in W that does not pass through any zero of f. We are interested in solving the problem of computing all the zeros of f that lie in the interior of γ. Then, let N_γ denotes the number of zeros of f enclosed by γ, i.e., the number of zeros where each zero is counted according to its multiplicity. Thus, from now we assume $N_\gamma > 0$ and the sequence $\alpha_{n,1}, \ldots, \alpha_{n,N_\gamma}$ represents the zeros of f that

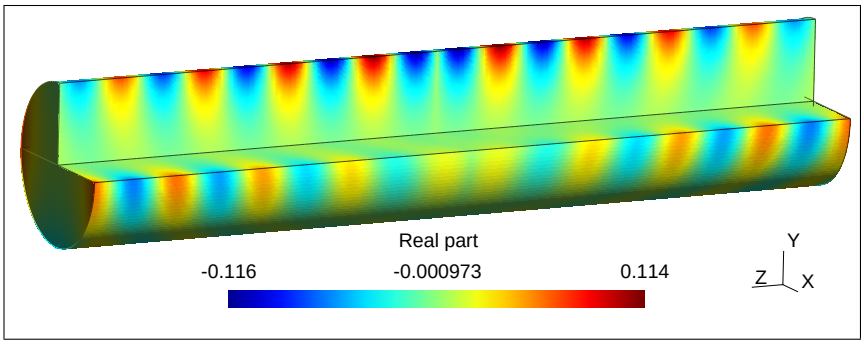

(a) $\mathfrak{Re}\, G$

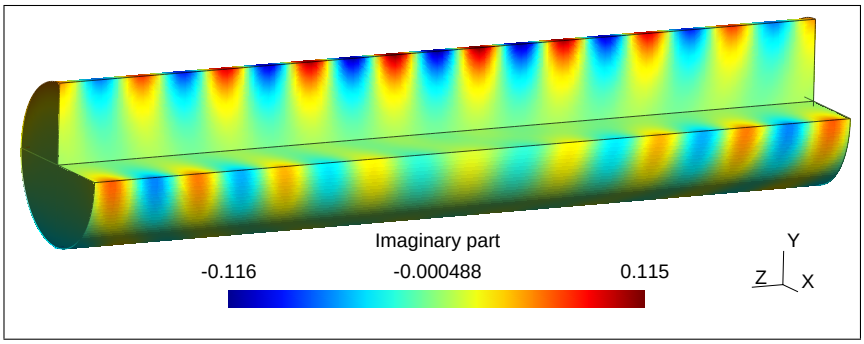

(b) $\mathfrak{Im}\, G$

FIGURE 5.5. Surface wave part of the Green's function.

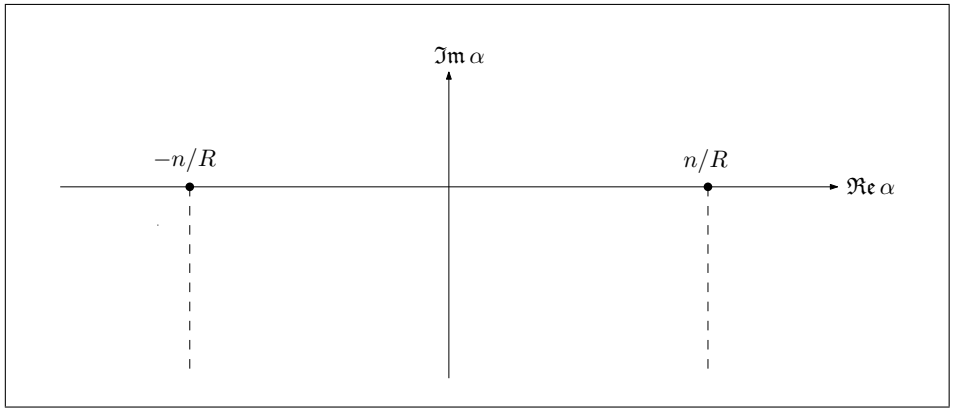

FIGURE 5.6. Domain of the complex square root function defined in (5.7).

lie inside γ. Each zero is repeated according to its multiplicity. Since f is analytic on and

inside γ, we obtain from the Cauchy theorem (cf. Silverman 1984) that

$$N_\gamma = \frac{1}{2\pi \mathrm{i}} \int_\gamma \frac{f'(\alpha)}{f(\alpha)} \, \mathrm{d}\alpha. \tag{5.8}$$

It allow us to obtain numerically, by quadrature methods, the number of zeros enclosed by γ. Likewise, employing numerical quadrature method, we compute the complex integrals

$$s_p = \frac{1}{2\pi \mathrm{i}} \int_\gamma \alpha^p \frac{f'(\alpha)}{f(\alpha)} \, \mathrm{d}\alpha, \;\; p = 1, \ldots, N_\gamma, \tag{5.9}$$

which by the residues theorem (cf. Silverman 1984), are

$$s_p = \alpha_{n,1}^p + \cdots + \alpha_{n,N_\gamma}^p, \;\; p = 1, \ldots, N_\gamma. \tag{5.10}$$

Subsequently, we construct a polynomial of degree N_γ that shares the zeros $\alpha_{n,1}, \ldots, \alpha_{n,N_\gamma}$ with f. Like Delves & Lyness (1967), we make use of the monic polynomial

$$P_{N_\gamma}(\alpha) = \prod_{l=1}^{N_\gamma} (\alpha - \alpha_{n,l}) = \alpha^{N_\gamma} + \sigma_1 \alpha^{N_{\gamma-1}} + \cdots + \sigma_{N_\gamma}.$$

where the coefficients that define it are given by the Newton's identities (Kravanja & Barel 2000)

$$\begin{aligned} s_1 + \sigma_1 &= 0 \\ s_2 + s_2\sigma_1 + 2\sigma_2 &= 0 \\ \vdots &\;\; \vdots \\ s_{N_\gamma} + s_{N_\gamma - 1}\sigma_1 + \cdots + s_1\sigma_{N_\gamma - 1} + N_\gamma \sigma_1 &= 0. \end{aligned} \tag{5.11}$$

Therefore, since (5.11) is a linear system of algebraic equations, it can be easily solved. Once we have computed these coefficients, we find the zeros of the polynomial P_{N_γ} obtaining an approximation of $\alpha_{n,1}, \ldots, \alpha_{n,N_\gamma}$. To do this, we employ some of the several highly efficient method for finding roots of polynomials, such as the one implemented in the function `roots.m` of MATLAB.

Table 5.2 shows the values of $\alpha_{n,l}$ for different n's, computed with the Delves-Lyness algorithm implemented in MATLAB. From these results we may notice that the non-simple

zero arising due to the impedance parameter $\alpha_{n,l}$, is the l-th root of $D_n(\cdot, \alpha_{n,l})$, i.e. $z_{n,m}$ with $m = l$.

Remark V.1. *Let us observe that the Delves-Lyness algorithm can be applied to compute the numbers $z_{n,m}$ in the case of a complex impedance parameter, instead the finite element method in one dimension described in the Subsection 5.1.2.*

TABLE 5.2. Numerical values of the first (in norm) five impedance parameters $\alpha_{n,l}$ leading to a non-simple root $z_{n,l}$ of the $D_n(\cdot, \alpha)$ computed with the Delves-Lyness algorithm for $R = 1$ and $n = 0, 1, 2, 3, 4$.

n	l	$\alpha_{n,l}$	$z_{n,l}$	$\lvert D_n(z_{n,l}, \alpha_{n,l})\rvert$	$\lvert D_n'(z_{n,l}, \alpha_{n,l})\rvert$
0	1	$1.2796 + 2.9804$i	$2.9804 - 1.2796$i	$0.0031 \cdot 10^{-6}$	$0.0031 \cdot 10^{-6}$
	2	$1.6187 + 6.1752$i	$6.1752 - 1.6187$i	$0.0281 \cdot 10^{-6}$	$0.0281 \cdot 10^{-6}$
	3	$1.8189 + 9.3420$i	$9.3420 - 1.8189$i	$0.0788 \cdot 10^{-6}$	$0.0788 \cdot 10^{-6}$
	4	$1.9615 + 12.4985$i	$12.4985 - 1.9615$i	$0.1260 \cdot 10^{-6}$	$0.1260 \cdot 10^{-6}$
	5	$2.0723 + 15.6501$i	$15.6501 - 2.0723$i	$0.1347 \cdot 10^{-6}$	$0.1347 \cdot 10^{-6}$
1	1	$1.5017 + 4.3646$i	$4.4663 - 1.4675$i	$0.0073 \cdot 10^{-5}$	$0.0071 \cdot 10^{-5}$
	2	$1.7410 + 7.6320$i	$7.6941 - 1.7270$i	$0.0345 \cdot 10^{-5}$	$0.0342 \cdot 10^{-5}$
	3	$1.9028 + 10.8299$i	$10.8746 - 1.8949$i	$0.0862 \cdot 10^{-5}$	$0.0858 \cdot 10^{-5}$
	4	$2.0251 + 14.0040$i	$14.0389 - 2.0201$i	$0.1344 \cdot 10^{-5}$	$0.1341 \cdot 10^{-5}$
	5	$2.1235 + 17.1669$i	$17.1956 - 2.1199$i	$0.1409 \cdot 10^{-5}$	$0.1407 \cdot 10^{-5}$
2	1	$1.6950 + 5.4908$i	$5.8169 - 1.6000$i	$0.0491 \cdot 10^{-6}$	$0.0467 \cdot 10^{-6}$
	2	$1.8590 + 8.9054$i	$9.1185 - 1.8155$i	$0.2383 \cdot 10^{-6}$	$0.2331 \cdot 10^{-6}$
	3	$1.9870 + 12.1756$i	$12.3346 - 1.9613$i	$0.5460 \cdot 10^{-6}$	$0.5393 \cdot 10^{-6}$
	4	$2.0902 + 15.3933$i	$15.5204 - 2.0731$i	$0.7386 \cdot 10^{-6}$	$0.7327 \cdot 10^{-6}$
	5	$2.1764 + 18.5855$i	$18.6914 - 2.1640$i	$0.6197 \cdot 10^{-6}$	$0.6162 \cdot 10^{-6}$
3	1	$1.8701 + 6.4813$i	$7.1010 - 1.7069$i	$0.0200 \cdot 10^{-5}$	$0.0185 \cdot 10^{-5}$
	2	$1.9716 + 10.0606$i	$10.4837 - 1.8921$i	$0.1088 \cdot 10^{-5}$	$0.1047 \cdot 10^{-5}$
	3	$2.0698 + 13.4197$i	$13.7437 - 2.0210$i	$0.2691 \cdot 10^{-5}$	$0.2630 \cdot 10^{-5}$
	4	$2.1553 + 16.6943$i	$16.9575 - 2.1219$i	$0.3827 \cdot 10^{-5}$	$0.3769 \cdot 10^{-5}$
	5	$2.2298 + 19.9263$i	$20.1482 - 2.2053$i	$0.3339 \cdot 10^{-5}$	$0.3303 \cdot 10^{-5}$
4	1	$2.0323 + 7.3836$i	$8.3439 - 1.7984$i	$0.0160 \cdot 10^{-4}$	$0.0144 \cdot 10^{-4}$
	2	$2.0794 + 11.1310$i	$11.8075 - 1.9603$i	$0.0778 \cdot 10^{-4}$	$0.0736 \cdot 10^{-4}$
	3	$2.1506 + 14.5865$i	$15.1145 - 2.0755$i	$0.1657 \cdot 10^{-4}$	$0.1602 \cdot 10^{-4}$
	4	$2.2198 + 17.9251$i	$18.3597 - 2.1673$i	$0.1931 \cdot 10^{-4}$	$0.1886 \cdot 10^{-4}$
	5	$2.2833 + 21.2031$i	$21.5730 - 2.2441$i	$0.1286 \cdot 10^{-4}$	$0.1265 \cdot 10^{-4}$

5.2 The Dirichlet-to-Neumann Finite Element Method (DtN FEM)

In this section we introduce the finite element method in order to solve the problems (2.24) (scattering problem) and (2.28) (resonance problem) by resorting to the use of Galerkin discretization of their variational forms (4.27) and (4.27), derived from the utilization of the DtN map absorbing boundary condition. The use of the finite element method allow us to transform the scattering problem into a linear algebraic system of equations and the resonance problem in a non-linear matrix eigenvalue problem similar to those arising in the use of the boundary element method for the solution of resonance problems (cf. Durán et al. 2001, 2007, Durán et al. 2009). Several well-known algorithm are available to solve these algebraic problems.

Good references concerning both theoretical and practical issues of the finite element method, are the classical books of Ciarlet (2002) and Zienkiewicz et al. (2005). Specific references concerning to the use of the finite element method in conjunction with the DtN absorbing boundary condition for the solution of scattering problems are Ihlenburg (1998) and Givoli (1999), while the implementation of the DtN FEM in waveguides is analyzed in Goldstein (1982) and Harari et al. (1998) for lossless boundary conditions.

Benchmark problems are developed to test the DtN FEM in solving both the scattering and the resonance problem with impedance boundary condition in axisymmetric and non-axisymmetric geometries and boundary data.

5.2.1 Numerical discretization by the finite element method

Let $\mathcal{T}_h$ a family of regular tetrahedral meshes of $\Omega_i \setminus \overline{\Omega_d}$ (in the sense of Ciarlet 2002, Chapter 2), such that $\overline{\Omega_i \setminus \Omega_d} = \bigcup_{T\in\mathcal{T}_h} T$, i.e., $\Omega_i \setminus \overline{\Omega_d}$ is assumed a tetrahedral domain. Parameter h measures the size of the elements (the tetrahedrons) of the mesh in the following sense:

$$h = \max\{\text{diam}\, T : T \in \mathcal{T}_h\},$$

with $\text{diam}\, T = \max\{|\boldsymbol{x}_1 - \boldsymbol{x}_2| : \boldsymbol{x}_1, \boldsymbol{x}_2 \in T\}$. Throughout this section we use the standard linear Lagrange element space to discretize (4.27) and (4.30). Thus, the approximate

solutions can be written as

$$p_h(\boldsymbol{x}) := \sum_{n=1}^{N} p_n \, \phi_n(\boldsymbol{x}) \tag{5.12}$$

where N is the number of nodes of the mesh and $\{\phi_1, \phi_2, \ldots, \phi_N\}$ is the nodal basis of the finite dimensional function space

$$V_h := \left\{ q \in H^1(\Omega_i \setminus \overline{\Omega_d}) : q \mid_T \in \mathcal{P}_1(T), \ \forall\, T \in \mathcal{T}_h \right\}, \tag{5.13}$$

with $\mathcal{P}_1(T)$ denoting the polynomials of first order defined on T.

The finite elements space (5.13) leads to the following discrete form of the variational formulation of the scattering problem (4.27):

$$\begin{cases} \text{Find } p_h \in V_h \text{ such that:} \\ \\ a(p_h, q_h) \;\; = \;\; b(q_h), \quad \forall q_h \in V_h, \end{cases} \tag{5.14}$$

where the bilinear form and the functional on the right hand are defined in (4.28). Replacing p_h by (5.12) and q_h by each basis function in the discrete variational formulation (5.14), we obtain the matrix form of the finite element discretization of the scattering problem, which can be written as:

$$\mathbf{M}_\omega \boldsymbol{p} = \boldsymbol{b}, \tag{5.15}$$

where the matrix $\mathbf{M}_\omega \in \mathbb{M}_{N\times N}(\mathbb{C})$ and the vectors $\boldsymbol{b}, \boldsymbol{p} \in \mathbb{C}^N$ are given by

$$[\mathbf{M}_\omega]_{i,j} := \; a(\phi_i, \phi_j), \qquad i, j = 1, \ldots, N, \tag{5.16a}$$

$$[\boldsymbol{b}]_i \;\; := \; b(\phi_i), \qquad i = 1, \ldots, N, \tag{5.16b}$$

$$[\boldsymbol{p}]_i \;\; := \; p_i, \qquad i = 1, \ldots, N. \tag{5.16c}$$

Because the different kind of integrals present in the variational formulation, we express the matrix $\mathbf{M}_\omega$ as

$$\mathbf{M}_\omega = \mathbf{A}_\omega - \mathbf{B} + \mathbf{C}_\omega + \mathbf{D}_\omega^+ + \mathbf{D}_\omega^-. \tag{5.17}$$

So that, the following matrices and vectors must be computed in order to obtain a solution of the linear algebraic system (5.15):

$$[\mathbf{A}_\omega]_{i,j} := \int_{\Omega_i \setminus \overline{\Omega_d}} k^2 \phi_i \, \phi_j \, \mathrm{d}\boldsymbol{x}, \qquad i,j = 1,\ldots,N \tag{5.18a}$$

$$[\mathbf{B}]_{i,j} := \int_{\Omega_i \setminus \overline{\Omega_d}} \nabla\phi_i \cdot \nabla\phi_j \, \mathrm{d}\boldsymbol{x}, \qquad i,j = 1,\ldots,N \tag{5.18b}$$

$$[\mathbf{C}_\omega]_{i,j} := \int_{\Gamma_i} \alpha \, \phi_i \, \phi_j \, \mathrm{d}\sigma, \qquad i,j = 1,\ldots,N \tag{5.18c}$$

$$\left[\mathbf{D}_\omega^{\pm}\right]_{i,j} := \int_{\Gamma_H^{\pm}} \phi_i \, \mathcal{DN}_t^{\pm} \, \phi_j \, \mathrm{d}\sigma, \qquad i,j = 1,\ldots,N \tag{5.18d}$$

$$[\boldsymbol{b}]_i := -\int_{\Gamma_d} \phi_i \, g \, \mathrm{d}\sigma, \qquad i = 1,\ldots,N. \tag{5.18e}$$

The symbol ω makes explicit the fact that these matrices depend on the angular frequency at which the radiating obstacle works. As can be easily observed from the definition of the DtN operators, it is impossible to perform the series that defined them because they have an infinite number of terms. Consequently, the symbols $\mathcal{DN}_t^+$ and $\mathcal{DN}_t^-$ in (5.18d) represent the truncated DtN operators, which consider only t terms in the series that defines them. These terms correspond to the first t (smallest in norm) numbers $\lambda_{n,m}$. Throughout this dissertation we assume that $t > |\Lambda|$, with Λ defined in (3.90), when undamped problems are attempted to solve. This is because considering less terms may cause problems of unicity of solutions in the sense described in Harari et al. (1998).

Let us note that each of the matrices in (5.18) is sparse and consequently, despite the huge number of nodes that the mesh could have, the linear algebraic system can be efficiently solved without requiring large amounts of memory.

Using the matrices defined above, we can achieve an approximate solution of the resonance problem (4.30), which is given by the solution of the non-linear eigenvalue problem that consists of finding a $\omega \in \mathbb{R}_+$ and $\mathbf{0} \neq \boldsymbol{p} \in \mathbb{C}^N$ such that

$$\mathbf{M}_\omega \boldsymbol{p} = 0. \tag{5.19}$$

To attempt to solve this algebraic problem, we look for the values $\omega_1 < \omega_2 < \cdots$ that lead to a matrix $\mathbf{M}_\omega$ having a zero eigenvalue. To do this, we first consider the eigenvalue problem

$$\mathbf{M}_\omega \boldsymbol{u} = \boldsymbol{\lambda}(\omega)\boldsymbol{u}$$

for a fixed ω. Then, we define the function

$$\Theta(\omega) := \frac{\max_{1\leqslant i\leqslant N} |\boldsymbol{\lambda}_i(\omega)|}{\min_{1\leqslant i\leqslant N} |\boldsymbol{\lambda}_i(\omega)|} \tag{5.20}$$

where $\boldsymbol{\lambda}_i(\omega) \in \mathbb{C}$, $1 \leqslant i \leqslant N$ denote the eigenvalues of matrix $\mathbf{M}_\omega$. There are several highly efficient algorithms to compute the nominator and denominator of the function in (5.20), such as the ones implemented in MATLAB by the function `eigs.m`. Hence, we can evaluate the function Θ for different values of ω in order to identify its local maxima. The local maxima of Θ (located at ω_j), will correspond to the approximate resonance frequencies that we are looking for and the generators of the eigenspace

$$\ker\left(\mathbf{M}_{\omega_j} - \boldsymbol{\lambda}_{i^*}(\omega_j)\mathbf{I}\right) \subset \mathbb{R}^N \quad \text{with} \quad i^* = \arg\min_{1\leqslant i\leqslant N} |\boldsymbol{\lambda}_i(\omega_j)|, \tag{5.21}$$

are the approximate resonance states associated with the resonance frequency ω_i.

Axisymmetric problems. From the paragraph at the end of the Section 4.3, we can infer that the same finite element discretization described above could be applied to problems having axisymmetric geometry and boundary data, introducing a triangular mesh instead a tetrahedral mesh. Of course, the use of a triangular mesh implies a great improvement in the computational performance of the DtN FEM, because much finer meshes can be employed in the discretization.

5.2.2 Non-axisymmetric scattering benchmark problem

Now we are in a position to perform a numerical benchmark problem designed to test the DtN FEM for the solution of scattering problems. To construct that problem, we choose a geometry and a boundary condition that allow us to work out the exact solution of (2.24).

Subsequently, the DtN FEM is applied to approximate this function and a comparison between both solutions will give us an idea of the accuracy of this method. Thus, let us consider that the interior domain is given by an unperturbed cylinder of finite length, i.e.

$$\Omega_i = \left\{ \boldsymbol{x} = (x_1, x_2, x_3) \in \mathbb{R}^3 : x_1^2 + x_2^2 < R^2, x_3 \in (-H, H) \right\}, \tag{5.22}$$

with $H > 0$. Next, consider that the obstacle is given by the ball

$$\Omega_d = \left\{ \boldsymbol{x} \in \Omega_i : |\boldsymbol{y} - \boldsymbol{x}| < \delta \right\}, \tag{5.23}$$

where $\boldsymbol{y} = (y_1, y_2, y_3) \in \Omega_i$, $(y_1, y_2) \neq (0, 0)$, and $\delta > 0$ is small enough such that $\Omega_d \subset \Omega_i$. Then now we attempt to solve the problem of finding $u : \Omega_i \setminus \overline{\Omega_d} \to \mathbb{C}$, $u \in H^1(\Omega_i \setminus \overline{\Omega_d})$ such that:

$$\begin{cases} \Delta u + k^2 u &= 0, \quad \text{in} \quad \Omega_i \setminus \overline{\Omega_d}, \\ \dfrac{\partial u}{\partial n} - \alpha\, u &= 0, \quad \text{on} \quad \Gamma_i, \\ \dfrac{\partial u}{\partial n} &= g, \quad \text{on} \quad \Gamma_d, \\ \dfrac{\partial u}{\partial n} &= \mathcal{DN}_t^+ u, \quad \text{on} \quad \Gamma_H^+, \\ \dfrac{\partial u}{\partial n} &= \mathcal{DN}_t^- u, \quad \text{on} \quad \Gamma_H^-, \end{cases} \tag{5.24}$$

where

$$g(\boldsymbol{x}) := \frac{\partial G(\boldsymbol{x}, \boldsymbol{y})}{\partial n_{\boldsymbol{x}}}, \quad \boldsymbol{x} \in \Gamma_d \tag{5.25}$$

with G being the Green's functions of the infinite cylinder. It is easy to see that the exact solution of (5.24) is given by

$$u(\boldsymbol{x}) = G(\boldsymbol{x}, \boldsymbol{y}). \tag{5.26}$$

Then now we can obtain an approximate solution of (5.24) by the DtN FEM (denoted by u_h) and compare it with the exact solution at each point of a mesh. To compare both

functions we compute the relative error in the following sense:

$$\text{Error} := \frac{\|u_h - \Pi_h u\|_{L^2\left(\Omega_i \setminus \overline{\Omega_d}\right)}}{\|\Pi_h u\|_{L^2\left(\Omega_i \setminus \overline{\Omega_d}\right)}}, \tag{5.27}$$

where $\Pi_h u$ denotes the Lagrange interpolation of the exact solution over the mesh.

TABLE 5.3. Relative error obtained in the solution of the non-axisymmetric benchmark problem for different meshes and wave numbers.

k	h	Number of nodes	Number of triangles	Number of tetrahedra	Relative error $\alpha = 2.5$	Relative error $\alpha = 2.5 + \mathrm{i}$
5	0.1893	3148	2320	16131	4.33×10^{-2}	1.95×10^{-2}
	0.1705	6020	3826	31918	2.00×10^{-2}	1.16×10^{-2}
	0.1441	7748	4584	41730	1.15×10^{-2}	7.86×10^{-3}
	0.1321	10189	5350	56155	9.21×10^{-3}	6.91×10^{-3}
	0.1122	14885	7250	83018	5.85×10^{-3}	4.86×10^{-3}
	0.0997	24481	9830	139949	3.46×10^{-3}	3.79×10^{-3}
	0.0907	33785	12362	195292	2.77×10^{-3}	3.42×10^{-3}
10	0.1893	3148	2320	16131	7.78×10^{-1}	2.01×10^{-1}
	0.1705	6020	3826	31918	3.94×10^{-1}	1.69×10^{-1}
	0.1441	7748	4584	41730	2.55×10^{-1}	1.12×10^{-1}
	0.1321	10189	5350	56155	1.85×10^{-1}	8.67×10^{-2}
	0.1122	14885	7250	83018	1.07×10^{-1}	5.65×10^{-2}
	0.0997	24481	9830	139949	5.79×10^{-2}	3.38×10^{-2}
	0.0907	33785	12362	195292	4.93×10^{-2}	2.76×10^{-2}

Employing the parameters $R = 0.5$, $H = 1.5$, $\boldsymbol{y} = (0, 0.25, 0)$, $\delta = 0.2$ and $t = |\Lambda| + 10$ (the same number of terms is used in the damped case), we compute the relative error for different mesh resolutions. The meshes used are uniform and are constructed through the freeware software GMSH (Geuzaine & Remacle 2009). The finite element method codes are programmed in MATLAB. The elemental calculations needed to assemble the matrices in (5.18) are taken from Zienkiewicz et al. (2005), and six-point gaussian quadrature (cf. Cowper 1973) is used to compute the integrals in both (5.18d) and (5.18e).

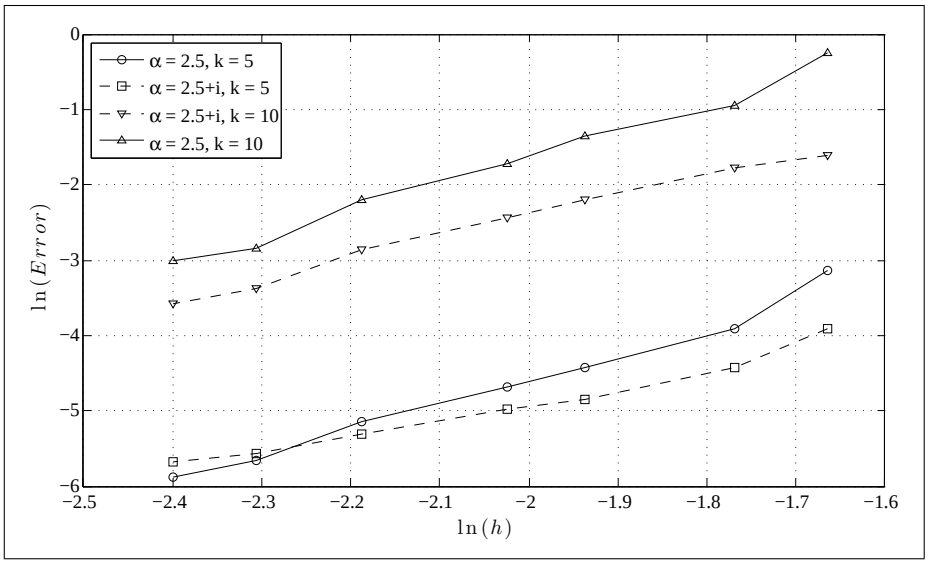

FIGURE 5.7. Relative error obtained in the solution of the non-axisymmetric benchmark problem for different values of the mesh resolution (in logarithmic scale).

Numerical results are shown in Table 5.3 and in Figure 5.7. Figures 5.8 and 5.9 compare the interpolated exact and the approximate solution of (5.24) on plane surfaces $\{\boldsymbol{x} = (x, y, z) \in \mathbb{R}^3 : y = 0\} \cap \Omega_i$ and $\{\boldsymbol{x} = (x, y, z) \in \mathbb{R}^3 : x = 0\} \cap \Omega_i$ respectively. The results displayed correspond to $k = 5$, $\alpha = 2.5$, $h = 0.1122$ and Error $= 0.0058$.

5.2.3 Axisymmetric scattering benchmark problem

As was stated in the paragraphs at the end of Sections 4.3 and 5.2.1, for problems with axisymmetric domain and boundary data (i.e. problems where the domain and the boundary data do not depend on the angular variable in cylindrical coordinates), the three-dimensional mesh used in Subsection 5.2.2 can be replaced by a two-dimensional one. To test the DtN FEM in axisymmetric problems employing a two-dimensional mesh, we consider the same benchmark problem (5.24) with the interior domain given by (5.22) and radiating obstacle given by (5.23). However, to get an axisymmetric boundary datum on Γ_d, we set the punctual source at $\boldsymbol{y} = (y_1, y_2, y_3) \in \Omega_i$, with $(y_1, y_2) = (0, 0)$. Assuming this and a constant impedance parameter, the boundary data become axisymmetric and the finite

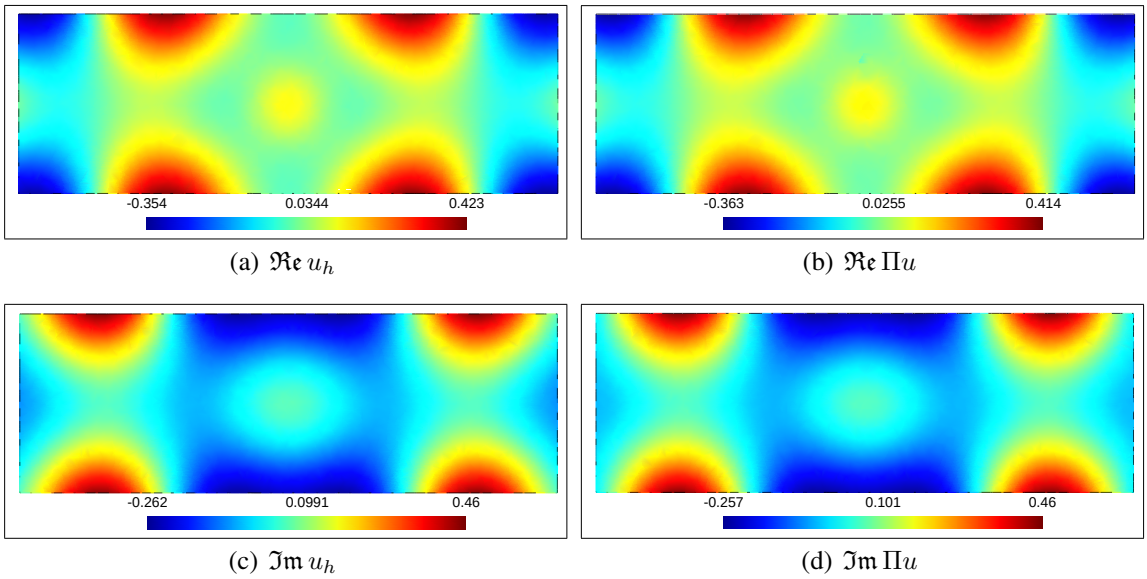

(a) $\mathfrak{Re}\, u_h$ (b) $\mathfrak{Re}\, \Pi u$

(c) $\mathfrak{Im}\, u_h$ (d) $\mathfrak{Im}\, \Pi u$

FIGURE 5.8. Level surfaces on the XZ-plane of the approximate and the exact solution of the scattering benchmark problem (non-axisymmetric case).

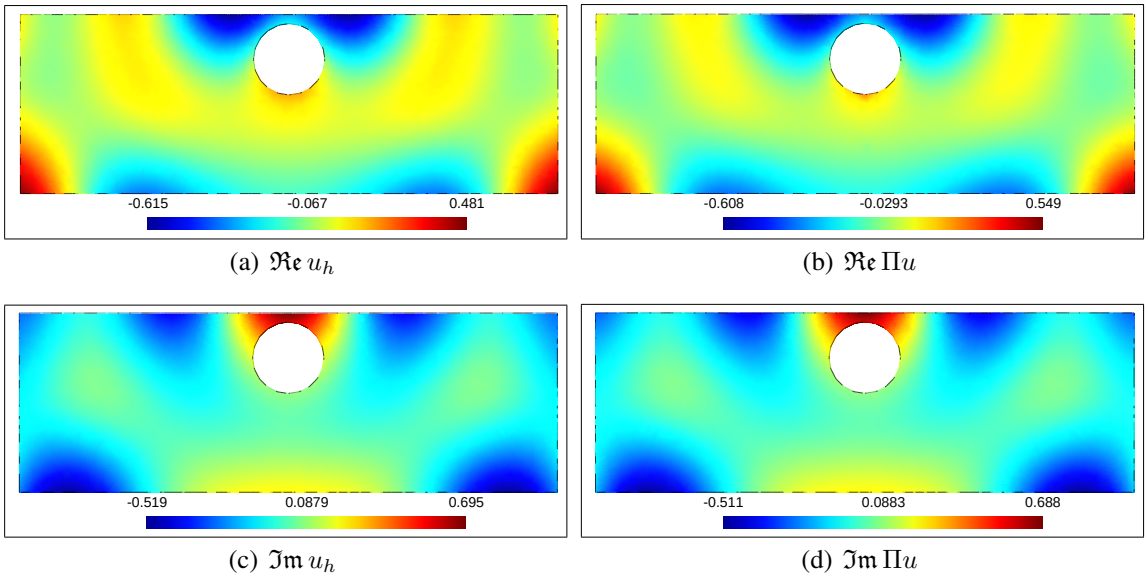

(a) $\mathfrak{Re}\, u_h$ (b) $\mathfrak{Re}\, \Pi u$

(c) $\mathfrak{Im}\, u_h$ (d) $\mathfrak{Im}\, \Pi u$

FIGURE 5.9. Level surfaces on the YZ-plane of the approximate and the exact solution of the scattering benchmark problem (non-axisymmetric case).

element discretization described in Subsection 5.2.1 can be applied on a two-dimensional mesh.

Employing the same parameters: $R = 0.5$, $H = 1.5$, $\delta = 0.2$ and $t = |\Lambda| + 10$ (the same number of terms is used in the damped case) with the exception of $\boldsymbol{y} = (0, 0, 0)$, we compute the relative error for different regular meshes. The values of the relative error are shown in Table 5.4 and in Figure 5.10. Figure 5.11 compares both solutions for $k = 5$, $\alpha = 2.5$, $h = 0.0827$ and Error $= 0.00907$.

TABLE 5.4. Relative error obtained in the solution of the axisymmetric benchmark problem for different meshes and wave numbers.

k	h	Number of nodes	Number of segments	Number of triangles	Relative error $\alpha = 2.5$	Relative error $\alpha = 2.5 + \mathrm{i}$
5	0.1553	110	49	169	2.50×10^{-2}	9.59×10^{-3}
	0.1337	141	56	224	1.72×10^{-2}	7.11×10^{-3}
	0.1112	176	58	292	1.23×10^{-2}	5.24×10^{-3}
	0.0896	197	63	329	1.05×10^{-2}	4.20×10^{-3}
	0.0827	223	68	376	9.07×10^{-3}	4.16×10^{-3}
	0.0811	276	74	476	8.60×10^{-3}	4.11×10^{-3}
	0.0790	326	84	566	7.03×10^{-3}	3.87×10^{-3}
10	0.1553	110	49	169	5.77×10^{-1}	4.67×10^{-1}
	0.1337	141	56	224	3.43×10^{-1}	2.72×10^{-1}
	0.1112	176	58	292	2.30×10^{-1}	1.75×10^{-1}
	0.0896	197	63	329	1.53×10^{-1}	1.20×10^{-1}
	0.0827	223	68	376	1.22×10^{-1}	9.65×10^{-2}
	0.0811	276	74	476	8.18×10^{-2}	6.45×10^{-2}
	0.0790	326	84	566	5.63×10^{-2}	4.44×10^{-2}

5.2.4 Non-axisymmetric resonance benchmark problem

This subsection aims to construct a benchmark problem designed to test the DtN FEM in order to solve resonance problems. With this end in view, we attempt to solve analytically (2.28), where the interior domain considered is the unperturbed cylinder of finite length given by

$$\Omega_i = \left\{ \boldsymbol{x} = (x_1, x_2, x_3) \in \mathbb{R}^3 : x_1^2 + x_2^2 < R^2, x_3 \in (-H, H) \right\} \tag{5.28}$$

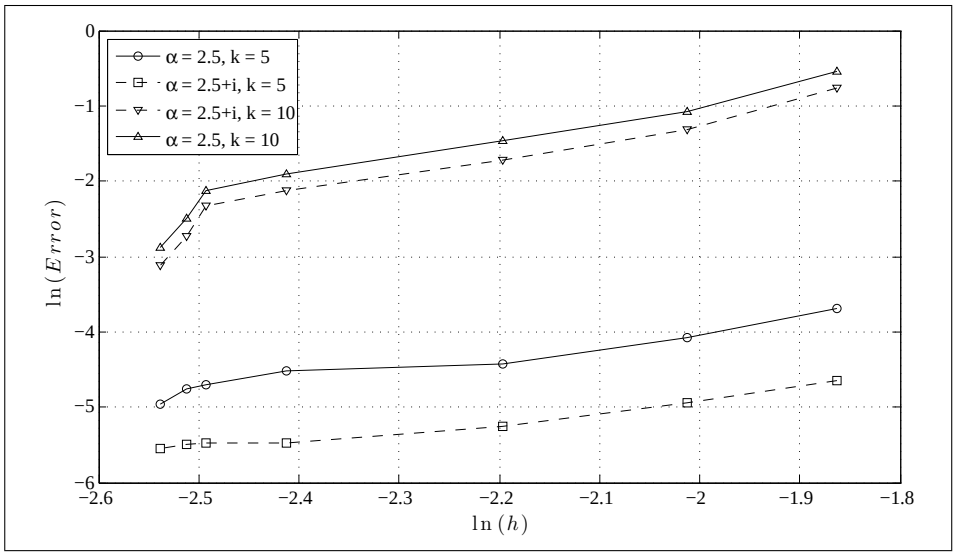

FIGURE 5.10. Relative error obtained in the solution of the axisymmetric benchmark problem for different values of the mesh resolution (in logarithmic scale).

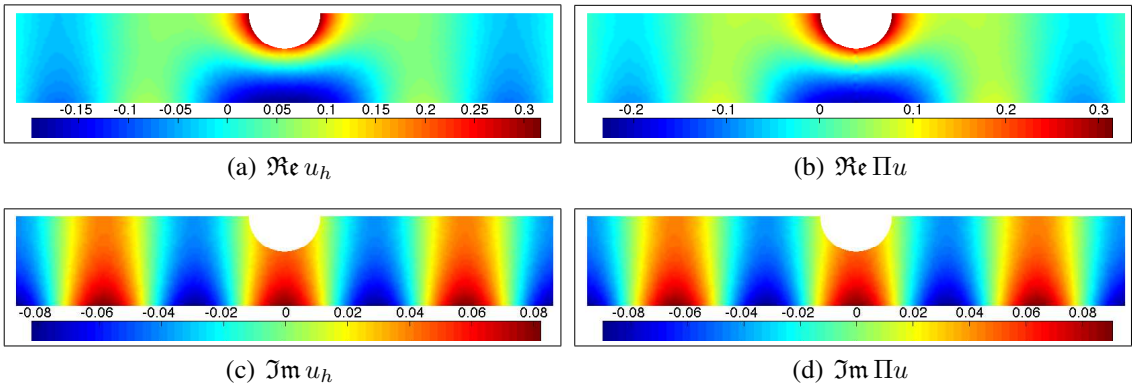

(a) $\mathfrak{Re}\, u_h$ (b) $\mathfrak{Re}\, \Pi u$

(c) $\mathfrak{Im}\, u_h$ (d) $\mathfrak{Im}\, \Pi u$

FIGURE 5.11. Level plots of the approximate and the exact solution of the scattering benchmark problem (axisymmetric case).

and the domain occupied by the obstacle is assumed empty, i.e. $\Omega_d = \emptyset$.

Under these assumptions we get that (2.28) can be written as:

Find $\omega \in \mathbb{R}$ that leads to a wave number $k \neq 0$ and a non-identically zero resonance state $\phi : \Omega_\infty \to \mathbb{C}$, such that

$$\begin{cases} \Delta\phi + k^2\phi &= 0, \quad \text{in } \Omega_\infty, \\ \dfrac{\partial\phi}{\partial n} - \alpha\phi &= 0, \quad \text{on } \Gamma_\infty, \\ + \text{ radiation condition at } |\boldsymbol{x}| \to \infty, \text{ if } \mathfrak{Im}\,\alpha = \mathfrak{Im}\,k = 0 \end{cases} \tag{5.29}$$

where Ω_∞ and Γ_∞ are defined in (3.2). In order to use the separation of variables techniques we assume that a resonant state can be expressed as $\phi(r,\theta,z) = A(\theta)B(r)C(z)$ in cylindrical coordinates. Replacing it in (5.29), we get the following one-dimensional eigenvalue problems:

$$\begin{cases} A'' + \alpha A &= 0, & \theta \in [0, 2\pi), \\ A(\theta + 2\pi) &= A(\theta), & \theta \in [0, 2\pi), \\ A'(\theta + 2\pi) &= A'(\theta), & \theta \in [0, 2\pi), \end{cases} \tag{5.30}$$

$$\begin{cases} -(rB')' + \dfrac{\alpha}{r}B - \beta rB &= 0, & r \in (0, R), \\ B' - \alpha B &= 0, & r = R, \\ \lim\limits_{r\to 0^+} |B(r)| &< 0, \end{cases} \tag{5.31}$$

and

$$C'' + (k^2 - \beta)C = 0, \qquad z \in \mathbb{R}. \tag{5.32}$$

Throughout this subsection we assume that the angular frequency and the wave number are related by the equation $k = \omega/c$ with c the speed of sound, and the impedance parameter such that $\mathfrak{Im}\,\alpha = 0$. These assumptions lead to $k \in \mathbb{R}$ and $\lambda_{n,m} \in \mathbb{R}, (n,m) \in \mathbb{N}_0 \times \mathbb{N}$ and consequently we need to impose the radiation conditions (4.13) and (4.19) to the generic resonant state so as to guarantee that it corresponds to an outgoing wave. These can be

expressed as follows:

$$\begin{aligned}\lim_{z\to\infty}\left(\frac{\mathrm{d}C}{\mathrm{d}z}-\mathrm{i}\,k_{n,m}C\right)\left(\int_0^{2\pi}A(\theta)\,\mathrm{e}^{\mathrm{i}\,n\theta}\,\mathrm{d}\theta\right)\left(\int_0^{R}B(r)\varphi_{n,m}(r)r\,\mathrm{d}r\right) &= 0,\\ \lim_{z\to-\infty}\left(\frac{\mathrm{d}C}{\mathrm{d}z}+\mathrm{i}\,k_{n,m}C\right)\left(\int_0^{2\pi}A(\theta)\,\mathrm{e}^{\mathrm{i}\,n\theta}\,\mathrm{d}\theta\right)\left(\int_0^{R}B(r)\varphi_{n,m}(r)r\,\mathrm{d}r\right) &= 0,\end{aligned} \tag{5.33}$$

with $(n,m)\in\Lambda$.

It can be easily seen that the solutions of (5.30) are

$$\alpha = n^2, \qquad A_n(\theta) = a\,\mathrm{e}^{\mathrm{i}\,n\theta}+b\,\mathrm{e}^{-\mathrm{i}\,n\theta},\ \ n\in\mathbb{Z},$$

while the solutions of (5.31) are given by

$$\beta=\lambda_{n,m}, \qquad B_{n,m}(r)=\varphi_{n,m}(r),\ \ (n,m)\in\mathbb{Z}\times\mathbb{N},$$

where the numbers $\lambda_{n,m}$ are defined in (3.37) and the functions $\varphi_{n,m}$ are defined in (3.87) and (3.88). Regarding the fact that

$$\int_0^{2\pi}A_n(\theta)\,\mathrm{e}^{\mathrm{i}\,p\,\theta}\,\mathrm{d}\theta = 2\pi b\,\delta_{n,p} \quad \text{and} \quad \int_0^{R}B_{n,m}(r)\varphi_{n,q}(r)r\,\mathrm{d}r=\delta_{m,q}, \tag{5.34}$$

we find that the continuous solutions of (5.32) satisfying the radiation condition are

$$C_{n,m}(z)=\begin{cases}\mathrm{e}^{-\mathrm{i}\,k_{n,m}|z|} & \text{if } k^2\neq\lambda_{n,m}\\ 1 & \text{if } k^2=\lambda_{n,m}.\end{cases} \tag{5.35}$$

From here it is possible to infer that the sought resonance frequencies are

$$\omega_{n,m}=c\sqrt{\lambda_{n,m}},\quad (n,m)\in\mathbb{N}_0\times\mathbb{N} \tag{5.36}$$

and their associated resonant states are

$$\phi_{n,m}(\boldsymbol{x}) := \varphi_{n,m}(r)\left\{a\,\mathrm{e}^{\mathrm{i}\,n\theta}+b\,\mathrm{e}^{-\mathrm{i}\,n\theta}\right\} \tag{5.37}$$

where a and b are arbitrary complex constants.

Resorting to use of the DtN FEM in the way described in Subsection 5.2.1, we obtain the results shown in Table 5.5. Those results were worked out assuming that the exact value of the eigenfrequencies are supplied by the method described in Subsection 5.1.1. The parameters employed in these computations are $R = 0.5$, $c = 1$, $H = 1.5$, $t = |\Lambda| + 10$ and $\alpha = 2.5$ with a mesh size of $h = 0.0997$. Figure 5.12 shown the local maxima of the Θ function and the exact values of the resonance frequencies. Figure 5.13 displays the level sets on the YZ-plane of the approximate and the exact (with $b = 0$) eigenfunction associated with the eigenvalue at $\omega_{2,1} = \sqrt{\lambda_{2,1}} = z_{2,1} = 4.047$.

TABLE 5.5. Results obtained in the solution of the non-axisymmetric resonance benchmark problem.

Eigenfrequencies		Exact	Approximate	Relative
n	m	eigenfrequencies	eigenfrequencies	error
2	1	4.047	4.000	1.16×10^{-2}
3	1	6.844	6.985	2.06×10^{-2}
0	2	7.008	7.050	6.06×10^{-3}
4	1	9.315	9.475	1.72×10^{-2}
1	2	10.174	10.325	1.48×10^{-2}

5.2.5 Axisymmetric resonance benchmark problem

The same benchmark problem (5.29) can be worked out using the DtN FEM for axisymmetric problems. Of course, in this case the function Θ does not have local maxima in the points corresponding to resonant frequencies that lead to resonant states with angular variation, due to the fact that the exact axisymmetric resonant states are

$$\phi_{0,m} = \varphi_{0,m} \tag{5.38}$$

and the resonance frequencies are

$$\omega_{0,m} = c\sqrt{\lambda_{0,m}}, m \in \mathbb{N}. \tag{5.39}$$

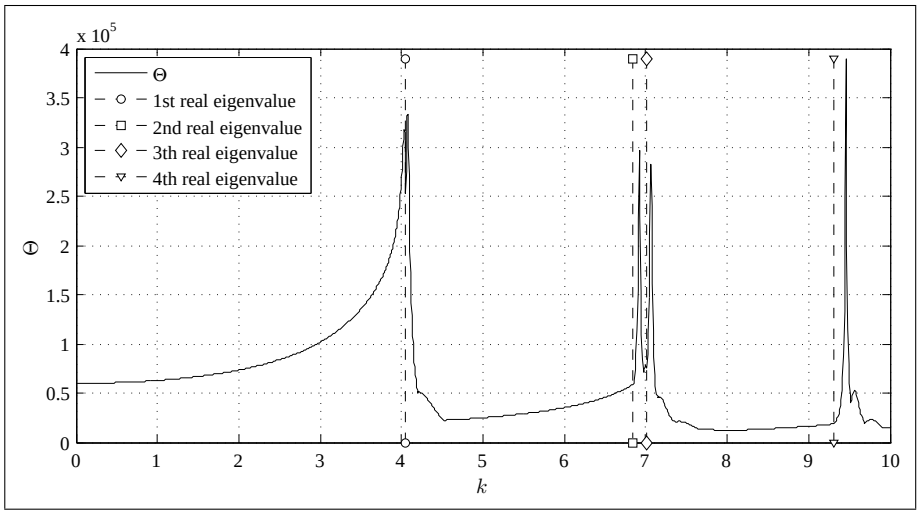

FIGURE 5.12. Location of the eigenfrequencies of the benchmark problem as local maxima of the Θ function (non-axisymmetric case).

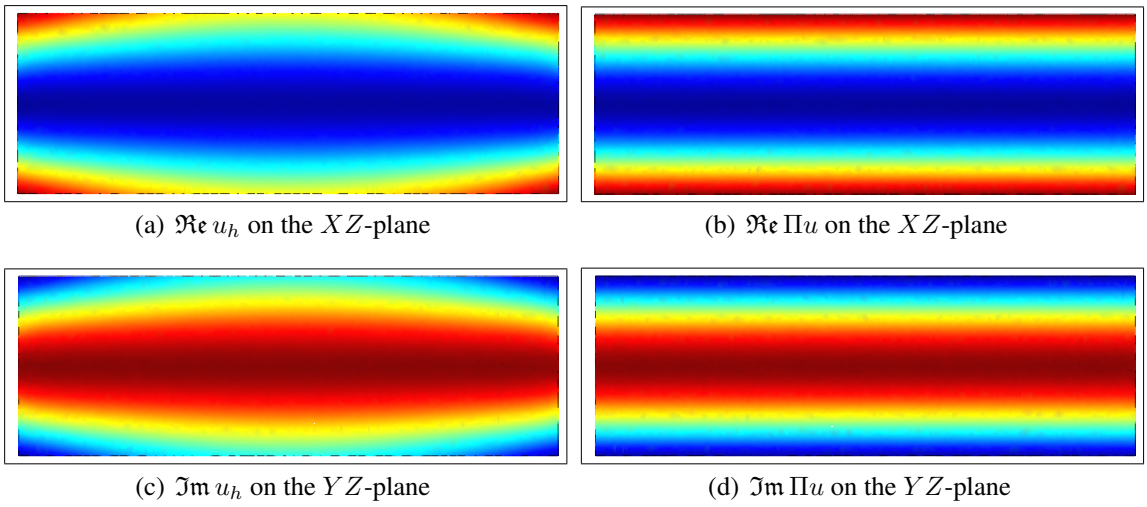

(a) $\mathfrak{Re}\, u_h$ on the XZ-plane

(b) $\mathfrak{Re}\, \Pi u$ on the XZ-plane

(c) $\mathfrak{Im}\, u_h$ on the YZ-plane

(d) $\mathfrak{Im}\, \Pi u$ on the YZ-plane

FIGURE 5.13. Plots of the approximated and the exact resonant state of the benchmark problem.

Some results are shown in Table 5.6. Figure 5.14 displays the local maxima of the Θ function in the real line. Clearly we can observe that this function does not have maxima in the non-axisymmetric eigenfrequencies located at $\omega_{2,1} = 4.047$, $\omega_{3,1} = 6.844$, $\omega_{4,1} = 9.315$ and so on. These results were performed for $R = 0.5$. $c = 1$, $H = 1.5$, $\alpha = 2.5$, $t = |\Lambda| + 10$ and a mesh resolution of $h = 0.0107$.

TABLE 5.6. Results obtained in the solution of the axisymmetric resonance benchmark problem.

Eigenfrequencies m	Exact eigenfrequencies	Approximated eigenfrequencies	Relative error
2	7.008	7.008	7.14×10^{-5}
3	13.674	13.675	6.58×10^{-5}
4	20.101	20.149	2.39×10^{-3}
5	26.460	26.562	3.87×10^{-3}
6	32.789	32.973	5.60×10^{-3}

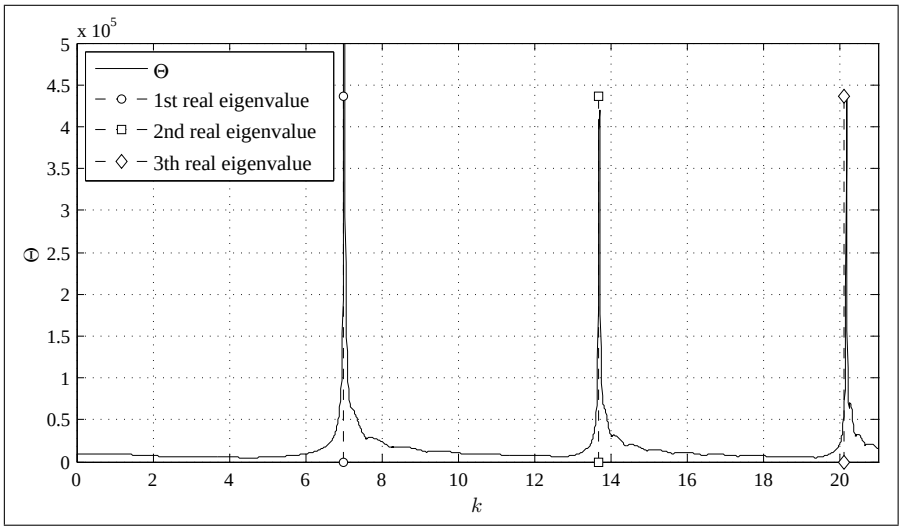

FIGURE 5.14. Location of the eigenfrequencies of the benchmark problem as local maxima of the Θ function (axisymmetric case).

5.2.6 Discussion

The numerical results of the scattering problems show that the approximate order of convergence, derived from the slope of the curves in Figures 5.7 and 5.10, is 3.05 for non-axisymmetric problems, and 2.17 for axisymmetric problems. Less relative error is obtained when a complex impedance parameter is used instead of a real one. A possible reason for this is that the dissipation attenuates the spurious waves reflection arising due to the artificial boundaries. Likewise, we may notice that less error is obtained for small

wave numbers. It is related with the well-known errors estimates for the finite element solution of the Helmholtz equation, which depend on kh (cf. Ihlenburg 1998). It tells us that the variable that truly explains the error is the number of nodes per wave-lenght rather than the mesh size by itself. The same effect may be appreciated in the computation of the eigenfrequencies from the local maxima of function Θ. From Figures 5.12 and 5.14 we can appreciate that the approximation of the exact eigenfrequencies gets worse as the wave number grows because the graphs of Θ were made with the mesh size remaining constant.

VI. NUMERICAL SIMULATION OF THE ACOUSTIC WELL STIMULATION METHOD

In this chapter we perform simulations of the AWS for a realistic geometry and realistic physical constants. Applying the method developed in the previous chapters, we set two problems relevant for the design of the AWS method. The first one consists of simulating the energy emission at different frequencies, determining for each frequency how much of the radiated energy is transmitted to the reservoir porous rock through the perforations. The second one consists of finding the resonance frequencies that stem from the real interaction between an oil well geometry and the acoustic device, determining for each resonance frequency how much energy is trapped inside the perforations.

6.1 Physical and geometric data

In Chapter II we defined the domain considered throughout this dissertation from an abstract point of view. In the same manner, there we pointed out which are the physical variables involved in the phenomenological model. At this stage we have to specify the quantitative value of the geometric and physical parameters used so as to show how the interaction of the geometry and physical variables may affect the performance of the AWS method. We take these values from previous articles where oil-well problems are considered. Table 6.1 summarizes the geometrical and physical data employed in both of the problems and Figure 6.1 explains the geometrical parameters.

The geometrical data of the oil well are taken from Hagoort (2007), while the geometrical data of the AWS device is taken from Mullakaev, Abramov & Pechkov (2009). The fluid density and the speed of sound are taken from Cheng & Blanch (2008).

However, no empirical model for the normal impedance have been found for the sound transmission between oil-like fluid media and porous materials. Usually these models are based on experimental data and depend strongly on the particular features of the materials studied. To face that problem in this chapter we use another impedance model successfully employed for sound transmission from air to porous media. Specifically, we use the so-called Delany-Bazley empirical model (cf. Delany & Bazley 1970), which allows us to

TABLE 6.1. Geometrical and physical input data for numerical computations performed in the realistic geometry.

Parameter	Value
Wellbore radius (R) [cm]	11.1
Perforation width [cm]	2.0
Perforation depth [cm]	30.5
Acoustic device length [cm]	70.5
Acoustic device radius [cm]	5.4
Phasing angle between the perforations [rad]	$\pi/2$
Perforation density [perforations·m^{-1}]	3.33
Speed of sound (c) [m·s^{-1}]	1524
Fluid density (ρ_0) [kg·m^{-3}]	1100

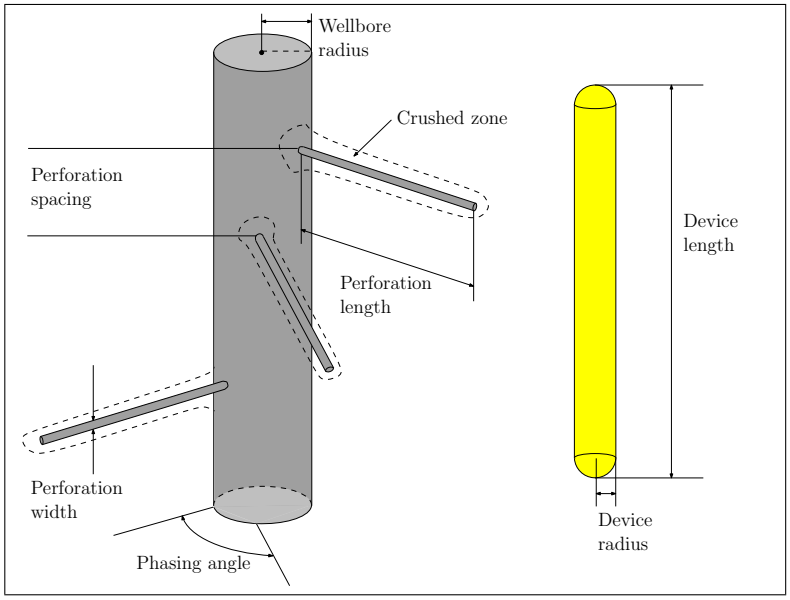

FIGURE 6.1. Explanation of the geometrical parameters of the well and the AWS device.

express the dimensionless normal impedance (see 2.17) as a function of frequency and

flow resistivity (a standard variable that characterize porous media). This model holds that

$$\chi = 1 + 0.0571 \left(\frac{\sigma}{\rho_0 f} \right)^{0.754} \tag{6.1a}$$

$$\xi = 0.087 \left(\frac{\sigma}{\rho_0 f} \right)^{0.732} \tag{6.1b}$$

where ρ_0 is the fluid density, $f = \omega/2\pi$ is the frequency and σ is flow resistivity.

The numerical values obtained from the simulations performed employing this impedance model will differ greatly from the real phenomenon because it is derived from the interaction of materials different to those involved in our problem. Nevertheless, they will give us key qualitative information showing the existence of locally optimal emission and resonance frequencies.

In this chapter we assume that oil does not dissipate energy and is homogenous, thus we are assuming that the wave number is a real constant and it does not vary with the spatial variables, i.e. $k = \omega/c \in \mathbb{R}$. The finite element mesh of the geometry with the parameters shown in Table 6.1 is constructed by resorting to the freeware software GMSH (Geuzaine & Remacle 2009). Figure 6.2 displays the mesh of the computational domain $\Omega_i \setminus \Omega_d$, where the color-bar depicts the quality of the elements using the Gamma factor, which is defined as the quotient between the radius of the inscribed and circumscribed sphere.

6.2 Energy transmission

Assuming that the flow resistivity of the casing and the damaged zone are given by $\sigma_c = 1.00 \times 10^{12}$[N·s·m^{-4}] and $\sigma_p = 2.77 \times 10^8$ [N·s·m^{-4}] respectively, we can solve the scattering problem (2.24) for different frequencies so as to determine the optimal ones in the sense that the energy transmission through the perforations' surface reach a local maximum.

To solve the direct scattering problem we need to specify the boundary datum on Γ_d, which will depend on the particular AWS device studied. Thus, for the sake of simplicity we assume that the energy is radiated uniformly throughout the surface of the AWS device.

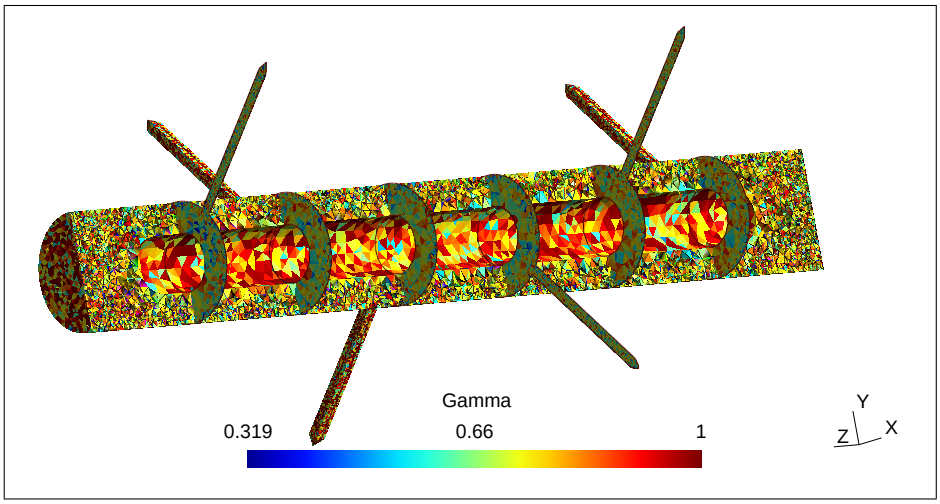

FIGURE 6.2. Mesh of the realistic geometry of the well and the device.

It leads to consider as boundary datum, a constant function given by $g = 1$ [N·m]. We claim that results obtained using this boundary datum will best display the effect of the geometry, because we are not privileging any particular direction. Of course we may choose any function $g \in H^{-1/2}(\Gamma_d)$ if we want to model others AWS devices.

To determine the acoustic energy transmission through the perforations' surface, we use the formulas (2.20) and (2.23) which give the time-averaged energy flux density dissipated by the locally reacting surface and the effective power density supplied by the AWS device respectively. To obtain how much energy can be transmitted through each perforation's surface, we denote these surfaces by the symbols $\Gamma_i^j \subset \Gamma_i$, $j = 1, \cdots, 6$, where the perforations are considered sorted in descending order according to their z-coordinate. These definitions lead us to achieve the proportion of energy transmitted by each perforation's surface, which is expressed by the formulas

$$\mathbf{p}_j := k\chi \frac{\displaystyle\int_{\Gamma_i^j} \frac{|p(\boldsymbol{x})|^2}{|\zeta(\boldsymbol{x})|^2}\, \mathrm{d}\sigma}{\displaystyle\int_{\Gamma_d} \mathfrak{Im}\left\{p(\boldsymbol{x})\overline{g(\boldsymbol{x})}\right\}\, \mathrm{d}\sigma}, \quad j = 1, \ldots, 6 \tag{6.2a}$$

$$\mathbf{p} := \sum_{j=1}^{6} \mathbf{p}_j, \tag{6.2b}$$

where the nominator in (6.2a) corresponds to the energy dissipated by the j-th perforation, and the denominator is the effective energy supplied by the AWS device. As it might be expected, by the conservation of energy principle, the energy supplied by the acoustic device is the total energy entering the domain and thus it is greater than the total energy radiated by the perforations' surface. Therefore $100 \times \mathbf{p}$ is the total percent of energy dissipated through the perforations' surface.

Figures 6.3 and 6.4 show the values of $\mathbf{p}_j$, $j = 1, \cdots, 6$ and $\mathbf{p}$ for different frequencies.

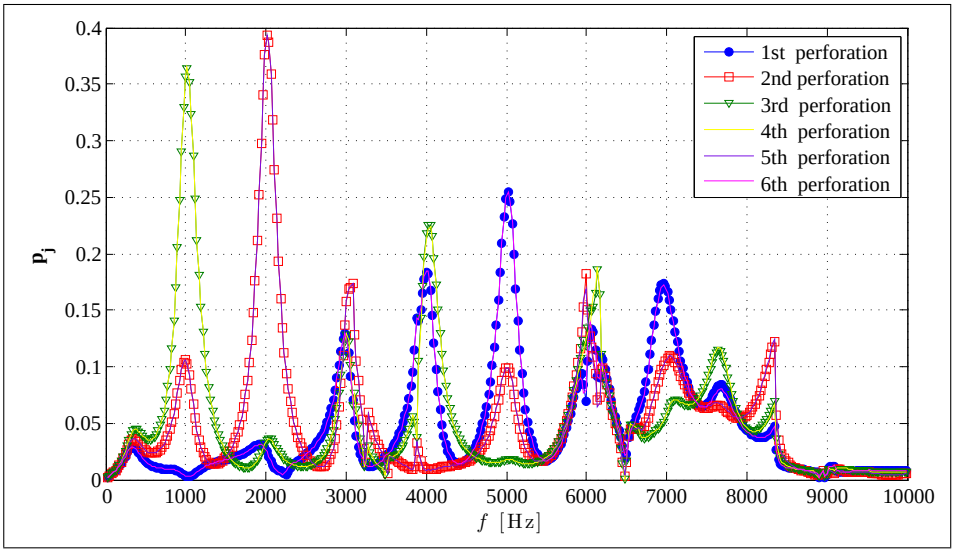

FIGURE 6.3. Proportion of time-averaged energy dissipated by each perforation's surface for different frequencies.

Due to the use of a symmetric source of excitation we observe in Figure 6.3 that the energy curves of the first and sixth perforation are the same, as well as the curves of the second and fifth, and the curves of the third and the fourth perforation. From these results it is also possible to observe that some particular frequencies lead to better energy transmission through specific perforations. For instance, at frequencies near 1 [kHz] the AWS device transmits energy through the third and the fourth perforation, at frequencies near 2 [kHz] it transmits energy through the second and the fifth perforation, while at frequencies near 5 [kHz] the energy is transmitted through the first and sixth perforation.

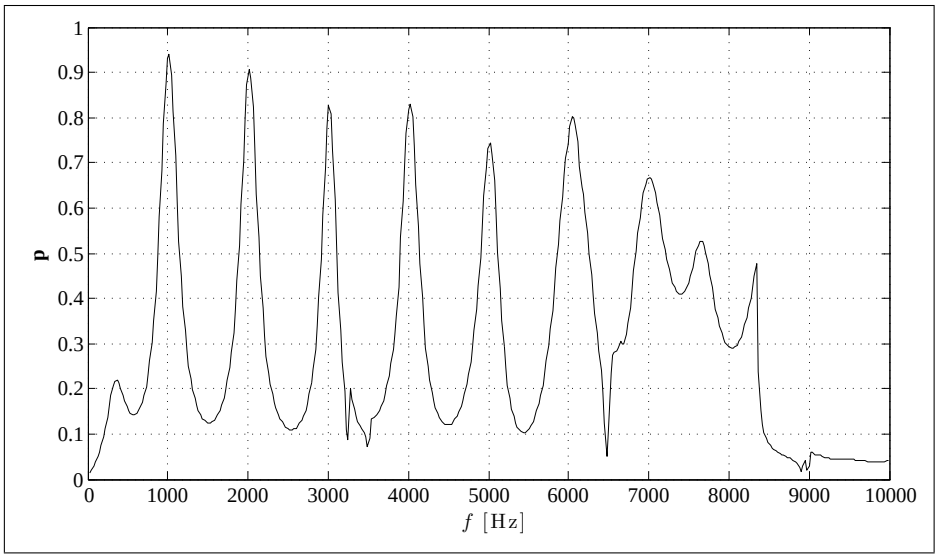

FIGURE 6.4. Proportion of time-averaged total energy dissipated through the perforations' surface for different frequencies.

Finally, from Figure 6.4, which displays the consolidated plot of the energy curves, we infer the existence of frequencies that allow us to effectively transmit about 80% of the energy radiated by the acoustic device, to the damaged zone of the well.

6.3 Resonance frequencies

An important feature of the AWS method that has not been exploited yet, is that the acoustical stimulation may trigger the occurrence of the resonance phenomenon when the frequency of the device matches some particular values so-called the resonance frequencies. The resonance phenomenon may be understood as a natural tendency of a mechanical system to accumulate energy when it is excited by a time-harmonic external force that oscillates at a resonance frequency and consequently it may produce severe damage to the components involved, as Parker & Stoneman (1989) point out in their famous paper. However, for the case studied here, the excitation of some resonance frequencies might be particulary useful to improve the design of the AWS method because at these frequencies the mechanical system can be easily excited by the acoustic source to generate high amplitude vibrations near the sealed pores of the rock formation. Herein we show that, using

the numerical procedures developed in the previous chapters, it is possible to find such resonance frequencies that lead to energy concentration inside the perforations.

As was already reported by Ursell (1991) and Linton & McIver (1998*a*,*b*) from a purely mathematical mathematical point of view, the presence of obstacles inside a circular cylindrical waveguide may trigger the occurrence of real resonances frequencies (trapped modes) when the Neumann boundary condition is fulfilled on the boundary of the device and the cylinder. Although these results do not apply directly to our problem, because the oil well has a local perturbation and thus it is not a perfect circular cylindrical waveguide, they provide a clue that it is possible to find them in our problem too. Moreover, from a physical point of view the Neumann boundary condition corresponds to acoustically hard surfaces that, from the insight given by the Delany-Bazley model, corresponds to an infinite flow resistivity, i.e., $\sigma_c = \sigma_p = \infty$. This boundary condition models pretty good totally depleted wells in which there is no oil flow.

Consequently, herein we address the problem of solving (2.28) for an identically null impedance parameter, i.e., for the Neumann boundary condition on Γ_i, Γ_e^-, Γ_e^+ and Γ_d. To do so, we use the method developed in the precedent chapters, and then we have to find the real local maxima of the function Θ defined in (5.20). A graph of this function showing its local maxima on the real line is displayed in Figure 6.5.

To evaluate how convenient could it be to excite a particular resonance frequency in the sense that the energy is concentrated inside the perforations, we define the sets $\Omega_i^j \subset \Omega_i$, $j = 1, \cdots, 6$, that denote the domain occupied by the j-th perforation, which again are considered sorted in descending order according to their z-coordinate. These definitions allow us to compute the energy ratio of each perforation over the whole interior domain Ω_i. According to Filippi et al. (1999) the time average energy density is given by $|p|^2/2\rho_0 c^2$. Thus the quotient of the energy accumulated inside the j-th perforation and the total energy

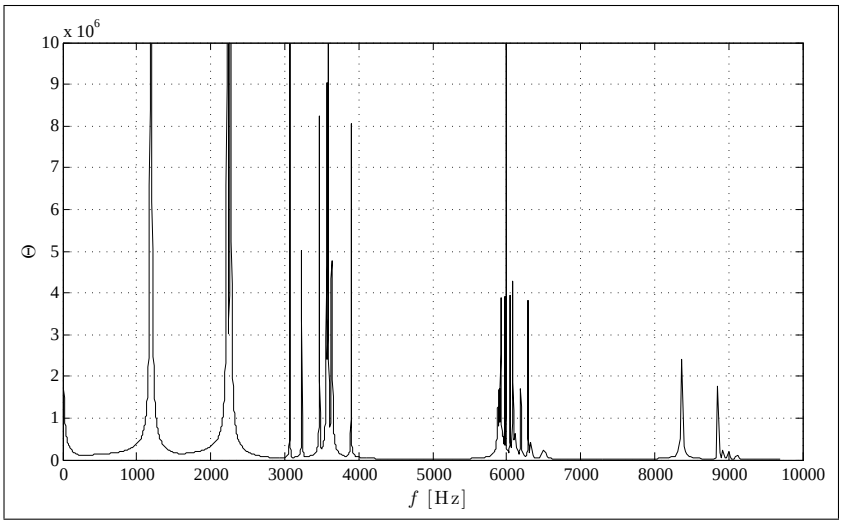

FIGURE 6.5. Real local maxima of the function Θ.

accumulated inside the interior domain may be expressed as follows

$$\mathbf{e}_j := \frac{\displaystyle\int_{\Omega_i^j} |p_i(\boldsymbol{x})|^2 \, \mathrm{d}\boldsymbol{x}}{\displaystyle\int_{\Omega_i} |p_i(\boldsymbol{x})|^2 \, \mathrm{d}\boldsymbol{x}}, \qquad j = 1, \ldots, 6, \tag{6.3a}$$

$$\mathbf{e} := \sum_{j=1}^{6} \mathbf{e}_j, \tag{6.3b}$$

where $100 \times \mathbf{e}_j$ corresponds to the average percent of energy accumulated in the j-th perforation and $100 \times \mathbf{e}$ represents the total average percent of energy concentrated in all the perforations. Table 6.2 shows the resonance frequencies, the value of the objective function at each resonance frequency and the value of the variables defined in (6.3).

From Table 6.2 it is possible to appreciate that, as we anticipated, some resonance frequencies lead to resonance states that trap energy inside the perforations. Moreover, Figure 6.6 shows how the energy is accumulated inside the perforations in the resonant states associated to the frequencies 1200.63 [Hz], 3567.94 [Hz], 5971.63 [Hz] and 6084.42 [Hz].

TABLE 6.2. Neumann approximated real resonances for a real well and device geometry.

f (Hz)	Θ	$\mathbf{e}_1\%$	$\mathbf{e}_2\%$	$\mathbf{e}_3\%$	$\mathbf{e}_4\%$	$\mathbf{e}_5\%$	$\mathbf{e}_6\%$	$\mathbf{e}\%$
1188.51	1.87×10^9	3.33	14.30	29.65	31.05	17.13	4.21	99.67
1200.63	5.70×10^7	3.82	16.94	28.31	28.75	16.45	3.59	97.86
2226.63	2.30×10^9	0.00	0.00	0.00	0.00	0.00	0.00	0.00
2265.44	8.56×10^7	0.00	0.00	0.00	0.00	0.00	0.00	0.00
2272.71	9.74×10^7	0.00	0.00	0.00	0.00	0.00	0.00	0.00
3068.29	8.41×10^7	0.00	0.08	1.42	0.22	0.54	0.00	2.26
3230.79	5.02×10^6	0.00	1.16	0.52	0.43	1.36	0.00	3.48
3470.92	8.23×10^6	0.03	5.44	1.73	1.84	4.98	0.03	14.05
3567.94	9.03×10^6	3.52	10.74	32.88	27.06	12.41	2.57	89.16
3587.35	1.73×10^7	33.65	1.71	0.87	0.97	1.63	33.38	72.21
3643.15	3.03×10^6	0.57	18.87	8.76	8.93	18.99	0.55	56.68
3897.81	8.05×10^6	0.02	0.31	0.82	0.68	0.38	0.01	2.22
5920.69	3.88×10^6	11.39	6.71	17.13	16.38	7.48	11.38	70.46
5971.63	3.90×10^6	3.50	14.35	18.38	18.66	14.63	3.38	72.90
5988.61	1.07×10^7	0.00	0.00	0.00	0.00	0.00	0.00	0.00
6046.82	3.93×10^6	0.01	0.00	0.00	0.00	0.02	0.04	0.07
6084.42	3.56×10^6	4.89	3.78	3.55	3.85	4.33	5.53	25.94
6291.80	3.82×10^6	0.00	0.00	0.00	0.00	0.00	0.00	0.00
8363.20	7.75×10^6	0.00	0.00	0.00	0.00	0.00	0.00	0.00

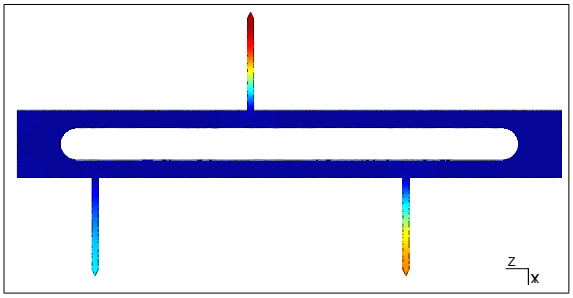

(a) Perforations 1, 3 and 5 for $f = 1200.63$Hz.

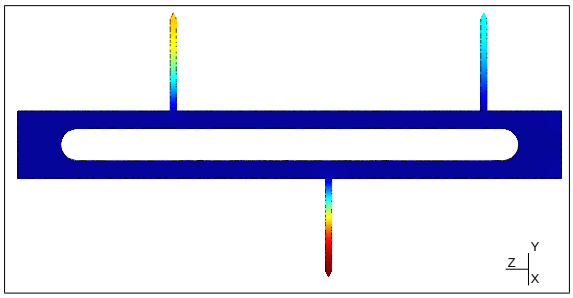

(b) Perforations 2, 4 and 6 for $f = 1200.63$Hz.

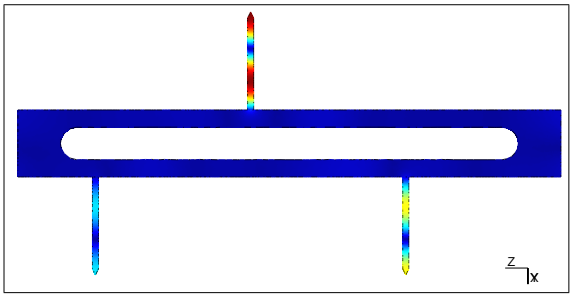

(c) Perforations 1, 3 and 5 for $f = 3567.94$Hz.

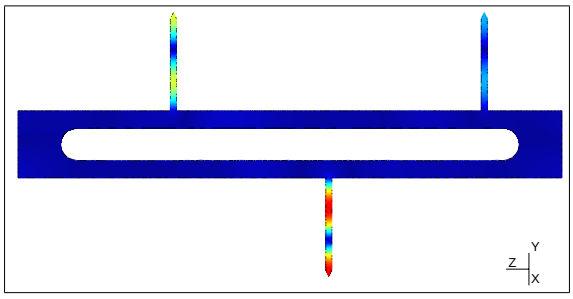

(d) Perforations 2, 4 and 6 for $f = 3567.94$Hz.

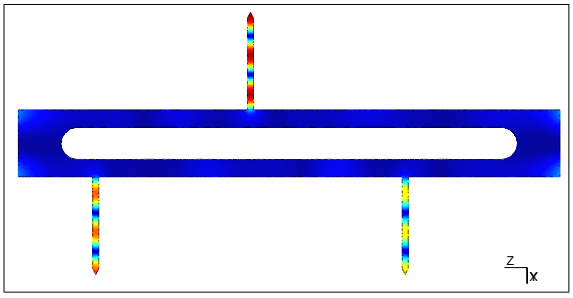

(e) Perforations 1, 3 and 5 for $f = 5971.63$Hz.

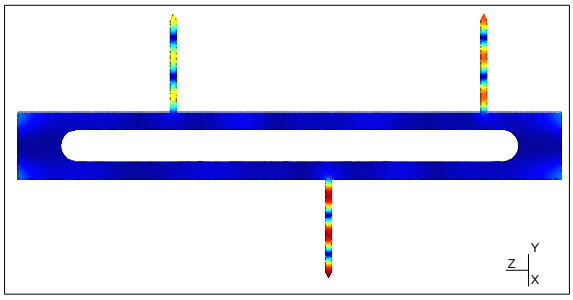

(f) Perforations 2, 4 and 6 for $f = 5971.63$Hz.

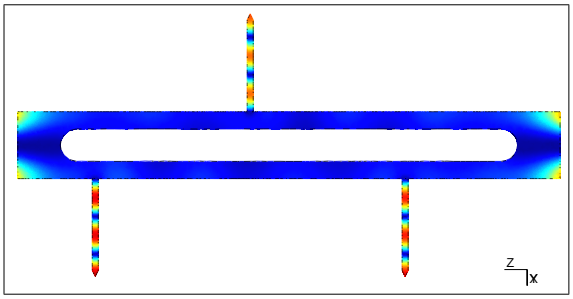

(g) Perforations 1, 3 and 5 for $f = 6084.42$Hz.

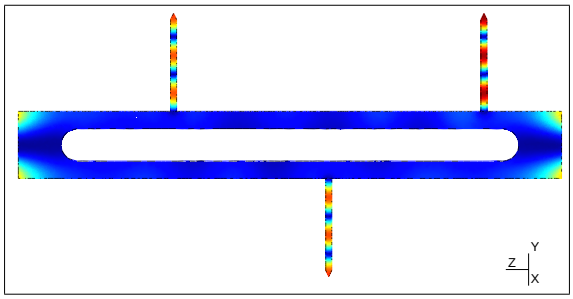

(h) Perforations 2, 4 and 6 for $f = 6084.42$Hz.

FIGURE 6.6. Level plots of the absolute value of some resonance states that accumulate energy inside the perforations.

VII. CONCLUSIONS

A phenomenological model for the study of the AWS method is for the first time developed. The seeking for optimal emission frequencies leads to a time-harmonic direct scattering and an eigenvalue problem defined on an unbounded domain with an impedance boundary condition. The problem that stems from the unbounded domain is faced by developing the DtN FEM for the impedance boundary condition, which is deduced from the Green's function for the Helmholtz operator in an infinite circular cylindrical waveguide. Benchmark problems show the accuracy of this numerical procedure by comparing the analytical and the approximated solution of problems defined on non-perturbed geometries. The use of the DtN FEM allow us to perform numerical simulations of the operation of the AWS method. They confirm our hypothesis of the existence of frequencies that lead to energy accumulation inside the perforations and optimal energy transmission from the acoustic device to the damaged zone of the well. Consequently, it is possible to conclude that the procedures developed in this thesis allow to improve the performance of the AWS stimulation by taking into account key geometrical and physical information not considered before.

This thesis presents an initial study on the mathematical modeling and simulation of the AWS method and consequently, many issues are still pending to clarify. The most important ones are the following:

- First of all, the preliminary results shown must be contrasted with experimental data that validate the phenomenological model and give accurate quantitative information about the physical constants involved. A key point in this possible future work, is the validity determination of the impedance boundary condition.
- Related to the previous point, it is the extension of the model to cover a portion of the porous solid that surounds the damaged zone. A model like this, may give results better adjusted to the real case without requiring the impedance boundary condition. However, to do that we need to work out accurate simulations of the wave propagation in a porous solid ruled by the Biot's model (Biot 1956*a*,*b*), and

it is not well studied yet a reliable method, like the DtN FEM, to truncate these kind of media.

- Another possible future work has to do with the frequency range at which the simulations have been performed. As can be observed from the numerical results, we do not cover the ultrasonic frequency range, that lies up to 20 [KHz]. It is mainly because the capacity of the computer used here, a MacBook, 2.4 GHz Intel Core 2 Duo with 2GB RAM, can not yield reliable results at these frequencies using the numerical procedures developed herein. Therefore, more efficient codes or numerical schemes could be performed in this sense.
- Several purely mathematical issues remain pending. For instance, studies of the existence and the properties of the eigenvalues may be very interesting, as well as the study of existence and unicity of solutions for the differential problems numerically solved here.
- Finally, it is important to point out that the mathematical procedures herein proposed cover a broad field of different applications such as other kind of acoustic wave propagation problems, like those arising in ventilation systems and mufflers (cf. Munjal 1987); they also can be used in electromagnetic communication in subterranean tunnels, where the impedance boundary condition on the inner wall models pretty well the real conditions (cf. Dudley & Mahamund 2006); in fiber-optic waveguides, where the surface impedance boundary conditions models a metal-dielectric cladding (cf. Hecht 1990); and so on. Thus, it seems to be attractive as future research to apply these procedures to other highly relevant engineering problems.

REFERENCES

Aarts, A. C. T. & Ooms, G. (1998), 'Net flow of compressible viscous liquids induced by travelling waves in porous media', *Journal of Engineering Mathematics,* **34**(4), 435–450.

Aarts, A. C. T., Ooms, G., Bil, K. J. & Bot, E. T. G. (1999), 'Enhancement of liquid flow through a porous medium by ultrasonic radiation', *SPE Journal,* **4**(4), 321–327.

Abismail, B., Canselier, J. P., Wilhelm, A. M., Delmas, H. & Gourdon, C. (1999), 'Emulsification by ultrasound: drop size distribution and stability', *Ultrasonic Sonochemestry,* **6**, 75–83.

Abramov, O., Abramov, V., Pechkov, A., Zolezzi-Garreton, A. A. & Paredes-Rojas, L. O. (2006), *U.S. Patent No. 7,059,413 B2*, Washington, DC: U.S. Patent and Trademark Office.

Abramov, O., Abramov, V., Zolezzi-Garreton, A. A., Paredes-Rojas, L. O. & Pechkov, A. (2006), *U.S. Patent No. 7.063.114 B2*, Washington, DC: U.S. Patent and Trademark Office.

Abramovitz, M. & Stegun, I. A. (1972), *Handbook of mathematical functions with formulas, graphs and mathematical tables*, Oxford University Press.

Ahmed, S. & Calogero, F. (1978), 'On the zeros of Bessel functions. III', *Lettere al Nuovo Cimento. Rivista Internazionale della Società Italiana di Fisica. Serie 2,* **21**(9), 311–314.

Allard, J.-F. & Champoux, Y. (1992), 'New empirical equations for sound propagation in rigid frame fibrous materials', *Journal of the Acoustical Society of America,* **91**(6), 3346–3353.

Amir, N., Pagneux, V. & Kergomard, J. (1997), 'A study of wave propagation in varying cross-section waveguides by modal decomposition .2. Results', *Journal of the Acoustical Society of America,* **101**(5), 2504–2517.

Aslanyan, A., Parnovski, L. & Vassiliev, D. (2000), 'Complex resonances in acoustic waveguides', *The Quarterly Journal of Mechanics and Applied Mathematics,* **53**(3), 429–447.

Astley, R. J. (2000), 'Infinite elements for wave problems: a review of current formulations and an assessment of accuracy', *International Journal for Numerical Methods in Engineering,* **49**(7), 951–976.

Astley, R. J. (2008), Infinite elements, *in* S. Marburg & B. Nolte, eds, 'Computational Acoustic of Noise Propagation in Fluids: Finite and Boundary Element Methods', Springer-Verlag, chapter 7, pp. 197–230.

Barrientos, M. A., Abramov, O., Abramov, V., Pechkov, A., Zolezzi-Garreton, A. A. & Paredes-Rojas, L. O. (2006), *U.S. Patent No. 7,059,403 B2*, Washington, DC: U.S. Patent and Trademark Office.

Bendali, A. & Guillaume, P. (1999), 'Non-reflecting boundary conditions for waveguides', *Mathematics of Computation,* **68**(225), 123–144.

Bérenger, J.-P. (1994), 'A perfectly matched layer for the absorption of electromagnetic waves', *Journal of Computational Physics,* **114**(2), 185–200.

Beresnev, I. A. & Johnson, P. A. (1994), 'Elastic-wave stimulation of oil production: A review of methods and results', *Geophysics,* **59**(6), 1000–1017.

Bermúdez, A., Hervella-Nieto, L., Prieto, A. & Rodríguez, R. (2008), Perfectly matched layers, *in* S. Marburg & B. Nolte, eds, 'Computational acoustic of noise propagation in fluids - finite and boundary element methods', Springer-Verlag, chapter 6, pp. 167–196.

Biot, M. A. (1956*a*), 'Theory of propagation of elastic waves in a fluid-saturated porous solid. I. Low-frequency range', *Journal of the Acoustical Society of America,* **28**, 168–178.

Biot, M. A. (1956*b*), 'Theory of propagation of elastic waves in a fluid-saturated porous solid. II. Higher frequency range', *Journal of the Acoustical Society of America,* **28**, 179–191.

Bonnet, M. (1995), *Boundary Integral Methods for Solids and Fluids*, John Wiley & Sons Ltd.

Brent, R. P. (1973), *Algorithms for minimization without derivatives*, first edn, Prentice-Hall Inc., Englewood Cliffs, N.J.

Champion, B., van der Bas, F. & Nitters, G. (2004), 'The application of high-power sound waves for wellbore cleaning', *SPE Production & Facilities,* **19**(3), 113–121.

Cheng, A. C. H. & Blanch, J. O. (2008), 'Numerical modeling of elastic wave propagation in fluid-filled borehole', *Communications in Computational Physics* **3**(1), 33–51.

Cheng, C. H. & Toksoz, M. N. (1981), 'Elastic wave propagation in a fluid-filled borehole and synthetic acoustic logs', *Geophysics,* **46**(7), 1042–1053.

Cherskiy, N. V., Tsarev, V. P., Konovalov, V. M. & Kusnetsov, O. L. (1977), 'The effect of ultrasound on permeability of rocks to water', *Transactions (Doklady) of the U.S.S.R. Academy of Sciences: Earth Science Sections,* **232**, 201–204.

Ciarlet, P. G. (2002), *The finite element method for elliptic problems*, Vol. 40 of *Classics in Applied Mathematics*, Society for Industrial and Applied Mathematics (SIAM), Philadelphia, PA.

Colton, D. L. & Kress, R. (1983), *Integral equation methods in scattering theory*, Pure and Applied Mathematics, first edn, John Wiley & Sons Inc., New York.

Cowper, G. (1973), 'Gaussian quadrature formulas for triangles', *International Journal for Numerical Methods in Engineering,* **7**(3), 405–408.

Davies, E. B. & Parnovski, L. (1998), 'Trapped modes in acoustic waveguides', *The Quarterly Journal of Mechanics and Applied Mathematics,* **51**(3), 477–492.

Delany, M. E. & Bazley, E. N. (1970), 'Acoustical properties of fibrous absorbent materials', *Applied Acoustics,* **3**(2), 105–116.

Delves, L. M. & Lyness, J. N. (1967), 'A numerical method for locating the zeros of an analytic function', *Mathematics of Computation* **21**, 543–560.

Dixon, A. C. (1903), 'On a property of Bessel functions', *Messenger XXXII* pp. 7–8.

Duan, Y., Koch, W., Linton, C. M. & McIver, M. (2007), 'Complex resonances and trapped modes in ducted domains', *Journal of Fluid Mechanics,* **571**, 119–147.

Duan, Y. & McIver, M. (2004), 'Rotational acoustic resonances in cylindrical waveguides', *Wave Motion,* **39**(3), 261–274.

Dudley, D. G. & Mahamund, S. F. (2006), 'Linear Source in a Circular Tunnel', *IEEE Transactions on Antennas and Propagation* **54**(7), 2034–2047.

Duffy, D. G. (2001), *Green's functions with applications*, Studies in Advanced Mathematics, Chapman & Hall/CRC, Boca Raton, FL.

Duffy, D. G. (2004), *Transform methods for solving partial differential equations*, second edn, Chapman & Hall/CRC, Boca Raton, FL.

Duhon, R. D. & Campbell, J. M. (1965), 'The effect of ultrasonic energy on the flow of fluids in porous media', *SPE 1316, presented at the 2nd Anual Eastern Regional Meeting of SPE/AIME, Charleston, WV, Nov. 4-5* .

Durán, M., Godoy, E. & Nedelec, J.-C. (2006), 'Computing Green's function of elasticity in a half-plane with impedance boundary condition', *Comptes Rendus Mécanique, Académie des Sciences. Paris,* **334**(12), 725–731.

Durán, M., Hein, R. & Nédélec, J.-C. (2007), 'Computing numerically the Green's function of the half-plane Helmholtz operator with impedance boundary conditions', *Numerische Mathematik,* **107**(2), 295–314.

Durán, M., Miguez, M. & Nédélec, J.-C. (2001), 'Numerical stability in the calculation of eigenfrequencies using integral equations', *Journal of Computational and Applied Mathematics,* **130**(1-2), 323–336.

Durán, M., Nédélec, J.-C. & Ossandón, S. (2009), 'An efficient Galerkin BEM to compute high acoustic eigenfrequencies', *Journal of Vibration and Acoustic* **131**(3).

Elbert, Á. & Siafarikas, P. D. (1992), 'On the zeros of $aC_\nu(x) + xC'_\nu(x)$, where $C_\nu(x)$ is a cylinder function', *Journal of Mathematical Analysis and Applications,* **164**(1), 21–33.

Ellingsen, O., Carvalho, C. R., Castro, C. A., Bonet, E. J., Villani, P. J. & Mezzomo, R. F. (1994), *U.S. Patent No. 5,282,508*, Washington, DC: U.S. Patent and Trademark Office.

Engquist, B. & Majda, A. (1977), 'Absorbing boundary conditions for the numerical simulation of waves', *Mathematics of Computation,* **31**(139), 629–651.

Evans, D. & Linton, C. (1994), 'Acoustic resonance in ducts', *Journal of Sound and Vibration* **173**, 85–94.

Evans, D. V., Levitin, M. & Vassiliev, D. (1994), 'Existence theorems for trapped modes', *Journal of Fluid Mechanics,* **261**, 21–31.

Evans, D. V., Linton, C. M. & Ursell, F. (1993), 'Trapped mode frequencies embedded in the continuous spectrum', *The Quarterly Journal of Mechanics and Applied Mathematics,* **46**(2), 253–274.

Fairbanks, H. V. & Chen, W. I. (1971), 'Ultrasonic acceleration of liquid flow through porous media', *Chem. Eng. Prog. Symp. Ser.* **67**, 108–116.

Filippi, P., Habault, D., Lefebvre, J. P. & Bergassoli, A. (1999), *Acoustic: Basic Physics, Theory and Methods*, first edn, Academic Press.

Folland, G. B. (1994), *Fourier analysis and its applications*, first edn, Brooks/Cole Publishing Company.

Gardes, K. (2000), 'A review of infinite element methods for exterior helmholtz problems', *J. Comput. Acoust.* **8**(1), 43–62.

Geuzaine, C. & Remacle, J.-F. (2009), 'Gmsh: A 3-D finite element mesh generator with built-in pre- and post-processing facilities', *International Journal for Numerical Methods in Engineering,* **79**(11), 1309–1331.

Givoli, D. (1999), 'Recent advances in DtN FE method', *Archive of Computational Method in Engineering* **6**(2), 71–116.

Givoli, D. (2004), 'High-order local non-reflecting boundary conditions: a review', *Wave Motion,* **39**(4), 319–326.

Givoli, D. (2008), Computational absorbing boundaries, *in* S. Marburg & B. Nolte, eds, 'Computational Acoustic of Noise Propagation in Fluids: Finite and Boundary Element Methods', Springer-Verlag, chapter 5, pp. 145–166.

Givoli, D., Patlashenko, I. & Keller, J. B. (1998), 'Discrete Dirichlet-to-Neumann maps for unbounded domains', *Computer Methods in Applied Mechanics and Engineering,* **164**(1-2), 173–185.

Goldstein, C. I. (1982), 'A finite element method for solving Helmholtz type equations in waveguides and other unbounded domains', *Mathematics of Computation,* **39**(160), 309–324.

Graham, D. R. & Higdon, J. J. L. (2000*a*), 'Oscillatory flow of droplets in capillary tubes. Part 1. Straight tubes', *Journal of Fluid Mechanics,* **425**, 55–77.

Graham, D. R. & Higdon, J. J. L. (2000*b*), 'Oscillatory flow of droplets in capillary tubes. Part 2. Constricted tubes', *Journal of Fluid Mechanics,* **425**, 55–77.

Graham, D. R. & Higdon, J. J. L. (2002*a*), 'Oscillatory forcing of flow through porous media. Part 1. Steady flow', *Journal of Fluid Mechanics,* **465**, 213–235.

Graham, D. R. & Higdon, J. J. L. (2002*b*), 'Oscillatory forcing of flow through porous media. Part 2. Unsteady flow', *Journal of Fluid Mechanics,* **465**, 237–260.

Guo, X., Du, Z., Li, G. & Shu, Z. (2004), 'High frequency vibration recovery enhancement technology in the heavy oil fields of China', *SPE 86956, Presented at the SPE Int. Thermal Operations and Heavy Oil Symposium and Western Regional Meeting, Bakersfield, CA, Mar. 16-18* .

Hagoort, J. (2007), 'An analytical model for predicting the productivity of perforated wells', *Journal of Petroleum Science and Engineering,* **56**, 199–218.

Hamida, T. & Babadagli, T. (2007), 'Analysis of capillary interaction and oil recovery under ultrasonic waves', *Transport in porous media* **70**, 231–255.

Harari, I. (2006), 'A survey of finite element methods for time-harmonic acoustics', *Computer Methods in Applied Mechanics and Engineering,* **195**(13-16), 1594–1607.

Harari, I., Patlashenko, I. & Givoli, D. (1998), 'Dirichlet-to-Neumann maps for unbounded wave guides', *Journal of Computational Physics,* **143**(1), 200–223.

Hazard, C. & Lunéville, E. (2008), 'An improved multimodel approach for non-uniform acoustic waveguides', *IMA J. Appl. Math.* **73**(4), 668–690.

Hecht, J. (1990), *Understanding Fiber Optics*, Oxford University Press.

Hein, S., Hohage, T. & Koch, W. (2004), 'On resonances in open systems', *Journal of Fluid Mechanics,* **506**, 255–284.

Hein, S. & Koch, W. (2008), 'Acoustic resonances and trapped modes in pipes and tunnels', *Journal of Fluid Mechanics,* **605**, 401–428.

Hyne, N. J. (2001), *Nontechnical Guide to Petrolium Goelogy, Explorations, Drilling and Production*, first edn, PennWell Corporation.

Ifantis, E. K. & Siafarikas, P. D. (1986), 'Ordering relations between the zeros of miscellaneous Bessel functions', *Applicable Analysis,* **23**(1-2), 85–110.

Ifantis, E. K. & Siafarikas, P. D. (1988), 'Bounds for the first positive zero of a mixed Bessel function', *Journal of Computational and Applied Mathematics,* **21**(2), 245–249.

Ifantis, E. K., Siafarikas, P. D. & Kouris, C. B. (1988), 'The imaginary zeros of a mixed Bessel function', *Z. Angew. Math. Phys.* **39**(2), 157–165.

Ihlenburg, F. (1998), *Finite element analysis of acoustic scattering*, Vol. 132 of *Applied Mathematical Sciences*, first edn, Springer-Verlag, New York.

Ismail, M. E. H. & Muldoon, M. E. (1995), 'Bounds for the small real and purely imaginary zeros of Bessel and related functions', *Methods and Applications of Analysis,* **2**(1), 1–21.

Johnson, C. & Nédélec, J.-C. (1980), 'On the coupling of boundary integral and finite element methods', *Mathematics of Computation,* **35**(152), 1063–1079.

Kinsler, L. E., Frey, A. R., Coppends, A. B. & Sanders, J. V. (1999), *Fundamentals of acoustics*, fourth edn, Wiley.

Kravanja, P. & Barel, M. V. (2000), *Computing the zeros of analytic functions*, first edn, Springer.

Krylov, Y. U., Nikolaevskiy, V. N. & El', G. A. (1991), 'Mathematical model of nonlinear generation of ultrasound by seismic waves', *Transactions (Doklady) of the U.S.S.R. Academy of Sciences: Earth Science Sections,* **318**(6), 1339–1345.

Lake, L. W. (1996), *Enhanced Oil Recovery*, Prentice Hall.

Landau, L. J. (1999), 'Ratios of Bessel functions and roots of $\alpha J_\nu(x) + xJ'_\nu(x) = 0$', *Journal of Mathematical Analysis and Applications,* **240**(1), 174–204.

Levitin, M. & Marletta, M. (2008), 'A simple method of calculating eigenvalues and resonances in domains with infinite regular ends', *Proceedings of the Royal Society of Edinburgh. Section A. Mathematics,* **138**(5), 1043–1065.

Linton, C. M. & Evans, D. V. (1992), 'Integral equations for a class of problems concerning obstacles in waveguides', *Journal of Fluid Mechanics,* **245**, 249–265.

Linton, C. M. & McIver, M. (1998*a*), 'Trapped modes in cylindrical waveguides', *The Quarterly Journal of Mechanics and Applied Mathematics,* **51**(3), 389–412.

Linton, C. M. & McIver, P. (1998*b*), 'Acoustic resonances in the presence of radial fins in circular cylindrical waveguides', *Wave Motion,* **28**(2), 99–117.

Linton, C. M. & McIver, P. (2007), 'Embedded trapped modes in water waves and acoustics', *Wave Motion,* **45**(1-2), 16–29.

Linton, C., McIver, M., McIver, P., Ratcliffe, K. & Zhang, J. (2002), 'Trapped modes for off-centre structures in guides', *Wave Motion,* **36**, 67–85.

Liu, Q. H., Schoen, E., Daube, F., Randall, C., Liu, H.-I. & Lee, P. (1996), 'A three-dimensional finite difference simulation of sonic logging', *Journal of the Acoustical Society of America,* **100**(1), 72–79.

Liu, Q. H. & Sinha, B. K. (2003), 'A 3D cylindrical PML/FDTD method for elastic wave in fluid-filled pressurized boreholes in triaxially stressed formations', *Geophysics,* **68**(5), 1731–1743.

Magnus, W. & Oberhettinger, F. (1954), *Formulas and theorems for the functions of mathematical physics*, second edn, Chelsea Publishin Company, New York.

Marburg, S. & Nolte, B. (2008), *Computational Acoustic of Noise Propagation in Fluids: Finite and Boundary Element Methods*, first edn, Springer - Verlag.

McIver, M. & Linton, C. M. (1995), 'On the non-existence of trapped modes in acoustic waveguides', *The Quarterly Journal of Mechanics and Applied Mathematics,* **48**(4), 543–555.

McIver, M., Linton, C. M., McIver, P., Zhang, J. & Porter, R. (2001), 'Embedded trapped modes for obstacles in two-dimensional waveguides', *The Quarterly Journal of Mechanics and Applied Mathematics,* **54**(2), 273–293.

McIver, M., Linton, C. & Zhang, J. (2002), 'Branch structure of embedded trapped modes in two-dimensional waveguide', *Quarterly Journal of Mechanics and Applied Mathematics,* **55**, 313–326.

Mettin, R., Akhatov, I., Parlitz, U., Ohl, C. D. & Lauterbom, W. (1997), 'Bjerknes forces between small cavitation bubbles in a strong acoustic field', *Physical Review E. Statistical Physics, Plasmas, Fluids, and Related Interdisciplinary Topics,* **56**(3), 2924–2931.

Meyer, R. J. & Tarnawskyj, C. J. (2002), *U.S. Patent No. 6,405,796 B1*, Washington, DC: U.S. Patent and Trademark Office.

Michler, C., Demkowicz, L. & Torres-Verdín, C. (2009), 'Numerical simulation of borehole acoustic logging in the frequency and time domains with hp-adaptive elements', *Computer methods in applied mechanics and Engineering* **198**(21-26), 1821–1838.

Miki, Y. (1990), 'Acoustical properties of porous materials - Modification of the Delany-Bazley models', *Journal of the Acoustical Society of America,* **11**(1), 19–28.

Morse, P. M. & Ingard, K. U. (1986), *Theoretical acoustics*, Princeton University Press.

Mullakaev, M. S., Abramov, O. V., Abramov, V. O., Gradov, O. M. & Pechkov, A. A. (2009), 'An ultrasonic technology for productivity restoration in low-flow boreholes', *Chemical and Petroleum Engineering,* **45**(3-4), 2009.

Mullakaev, M. S., Abramov, V. O. & Pechkov, A. A. (2009), 'Ultrasonic unit for restoring oil wells', *Chemical and Petroleum Engineering,* **45**(3-4), 133–137.

Munjal, M. L. (1987), *Acoustic of Ducts and Mufflers: With Applications to Exhaust and Ventilation System Design*, first edn, John Wiley & Sons.

Nédélec, J.-C. (2001), *Acoustic and electromagnetic equations: Integral representations for harmonic problems*, Vol. 144 of *Applied Mathematical Sciences*, first edn, Springer-Verlag, New York.

Nosich, A. I. (1994), 'Radiation conditions, limiting absortion principle and general relations in open waveguide scattering', *J. Electromag. Waves Applicat.* **8**(3), 329–353.

Pagneux, V., Amir, N. & Kergomard, J. (1996), 'A study of wave propagation in varying cross-section waveguides by modal decomposition .1. Theory and validation', *Journal of the Acoustical Society of America,* **100**(4), 2034–2048.

Paillet, F. L. & Cheng, C. H. (1991), *Acoustic waves in boreholes*, CRC Press, Inc.

Parker, R. & Stoneman, S. A. T. (1989), 'The excitation and consequences of acoustic resonances in enclosed fluid flow around solid bodies', *Proceedings of the Institution of Mechanical Engineers. Part C. Mechanical engineering science* **203**, 9–19.

Pechkov, A. A., Kouznetsov, O. L. & Drjaguin, V. V. (1993), *U.S. Patent No. 5,184,678*, Washington, DC: U.S. Patent and Trademark Office.

Poesio, P. (2009), 'Fouling by external particles and ultrasonic cleaning of a porous material', *SPE Journal,* **14**(1), 14–29.

Poesio, P. & Ooms, G. (2004), 'Formation and ultrasonic removal of fouling particle structures in a natural porous material', *Journal of Petroleum Science and Engineering,* **45**(3-4), 159–178.

Poesio, P. & Ooms, G. (2007), 'Removal of particles bridges from a porous material by ultrasonic irradiation', *Transport in Porous Media,* **66**(3), 235–257.

Poesio, P., Ooms, G., Dongen, M. E. V. & Smeulders, D. M. (2004), 'Removal of small particles from a porous material by ultrasonic irradiation', *Transport in Porous Media,* **54**(3), 239–264.

Polyanin, A. D. (2002), *Handbook of Linear Partial Differential Equations for Engineers and Scientists*, first edn, Chapman & Hall/CRC.

Rawlins, A. D. (1978), 'Radiation of sound from an unflanged rigid cylindrical duct with an acoustically absorbing internal surface', *Proceedings of the Royal Society. London. Series A. Mathematical, Physical and Engineering Sciences,* **361**(1704), 65–91.

Rawlins, A. D. (1995), 'A bifurcated circular waveguide problem', *IMA Journal of Applied Mathematics,* **54**(1), 59–81.

Rawlins, A. D. (2007), 'Wave propagation in a bifurcated impedance-lined cylindrical waveguide', *Journal of Engineering Mathematics,* **59**(4), 419–435.

Rawlins, A. D. & Mahmood-Ul-Hassan (2003), 'Wave propagation in a waveguide', *Zeitschrift für Angewandte Mathematik und Mechanik,* **83**(5), 333–343.

Roberts, P. M., Venkitaraman, A. & Sharma, M. M. (2000), 'Ultrasonic removal of organic deposits and polymer-induced formation damage', *SPE Drilling & Completion,* **15**(1), 19.

Roberts, P., Venkitaraman, A. & Sharma, M. M. (1996), 'Ultrasonic removal of organic depostis and polymer induced formation damage', *Paper SPE 31129 presented at the 1996 SPE Formation Damage Control Symposium* .

Schmitt, D. P. & Bouchon, M. (1985), 'Full-wave acoustic logging: synthetic microseismograms and frequency-wavenumber analysis', *Geophysics,* **50**(11), 1756–1778.

Schmitt, D. P., Bouchon, M. & Bonnet, G. (1988), 'Full-wave synthetic acoustic logs in a radially semiinfinite saturated porous media', *Geophysics,* **53**(6), 807–823.

Segura, J. & Gil, A. (1999), 'ELF and GNOME: two tiny codes to evaluate the real zeros of the Bessel functions of the first kind for real orders', *Computer Physics Communications,* **117**(3), 250–262.

Silverman, R. A. (1984), *Complex analysis with application*, second edn, Dover Publications.

Singer, I. & Turkel, E. (2004), 'A perfectly matched layer for the Helmholtz equation in a semi-infinite strip', *Journal of Computational Physics* **201**(2), 439–465.

Spigler, R. (1975), 'Sulle radici dell'equazione: $AJ_\nu(x) + BxJ'_\nu(x)$', *Atti. Sem. Mat. Fis. Univ. Modena* **24**, 399–419.

Spigler, R. (1978), 'Sulle radici dell'equazione: $A\mathcal{C}_\nu(x) + Bx\mathcal{C}'_\nu(x)$', *Atti. Sem. Mat. Fis. Univ. Modena* **27**, 153–166.

Stakgold, I. (1998), *Green's functions and boundary value problems*, Pure and Applied Mathematics (New York), second edn, John Wiley & Sons Inc., New York. A Wiley-Interscience Publication.

Stakgold, I. (2000), *Boundary value problems of mathematical physics. Vol. I, II*, Vol. 29 of *Classics in Applied Mathematics*, Society for Industrial and Applied Mathematics (SIAM), Philadelphia, PA. Corrected reprint of the 1967–68 original.

Stephen, R. A., Cardo-Casas, F. & Cheng, C. H. (1985), 'Finite-difference synthetic acoustic logs', *Geophysics,* **50**(10), 1588–1609.

Stuwe, H. C. & Werner, P. (1996), 'A Green's function approach to wave propagation and potential flow around obstacles in infinite cylindrical channels', *Mathematical Methods in the Applied Sciences,* **19**(8), 607–638.

Sveshnikov, A. G. (1951), 'Limiting absorption principle for a waveguide', *Dokl. Akad. Nauk SSSR,* **80**(3), 341–344.

Tadeu, A. J. B., Godinho, L. M. C. & António, J. M. P. (2000), 'Benchmark solutions for 3-D Scattering from cylindrical inclusions', *Journal of computational acoustics* **6**(4), 1311–1327.

Tang, X.-M. & Cheng, A. (2004), Quantitative borehole acoustic methods, *in* K. Helbig & S. Treitel, eds, 'Handbook of geophysical exploration: Seismic exploration', Vol. 24,

Elsevier.

Thomson, L. L. (2006), 'A review of finite-element methods for time-harmonic acoustics', *Journal of the Acoustical Society of America,* **119**(3), 1315–1330.

Tubman, K. M., Cheng, C. H. & Toksoz, M. N. (1984), 'Synthetic full waveform acoustic logs in cased boreholes', *Geophysics,* **49**(7), 1051–1059.

Ursell, F. (1991), 'Trapped modes in a circular cylindrical acoustic waveguide', *The Royal Society of London. Proceedings. Series A. Mathematical, Physical and Engineering Sciences,* **435**(1895), 575–589.

Venkitaraman, A., Roberts, P. M. & Sharma, M. M. (1995), 'Ultrasonic removal of near-wellbore damage caused by fines and mud solids', *SPE Drilling & Completion* **10**(3), 193.

Vrahatis, M. N., Ragos, O., Skiniotis, T., Zafiropoulos, F. A. & Grapsa, T. N. (1995), 'RFSFNS: A portable package for the numerical determination of the number and the calculation of roots of Bessel functions', *Computer Physics Communications,* **92**(2-3), 252–266.

Watson, G. N. (1966), *A treatise on the theory of Bessel functions*, second edn, Cambridge University Press.

Wegener, D. C., Maloney, D. R., Zornes, D. R., Reese, D. E. & Fraim, M. L. (2001), *U.S. Patent No. 6,184,228 B1*, Washington, DC: U.S. Patent and Trademark Office.

Wegener, D. C., Zornes, D. R., Maloney, D. R., Vienot, M. E. & Fraim, M. L. (2001), *U.S. Patent No. 6,279,653 B1*, Washington, DC: U.S. Patent and Trademark Office.

Westermark, R. & Brett, J. F. (2002), 'Enhanced oil recovery with downhole vibration stimulation, Osage County, Oklahoma', *SPE 75254, Proc. of SPE/DOE Thirteenth Symposium on Improved Oil Recovery, Tulsa, Oklahoma, 13-17 April* .

Westermark, R. V., Brett, J. F. & Maloney, D. R. (2001), 'Enhanced oil recovery with downhole vibration stimulation', *SPE 67303, Proc. of SPE Production and Operations Symposium, Oklahoma City, Oklahoma, 24-27 March* .

Wong, S. W., van der Bas, F., Zuiderwijk, P., Birchak, B., Han, W., Yoo, K. & van Batenburg, D. (2004), 'High-power/high-frequency acoustic stimulation: a novel and effective

wellbore stimulation technology', *SPE Product. Facilit.* **19**(4), 183–188.

Wu, Z. H. & Fang, J. Y. (1995), 'Numerical implementation and performance of perfectly matched layer boundary condition for waveguide structures', *IEEE Transactions on microwave theory and techniques* **43**(12), 2676–2683.

Zienkiewicz, O. C., Taylor, R. L. & Zhu, J. Z. (2005), *The finite element method: Its basis and fundamentals*, Elsevier.